UNIVERSITÀ DEL PIEMONTE ORIENTALE

Department of Translational Medicine

PhD Program in Medical Sciences and Biotechnology

XXIX cycle

Academic years 2014-2017

PhD THESIS

Unacylated ghrelin enhances satellite cell function and relieves the dystrophic phenotype in Duchenne muscular dystrophy mdx model

SSD: BIO/10

PhD coordinator:
Prof. Marisa Gariglio

Supervisor:
Prof. Andrea Graziani

Tutor:
Prof. Nicoletta Filigheddu

PhD candidate:

Elia Angelino

TABLE OF CONTENTS

SUMMARY

Injuries or pathological states such as muscular dystrophies trigger regeneration of the adult skeletal muscle. Muscle regeneration is mainly sustained by a heterogeneous population of quiescent resident precursors called satellite cells (SCs) characterized by the expression of the transcriptional factor Pax7 (Seale et al., 2000). In consequence of injury, SCs activate, proliferate, and eventually differentiate to repair the damaged tissue thus restoring muscle function. A portion of SCs undergoes self-renewal through asymmetric division, thus maintaining the quiescent SC pool and allowing the muscle to retain its regenerative potential (Collins et al., 2005; Kuang et al., 2007). The asymmetric division generates daughter cells with divergent fates: proliferating myoblasts, that express the marker of myogenic commitment MyoD (MyoD+), and MyoD- quiescent SCs, preserving stem features. The differential expression of MyoD depends on the asymmetric segregation of the Par polarity complex during SC activation that leads to a polarized activation of p38 MAPK pathway, triggering MyoD expression in only one daughter cell (Jones et al., 2005; Troy et al., 2012).

Ghrelin and unacylated ghrelin (UnAG) are circulating peptide hormones mainly produced by the stomach. Ghrelin derives from the octanoylation of the preprohormone by the ghrelin-O-acyltransferase (GOAT) enzyme (Gutierrez et al., 2008; Yang et al., 2008). Acylation is required for the binding to the growth hormone secretagogue receptor-1a (GHSR-1a) to induce growth hormone release and perform multiple endocrine functions (Kojima et al., 1999; Müller et al., 2015). UnAG, the main circulating form of the peptide, does not bind to GHSR-1a but features several biological activities, including the enhancement of skeletal muscle regeneration induced by hindlimb ischemia (Ruozi et al., 2015; Togliatto et al., 2013) and improvement of insulin sensitivity in skeletal muscle (Gortan Cappellari et al., 2016; Tam et al., 2015). Besides, UnAG shares with ghrelin numerous biological effects, among which the protection of skeletal muscle from atrophy (Porporato et al., 2013; Sheriff et al., 2012) and the promotion of myoblast differentiation (Filigheddu et al., 2007).

While the mechanisms through which UnAG protects skeletal muscle from atrophy and insulin resistance have been described (Gortan Cappellari et al., 2016; Porporato et al., 2013; Tam et al., 2015), the cellular and molecular mechanisms mediating UnAG ability to enhance muscle regeneration remain to be elucidated. Here we show that UnAG affects multiple stages of muscle regeneration, including SC activation, proliferation, and self-renewal, the latter through induction of SC asymmetric division mediated by PKCλ/ι-Par6 complex formation and asymmetric activation of p38 MAPK. Moreover, UnAG induces the differentiation of committed myoblasts, thus promoting the regeneration of an injured muscle. Based on UnAG ability to enhance skeletal muscle regeneration, we hypothesized that UnAG could have a therapeutic importance for muscle dystrophies.

Duchenne muscular dystrophy (DMD) is characterized by the absence of the dystrophin protein, whose main function is to connect the myofiber cytoskeleton to the extracellular matrix through the dystrophin-associated glycoprotein complex. In the absence of dystrophin, myofibers are extremely susceptible to contraction-induced damage, with the consequent chronic degeneration (Wallace and McNally, 2009). Moreover, dystrophin-null SCs display an impairment of self-renewal and asymmetric division that results in a faulty myogenic progression and, thus, in a defective regenerative process (Dumont et al., 2015; Jiang et al., 2014). We show that upregulation of circulating or local UnAG levels in mdx dystrophic mice improves the pathologic phenotype, including muscle architecture and functionality. Moreover, UnAG blunts the self-renewal defect of dystrophin-null SCs, thus preserving the SC pool at later stages of the pathology.

INTRODUCTION

Skeletal muscle regeneration

Skeletal muscle is the most abundant tissue in the vertebrate body. In human, it comprises the 30-40% of the total body mass, and its primary function is to convert chemical energy into mechanical force, allowing precise movement, force generation, posture maintenance, and respiration (Frontera and Ochala, 2015; Relaix and Zammit, 2012). Besides its mechanical function, skeletal muscle plays a crucial role in regulating metabolism, since it is a primary target of insulin-dependent glucose uptake and a huge amino acids reservoir, that serves as substrates for protein synthesis and hepatic gluconeogenesis, sustaining survival during critical conditions, such as fasting (Jensen et al., 2011; Wolfe, 2006).

The skeletal muscle is essentially composed of long multinucleated cells, the myofibers, composed of hundreds of post-mitotic nuclei and surrounded by the basal lamina. A synchronized framework of myofibrils is packed into a single myofiber, and each myofibril is formed by thousands of repeated contractile units called sarcomeres (Relaix and Zammit, 2012; **Figure 1**).

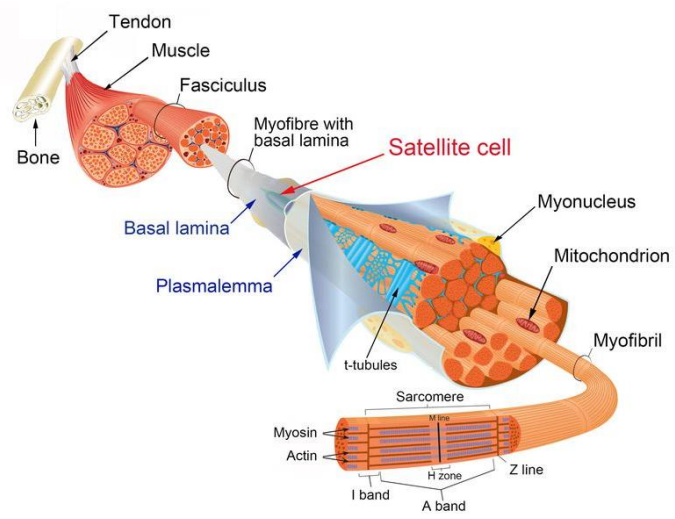

Figure 1. The structure and ultrastructure of skeletal muscle and myofiber.
The satellite cell (SC) is located between the basal lamina and the plasmalemma (adapted from Relaix and Zammit, 2012).

Although the myofiber is a terminally differentiated cell, muscle tissue has an extraordinary ability to regenerate. This regenerative capacity is mainly sustained by a pool of myogenic precursors, located underneath the basal lamina and intimately associated to the myofiber, called satellite cells (SCs), although other cells directly contribute to the regenerative process (Liu et al., 2017). After the first SC observation by electron microscopy, it was suggested that these cells were dormant myoblasts, escaped from differentiation during embryonic development, able to regenerate muscle following damage (Mauro, 1961). Several studies confirmed this hypothesis, demonstrating that SCs can fuse with other muscle precursors and differentiate into myofibers (Bischoff, 1975; Konigsberg et al., 1975; Partridge, 1978; Collins et al., 2005). The cell-autonomous stem property of SCs was then formally demonstrated via single cell transplant (Sacco et al., 2008).

In the adult skeletal muscle, SCs are normally quiescent and express the transcription factor paired-box 7 (Pax7) (Seale et al., 2000). Although other cells participate to muscle regeneration, genetic ablation experiments demonstrated that Pax7+ SCs are strictly required for muscle regeneration (Lepper et al., 2011). The SC quiescent state is ensured by the complex SC microenvironment (referred to as “SC niche”), which consists of extracellular matrix (ECM) components as well as cellular components, such as the myofiber, immune cells, and fibro-adipogenic progenitors (FAPs) (Joe et al., 2010; Yin et al., 2013). The connection between the SC and its niche is ensured by several SC transmembrane proteins, such as the syndecan proteoglycan family members syndecan-3 and syndecan-4 that interact with integrins and cadherins, defining both cell-cell and cell-matrix interactions (Cornelison et al., 2001; Rapraeger, 2000).

SC interactions with its niche translate into an intracellular response that eventually modulates the SC behavior. For example, delta-NOTCH interaction and the subsequent cleavage of the NOTCH intracellular domain (NICD) results in the induction of Pax7 and others quiescence-associated genes, such as Hes and Hey, that inhibit cell cycle entry (Almada and Wagers, 2016; Wen et al., 2012).

After injury or exercise, several growth factors and cytokines trigger the activation of SCs, inducing the expression of myogenic genes, such as the myogenic factor 5 (Myf5) and the myoblasts determination factor

(MyoD), thus SCs enter the cell cycle as a transient amplifying population, referred to as myoblasts (Singh and Dilworth, 2013; **Figure 2**).

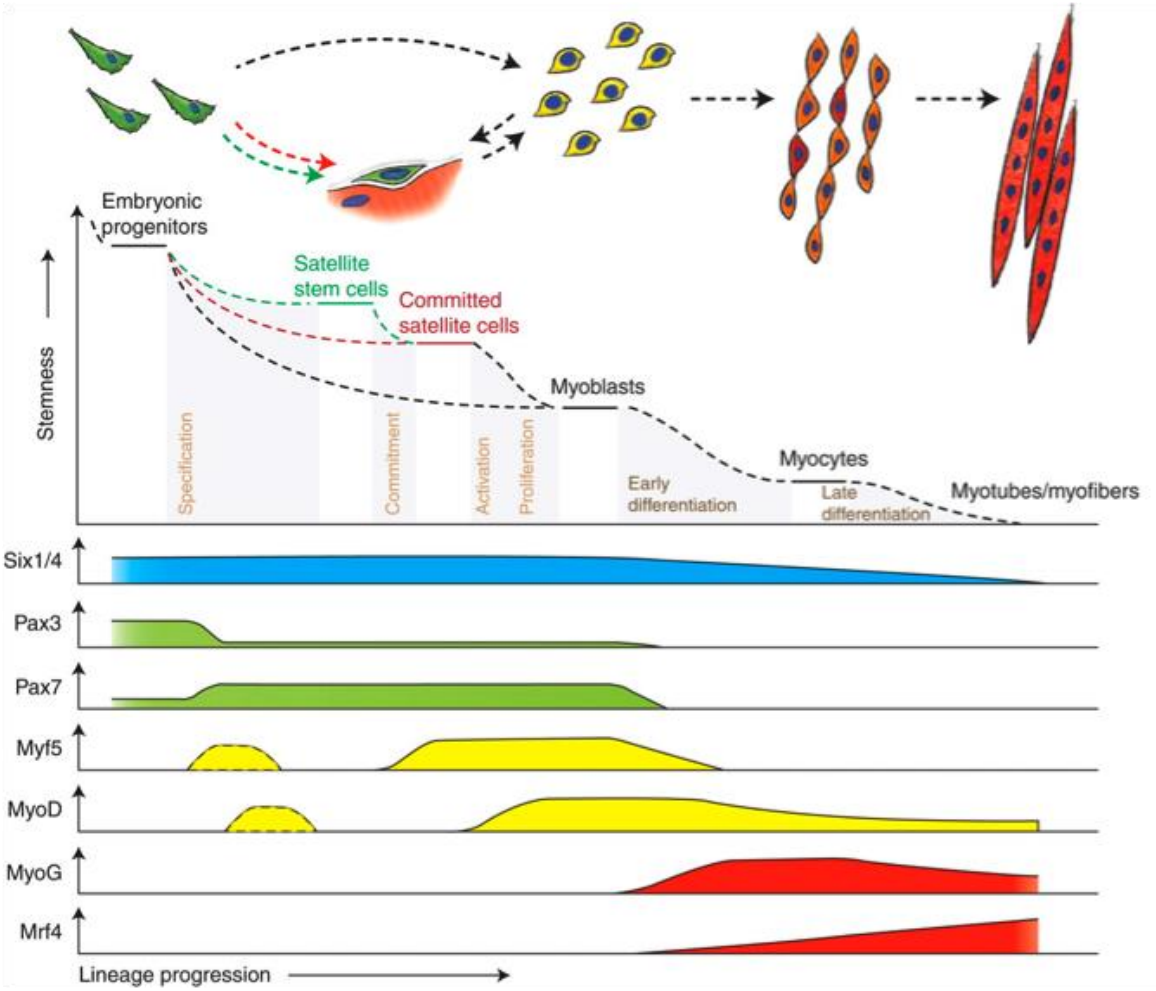

Figure 2. SC myogenic progression.
SCs derive from embryonic progenitor cells that escape from differentiation during muscle development. The SC pool comprises muscle stem cells and committed progenitors; after specific stimuli, SCs activates, proliferates as myoblasts and differentiates as myocytes; however, a subset of SCs exits the cell cycle and maintain the quiescent pool, through the mechanism of self-renewal. At later differentiation stage, myocytes fuse to each other, or to existing damaged myofibers, to repair the muscle. The myogenic process is defined by the expression of key genes: Pax3 during embryonic development; Pax7 in quiescent SCs and during myoblast proliferation; Myf5 and MyoD after SC activation (although transiently expressed in quiescent SCs); myogenin (MyoG) and Mrf4 in later stages of differentiation (from Bentzinger et al., 2012).

After several cellular divisions, myoblasts turn off Pax7 expression and start to express other key genes that orchestrate the final stages of differentiation, such as myogenin (MyoG). At this stage, myoblasts exit the cell cycle and fuse into existing myofibers or to each other to form de novo myofibers (Yin et al., 2013; **Figure 2**). SC activation is a dynamic process that consists in a precise regulation of protein expression at both transcriptional and post-transcriptional levels. Curiously, although MyoD and Myf5 are both target genes of Pax7 (McKinnell et al., 2008), their protein expression is inhibited in SC quiescent state (Almeida et al., 2016), suggesting the involvement of post-transcriptional events underlying SC transition from quiescence to activation. Indeed, in the quiescent SC, the RNA-binding protein tristetraprolin (TTP) promotes MyoD mRNA decay preventing its translation (Hausburg et al., 2015). During activation, external stimuli induce the phosphorylation of the mitogen-activated protein kinase (MAPK) p38α/β that, in turn, inhibits TTP and stabilizes MyoD mRNA, thus inducing MyoD expression (Hausburg et al., 2015; Jones et al., 2005).

Satellite cell asymmetric division

After the first cell division of SCs, not all the daughter cells undergo myogenic progression. Indeed, a portion of SCs exit the cell cycle exerting self-renewal and maintaining the SC pool (Collins et al., 2005; Kuang et al., 2007). Self-renewal ensures a continuous source of progenitors that can sustain several rounds of muscle regeneration. The divergent fates of the two daughter cell rely on SC asymmetric division, in which several cellular components, such as DNA strands, enzymes, and transcriptional factors are asymmetrically distributed in the two daughter cells (Kuang et al., 2007; Rocheteau et al., 2012; Troy et al., 2012). In particular, using a Cre-recombinase mediated lineage tracing, Kuang and colleagues demonstrated that a subpopulation of SCs that had never expressed Myf5 is able to perform apical-basal cell division, generating one committed progenitor (Myf5+) and one daughter cell with stem-like features (Myf5-) (Kuang et al., 2007). Moreover, the template DNA strand exhibits a non-random segregation and is maintained throughout several cell divisions by a subpopulation of Pax7 high-expressing SCs (Rocheteau et al., 2012; Shinin et al., 2006). The selective segregation of the “immortal” DNA strand prevents the accumulation of replication

errors and is a hallmark of stem cells (Cairns, 1975; Karpowicz et al., 2005). Although it is not clear if the Pax7 high-expressing SCs and the Myf5 never-expressing SCs are two overlapping subpopulations, these observations demonstrate that the SC pool is organized in a hierarchical structure of stem cells and committed progenitors (Tierney and Sacco, 2016).

The polarity of stem cells has been extensively studied in *Drosophila Melanogaster* neuroblasts in which several molecular key players define the apical-basal orientation during cell division (Knoblich, 2010).

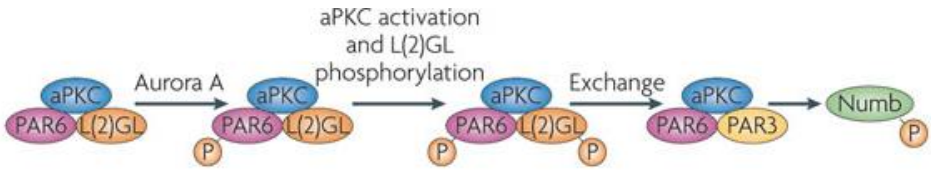

Figure 3. Model of activation of Par complex activation in Drosophila Melanogaster neuroblast.
The phosphorylation of L(2)GL by aurora kinase A in neuroblast during mitosis induces L(2)GL release, thus enabling Par3 to binds to Par6-aPKC and generating the Par Complex. See text for details (adapted from Knoblich, 2010).

The atypical protein kinase C (aPKC) forms a complex with Partitioning Defective 6 (Par6) and Lethal (2) Giant Larvae (L(2)GL). In this context, L(2)GL inhibits aPKC (Knoblich, 2010; Plant et al., 2003; **Figure 3**). During mitosis, aurora kinase A phosphorylates Par6 that, in turn, activates aPKC (Wirtz-Peitz et al., 2008). Activation of aPKC leads to L(2)GL release from the complex, exposing the aPKC PDZ domain for the binding with Bazooka (the *Drosophila* homolog of Partitioning Defective 3 – Par3) (**Figure 3**). This event generates a protein complex between aPKC-Par3-Par6, named Par complex, that orchestrates cell polarization through the activation and compartmentalization of several downstream targets, including Numb (an adaptor protein that inhibits NOTCH signaling) and the serine/threonine kinase Par1b (Chang et al., 2016). In epithelial cells,

the atypical PKC and Par1b are reciprocally regulated and localize in the apical and in the basal side respectively and after asymmetric division, the daughter cell receiving the Par complex will differentiate (Chang et al., 2016; Goulas et al., 2012). In a subset of dividing SCs, the Par complex segregates asymmetrically in only one daughter cell (committed to differentiation), activating p38α/β MAPK and inducing MyoD expression (Troy et al., 2012). Accordingly, the atypical PKCλ is required for both MyoD expression and myogenic commitment. On the other side, the MyoD negative daughter cell exits the cell cycle and displays stem-like features (Troy et al., 2012; Wang et al., 2014; **Figure 4**). The Par complex-dependent asymmetric segregation of active p38α/β MAPK and MyoD expression allows the generation of committed progenitors that sustain myogenesis and, at the same time, the maintenance of the SC pool (Wang et al., 2014).

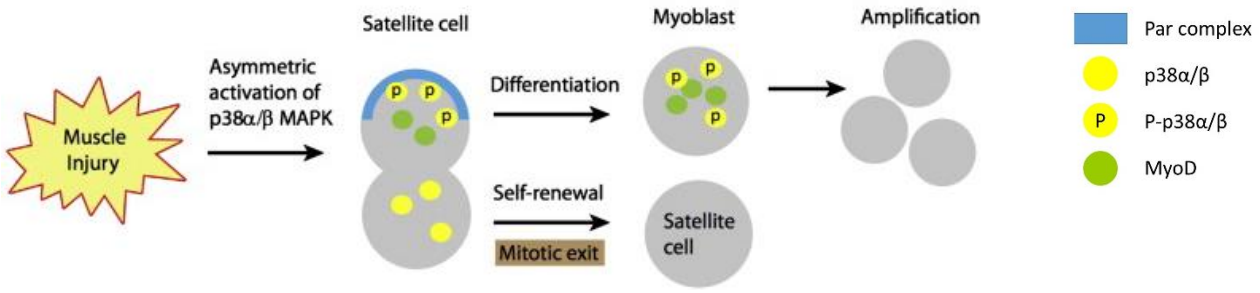

Figure 4. Asymmetric division of the SC.
After muscle injury, SC activates, and the Par complex (composed by Pard3-PKCλ-Par6) segregates in the committed progenitor, inducing phosphorylation of p38α/β MAPK only in one daughter cell. Active P-p38α/β MAPK trigger MyoD expression inducing amplification and myogenic progression of the myoblast. The daughter cell with the inactive p38α/β MAPK does not express MyoD, and exits the cell cycle, restoring a functional quiescent SC pool (adapted from Inaba and Yamashita, 2012).

Satellite cell symmetric division

The asymmetric division ensures the SC pool maintenance during muscle regeneration. However, SCs expand through symmetric division. While the apical-basal spindle orientation during SC mitosis defines a divergent fate of the two daughter cells, planar SC division generates two putative identical cells (Kuang et al., 2007). This cellular mechanism is regulated by the planar cell polarity (PCP) pathway (Le Grand et al., 2009). In particular, Wnt7a drives the symmetric SC expansion through the binding to the receptor Frizzled7 (Fzd7) and by inducing the polarization of the PCP effector Vangl2 and α7-integrin at the poles of the SC through the planar axis (Le Grand et al., 2009). As a direct consequence, both daughter cells will express α7-integrin that anchors the SC plasma membrane to the basal lamina, maintaining the stem state (Le Grand et al., 2009; Kuang et al., 2008). Moreover, the adhesion of the SC to the basal lamina is ensured by syndecan-4 (Sdc4), a Fzd7 co-receptor and binds the ECM protein fibronectin connecting the SC to the basal lamina and regulating Wnt7a-mediated symmetric division (Bentzinger et al., 2013; Cornelison et al., 2001, 2004).

The balance between self-renewal and differentiation of SCs is crucial for muscle homeostasis and assumes a particular relevance in chronic muscle wasting conditions, including sarcopenia and muscular dystrophies (Chang et al., 2016; Sacco and Puri, 2015). Sarcopenia is an age-associated loss of muscle mass and strength (Evans and Campbell, 1993), and the mechanisms underlying this disorder comprise both metabolic and regeneration defects (Grounds, 1998; Karakelides and Nair, 2005). Interestingly, aged SCs express senescence markers and exhibit a reduced capacity to regenerate muscles (Cosgrove et al., 2014; Sousa-Victor et al., 2014). Moreover, excessive activation of the p38α/β MAPK in SCs from aged mice results in asymmetric division defects and subsequent impairment of SC self-renewal ability (Bernet et al., 2014). Other intrinsic asymmetric division and self-renewal defects are associated with an impaired myogenesis and a progressive depletion of functional SCs in Duchenne muscular dystrophy (Chang et al., 2016; Jiang et al., 2014).

Duchenne muscular dystrophy

Muscular dystrophies are a group of inherited disorders characterized by chronic muscle degeneration that leads to progressive structural and functional impairment of skeletal and cardiac muscles (Rahimov and Kunkel, 2013). Among this group, Duchenne muscular dystrophy (DMD) is the most common and severe disorder (Mercuri and Muntoni, 2013). DMD affects approximately 1 to 5000 males and is caused by frameshift or nonsense mutations in the dystrophin gene that result, in almost all the cases, in the complete absence of the dystrophin protein (Rahimov and Kunkel, 2013; Straub et al., 2016). Death usually occurs around 20-25 years and is mainly due to respiratory and cardiac failure (Wallace and McNally, 2009). Dystrophin is a 427 kDa cytoskeletal protein that connects the filamentous actin of the myofiber cytoskeleton to the transmembrane protein β-dystroglycan which, through its extracellular domain, is linked to the α-dystroglycan, forming the dystroglycan complex (Hoffman et al., 1987; Ibraghimov-Beskrovnaya et al., 1992; Rybakova et al., 2000; Wallace and McNally, 2009). The binding between α-dystroglycan and laminin connects the myofiber to the ECM, stabilizing the muscle structure and preventing contraction-induced damage (Gumerson and Michele, 2011). In the absence of dystrophin, myofibers are extremely susceptible to damage. In this context, skeletal muscle undergoes continuous rounds of degeneration and regeneration. This leads to a gradual depletion of functional SCs and replacement of skeletal muscle with fat and fibrotic tissue, resulting in loss of structure and function of skeletal muscle (Jiang et al., 2014; Kharraz et al., 2014). Moreover, dystrophin is expressed in activated SCs and is involved in SC asymmetric division (Dumont et al., 2015). Indeed, dystrophin is connected to the ECM through the dystroglycan complex, thus is localized to the basal side of the SC (**Figure 5A**). During the first SC division, dystrophin is associated with Par1b (Mark2) and controls the localization to the opposite side (apical) of the Par complex member Par3 (Dumont and Rudnicki, 2016; **Figure 5A**). In dystrophin-null SCs, Par1b is downregulated, and Par3 polarization is impaired. The consequent defective asymmetric division leads to the generation of senescent daughter cells (Dumont et al., 2015; **Figure 5B**).

Although the contribution of the defective asymmetric division in the DMD progression is not completely elucidated yet, this intrinsic defect on SC mitosis could partially explain the parallel impairment of both myogenesis and self-renewal presents in DMD (Dumont et al., 2015; Jiang et al., 2014).

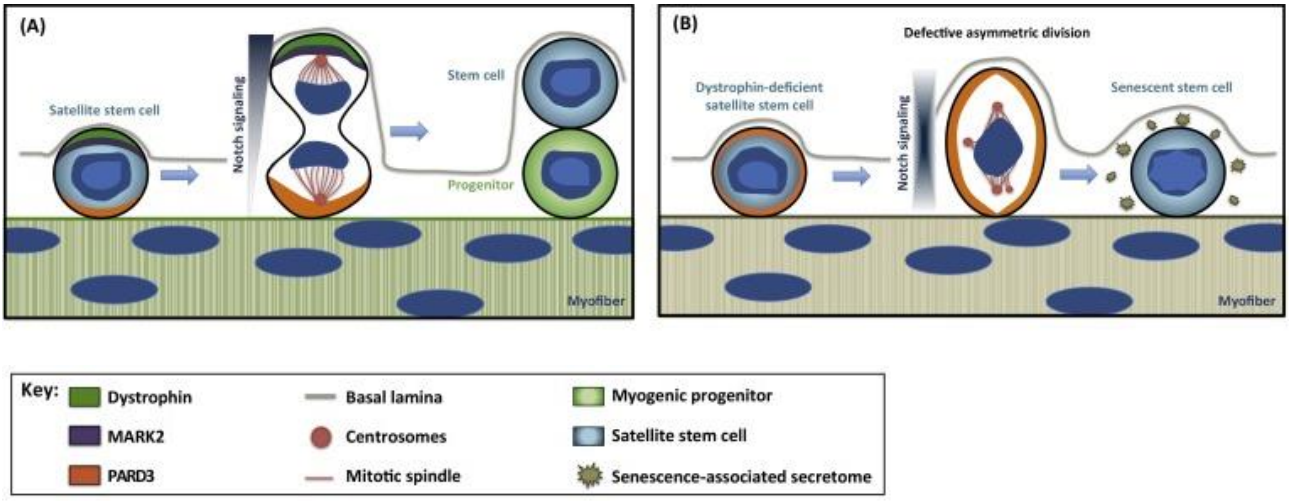

Figure 5. Defective asymmetric division in dystrophin-null SC.
(A) *Normal SC (i.e. dystrophin positive) undergoes asymmetric division during which dystrophin localizes in the basal side of the SC and co-localizes with Mark2 (or Par1b). Par3 (or Pard3-member of the Par complex) is localized in the opposite site (apical). The asymmetric distribution of the polarity determinants, including Notch signaling components, defines the opposite cell fate of the daughter cells: one quiescent stem cell and one committed progenitor.* ***(B)*** *In dystrophin-null SC, Mark2 is downregulated, and Par3 asymmetric distribution is impaired. Dysregulation of the polarity determinants results in a defective mitosis and myogenic progression (adapted from Chang et al., 2016).*

Two corticosteroids, prednisone and deflazacort, are the only drugs that had ultimately demonstrated to have beneficial effects on DMD patients and represent the standard of care for this pathology (Straub et al., 2016). In particular, treatment with corticosteroids improves muscle strength and functional outcomes as well as cardiac dysfunction and life expectancy (Angelini et al., 1994; Beytía et al., 2012; Fenichel et al., 1991). However, these beneficial effects are associated with several side effects that include excessive weight gain, behavioral changes, and osteoporosis (Angelini and Peterle, 2012; Vestergaard et al., 2001). The precise mechanisms of action through which corticosteroids ameliorate the DMD phenotype are not yet known.

However, they likely include inhibition of fibrotic tissue deposition, increased expression of utrophin (that partially compensates for dystrophin function), and reduction of inflammation (Angelini, 2015; Spuler and Engel, 1998).

Gene therapy

Although corticosteroid treatment slows down the progression of DMD, the effective cure of the pathology requires a full genetic correction of the affected tissues. Gene therapy is an attractive therapeutic approach for this monogenic disorder. Several viral vectors have been tested for applications in DMD, including adenoviral vector, lentiviral vectors, and adeno-associated viral (AAV) vectors (Guiraud et al., 2015; Konieczny et al., 2013). Considering the extremely large dimension of the dystrophin gene, one important issue is the limited packaging capacity of the vectors. However, the expression of a portion of the dystrophin protein (mini-dystrophin) is sufficient to ameliorate muscle dystrophic phenotype (Guiraud et al., 2015). In particular, AAV vectors expressing the mini-dystrophin gene have been tested in both preclinical and clinical studies. These studies reveal an unsatisfactory dystrophin expression and a concomitant T-cell reactivity against both the dystrophin and the viral vectors (Konieczny et al., 2013; Mendell et al., 2010). Another therapeutic approach regards the use of viral vector-free gene delivery. The full-length dystrophin cDNA injection in dystrophic mice results in a relative high dystrophin expression. However, this expression is not stable throughout time; this is thought to be related to the low stability of the extrachromosomal DNA (Bertoni et al., 2006; Liu et al., 2001; Molnar et al., 2004).

Currently, promising studies come from the observation that a subset of myofibers in DMD express a truncated form of dystrophin that lacks the mutated exon (Wilton et al., 1997). This is due to a spontaneous intrinsic exon skipping mechanism that restores the correct reading frame of the dystrophin mRNA (Dowling, 2016). The development of an antisense RNA against the mutated exon allows a forced RNA exon skipping and the expression of a truncated, but still functional, dystrophin (Adkin et al., 2012; Cirak et al., 2012). Most of the developed antisense RNA are against exon 51 since the relative majority of the DMD patients (about

the 13%) has mutations in this exon (Bladen et al., 2015). These antisense RNAs include the drug eteplirsen (Sarepta Therapeutics) that is currently tested in a phase III clinical trial (ClinicalTrials.gov identifier: NCT02255552). Previous clinical and pre-clinical studies demonstrate that treatment with this compound partially restores dystrophin expression (in about 40% of the myofibers) and moderately improves functional muscle performance (Dowling, 2016). However, since the antisense RNA targets a specific exon, treatment with these oligonucleotides must be mutation-, and consequently, patient-specific, thus their future application in DMD therapy would require a personalized approach (Kole and Leppert, 2012).

Cell therapy

Pioneering studies reported that intramuscular myoblasts transplant in mdx dystrophic mice, from a wild-type (WT) donor, results in a consistent dystrophin expression (Partridge et al., 1989). However, the translation of this paradigm into the clinical practice revealed several limitations, such as the immune response against the donor cells and inadequate engraftment of the myoblasts (Gussoni et al., 1999; Mendell et al., 1995). To improves engraftment and long-term survival of transplanted cells, several immunosuppressant agents have been tested in animal models (Maffioletti et al., 2014). However, the main bottleneck of myoblast transplantation is that these cells do not cross the vessel wall and have a limited capacity to migrate. Thus a proper treatment would require a huge number of local intramuscular injections, a practice infeasible for the diaphragm and other respiratory muscles (Price et al., 2007). Mesoangioblasts are myogenic pericyte-derived progenitor cells with a promising profile for the treatment of DMD since they can pass throughout vessels, enabling systemic delivery, and exhibit modulatory activities on the immune system (Benedetti et al., 2013; Sampaolesi et al., 2006). Pre-clinical studies reported a partial efficacy of mesoangioblast systemic delivery for the treatment of DMD (Konieczny et al., 2013). However, a recent phase I/IIa clinical trial failed to recapitulate this effect, suggesting that further studies are required to improve efficacy in the clinical practice (Cossu et al., 2015).

Gene and cell therapy represent two encouraging therapeutic options for the future cure of DMD. Moreover, their combination ideally allows autologous stem cell transplant after dystrophin gene correction. However, the investigation of key factors that can modulate transplant efficacy, muscle regeneration, and SC homeostasis is still central to boost the efficacy of these treatments and to slow down pathology progression (Consalvi et al., 2013; Skuk, 2013).

Ghrelin

Ghrelin is a 28 amino acid peptide hormone discovered in 1999 as the endogenous ligand of the growth hormone (GH) secretagogue receptor (GHSR1a) (Kojima et al., 1999), a G protein-coupled receptor (GPCR) mainly expressed in pituitary, hypothalamus, and pancreas. The hormone is produced by the X/A-like stomach cells and physiologically controls several metabolic functions, including GH-release, food intake, adiposity, glucose homeostasis, and body weight (Müller et al., 2015). The peptide sequence presents a biologically rare post-translational modification, consisting in the acylation of the serine-3 residue through esterification with octanoic acid (C8) or, to a lesser extent, with decanoic acid (C10) (Gutierrez et al., 2008; Yang et al., 2008). Ghrelin gene (Ghrl) encodes for a 117 amino acid precursor named preproghrelin, that, after prohormone convertase 1/3-dependent cleavage, generates two biologically active peptides: the unacylated form of ghrelin (unacylated ghrelin, UnAG) and obestatin (Nishi et al., 2011). The acylation of the prohormone occurs intracellularly and is mediated by the ghrelin O-acyl-transferase (GOAT) enzyme (a member of the membrane-bound O-acyltransferase family). Moreover, ghrelin acylation is strictly required for the activation of the GHSR1a and for its metabolic function (Gutierrez et al., 2008; Kojima et al., 1999; Yang et al., 2008).

For its central role in food intake regulation and energy expenditure, ghrelin has been named “the hunger hormone.” Indeed, its plasma levels increase in fasting condition while decrease immediately after food assumption (Cummings et al., 2004; Monteleone et al., 2003), and ghrelin treatment of both mice and human induces food intake indicating a direct role in regulating feeding behavior (Tschöp et al., 2000; Wren et al.,

2001). Consistently with its modulatory effects on energy balance, ghrelin interferes with insulin release and glucose homeostasis (Sangiao-Alvarellos and Cordido, 2010). Ghrelin infusion in both mice and human blunts insulin secretion, thus impairing peripheral glucose uptake (Dezaki et al., 2008; Tong et al., 2010). Moreover, inhibition of the ghrelin-GHSR1a axis results in increased insulin response and glucose tolerance in rats (Dezaki et al., 2008; Sangiao-Alvarellos and Cordido, 2010), confirming the negative action of ghrelin on insulin function. These effects have been confirmed in genetic ablation experiments, indeed, in GHSR- and Ghrl-null mice, insulin secretion, insulin sensitivity, and glucose uptake are increased (Longo et al., 2008; Qi et al., 2011; Sun et al., 2008).

In pathological conditions, such as chronic heart failure and cancer cachexia, high plasmatic ghrelin levels are associated with long-term energy deficit situations (Müller et al., 2015). The correlation between energy deficiency and ghrelin levels observed in several cachectic conditions, may be a consequence of decreased food uptake, thus have been considered as a compensation mechanism (DeBoer, 2011; Müller et al., 2015). Indeed, treatment with ghrelin or GHSR1a-analogues improves cancer-associated cachectic state in both animal models and patients (Garcia et al., 2013; Reano et al., 2014), suggesting that further increase of ghrelin levels through its exogenous administration positively modulates energy balance. The positive effects of ghrelin in the context of cancer cachexia reside in its primary ability to induce food intake and increase lean body mass, by positively regulating GH-IGF1 axis.

Moreover, ghrelin displays an anti-inflammatory action that contributes to the protection against cachexia (Chen et al., 2015; Dixit et al., 2004; Prodam and Filigheddu, 2014). Although ghrelin has anti-inflammatory effects in several contexts (Dixit et al., 2004; Hataya et al., 2003; Li et al., 2004; Waseem et al., 2008), it has also been demonstrated that GHSR-1a contributes to the development of experimental colitis (Liu et al., 2015) as well as to the expression of pro-inflammatory cytokines in macrophages of mice fed with high fructose diet (Ma et al., 2013). Consistently, pro-inflammatory cytokine release by macrophage is mediated by the GHSR-1a and genetic ablation of GHSR-1a attenuates age-associated increase of pro-inflammatory peritoneal macrophages in adipose tissue (Lin et al., 2016). Although opposite activities of ghrelin on

inflammation have been reported, several studies on animal model of chronic inflammation and consequent fibrosis development demonstrate that ghrelin has an overall protective effect (reviewed in Angelino et al., 2015, see attached paper in **Appendix 1**). Notably, in several chronic human pathologies, such as in chronic hepatitis, ghrelin plasma levels negatively correlate with the disease severity (Angelino et al., 2015; Moreno et al., 2010), suggesting a possible physiological role of this hormone in the attenuation of inflammation and fibrosis.

Interestingly, in both physiological and pathological conditions, the most abundant form of circulating ghrelin is the unacylated one (UnAG), that binds GHSR-1a with much lower affinity than acylated ghrelin (in the micromolar range compared to the nanomolar) (Gauna et al., 2007) and definitely lacks any GHSR-1a-dependent activity. For that reason UnAG was initially considered as an inactive catabolism product of acylated ghrelin (Chen et al., 2009; Kojima et al., 1999). However, UnAG shares with ghrelin several biological activities and common binding sites in cells that do not express GHSR1a, including cardiomyocytes, skeletal myoblasts, and pancreatic cells, indicating the presence of a common receptor for the these peptides (Baldanzi et al., 2002; Granata et al., 2007). In particular, several studies explored the GHSR1a-independent ghrelin/UnAG biological activities and their molecular pathways involved:

- Ghrelin and UnAG protect cardiomyocytes and endothelial cells against apoptosis through activation of ERK1/2 and AKT (Baldanzi et al., 2002).

- Ghrelin and UnAG prevent apoptosis of β-pancreatic cells through activation of adenylyl cyclase/3',5'-cyclic adenosine monophosphate (cAMP)/protein kinase A pathway. Moreover, in these cells, both peptides activate PI3K/AKT and ERK1/2 signaling (Granata et al., 2007).

- UnAG protects the heart against ischaemic damage and both UnAG and, to a lesser extent, ghrelin induce dysfunctional mitochondria removal (mitophagy) and promote ischemia-induced muscle regeneration (Ruozi et al., 2015). Moreover, UnAG stimulates autophagy in muscle cells and

decreases inflammation and reactive oxygen species (ROS) production (Gortan Cappellari et al., 2016). These activities result in the prevention of obesity-associated hyperglycemia and to a general improvement of insulin sensitivity (Gortan Cappellari et al., 2016).

- Ghrelin and UnAG impair skeletal muscle atrophy in mice in a GHSR1a-independend manner (Porporato et al., 2013, see attached paper in **Appendix 2**). Both ghrelin and UnAG activate the PI3Kβ-mTORC2-AKT pathway and p38α/β MAPK, thus inhibiting the expression of the atrophy-mediator genes Atrogin1 and MuRF1 (**Figure 6**). These activities are GHSR1a-independent since UnAG protects against atrophy even in Ghsr-null mice, giving the genetic proof of the existence of a ghrelin/UnAG receptor, different from the GHSR1a (Porporato et al., 2013). Although the identity of this receptor is still elusive, several experiments strongly suggest that this receptor is a Gαs protein-coupled receptor (GPCR) (Granata et al., 2007; Porporato et al., 2013; **Figure 6**).

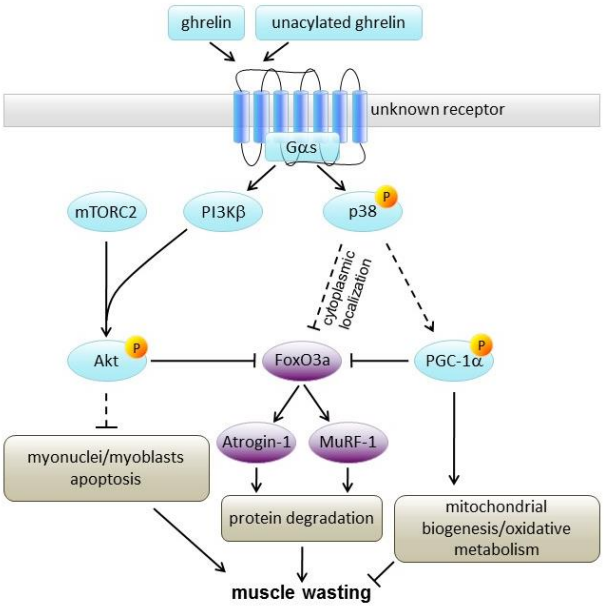

Figure 6. Signaling pathway involved in ghrelin/UnAG anti-atrophic activity.

Ghrelin and UnAG act through a Gαs protein-coupled receptor (GPCR), activating PI3Kβ/ mTORC2/AKT pathway and p38α/β MAPK. The activation of these proteins results in the inhibition of FoxO3a-dependent induction of muscle atrophy (adapted from Reano et al., 2014).

Altogether these data indicate that skeletal muscle represents a major target tissue of both ghrelin and UnAG. Their function in skeletal muscle, however, is not related exclusively to the differentiated myofibers. Indeed, both peptides promote differentiation and fusion of C2C12 myoblasts through activation of p38α/β MAPK (Filigheddu et al., 2007). Moreover, ghrelin and UnAG share common high-affinity binding sites in these cells, which lacks the Ghsr1a, confirming the presence of an unknown common receptor in myoblasts (Filigheddu et al., 2007). Also, these data reveal a direct activity of the two peptides in the skeletal muscle, that is independent from any endocrine effect (Reano et al., 2014).

Interestingly, Togliatto and colleagues demonstrated that UnAG, but not ghrelin, protects skeletal muscle against hindlimb ischemia thus improving muscle regeneration in mice. The authors also provide evidence of a direct effect of UnAG on myoblast proliferation (Togliatto et al., 2013).

Taken together, the data arising from our and others groups indicate that UnAG could be considered as a regulator of myogenesis (Filigheddu et al., 2007; Ruozi et al., 2015; Togliatto et al., 2013). Moreover, UnAG promotes muscle regeneration through the activation of p38α/β MAPK, a master regulator of SC activation, proliferation, differentiation and self-renewal (Kuang et al., 2008; Troy et al., 2012; Wang et al., 2012), suggesting a more complex function of UnAG in the regulation of SC behavior and indicating that exogenous administration of UnAG could ameliorate pathologic phenotype of muscle wasting diseases, in which degeneration and regeneration processes are involved, such as in dystrophies.

AIMS OF THE THESIS

Several experiments indicate that UnAG directly act on the skeletal muscle tissue in both differentiated myofibers and myogenic precursors, regulating protein breakdown, autophagy, ROS production, and myogenesis (Filigheddu et al., 2007; Gortan Cappellari et al., 2016; Porporato et al., 2013; Ruozi et al., 2015; Sheriff et al., 2012; Togliatto et al., 2013). UnAG effects on myogenesis include induction of both SC proliferation and myoblast differentiation and are mediated by p38α/β MAPK activation (Filigheddu et al., 2007; Togliatto et al., 2013). p38α/β MAPK activity is required in several steps throughout SC lineage progression, including activation, proliferation, differentiation, and fusion (Kuang et al., 2008). Moreover, during SC activation, the Par complex-dependent localized activation of p38 MAPK controls SC asymmetric division, a crucial cellular mechanism through which SCs generate daughter cells with opposite fates: committed progenitors and quiescent stem cells, linking a proper myogenesis with the maintenance of the SC pool (Troy et al., 2012). These observations indicate that p38 MAPK is a master regulator of myogenesis and SC homeostasis, and suggests that UnAG might control other important steps of the myogenesis, such as SC asymmetric division and self-renewal. Moreover, we explored the therapeutic potential of UnAG in the dystrophic *mdx* mouse.

In particular, this project aimed at investigation of:

- the pro-regenerative potential of UnAG *in vivo* by using a transgenic mouse carachterized by high levels of circulating UnAG.
- the direct effects of UnAG on SC behaviour, in particular on SC asymmetric division and self-renewal by *ex-vivo* UnAG treatment of myofiber-associated SCs.
- the molecular pathways involved in UnAG activity on SC asymmteric division and self-renewal.

- the potential protective effects of UnAG on skeletal muscle of mdx mice analyzing structural and functional parameters.
- the effects of UnAG on dystrophin-null SC defective asymmetric division and self-renewal by *ex vivo* UnAG treatment of mdx-derived SCs.

MATERIAL AND METHODS

Animals

Animal experiments were performed according to procedures approved by the Institutional Animal Care and Use Committee at the University of Piemonte Orientale. Male mice, matched for age and weight, were used for all experiments. Dystrophin-deficient mdx mice (C57BL/10ScSn-Dmdmdx/J) and C57BL/6-Tg(CAG-EGFP)131Osb/LeySopJ mice with ubiquitous GFP expression were from The Jackson Laboratory; FVB1-Myh6/Ghrl and C57BL/6-Myh6/Ghrl transgenic mice were generated as previously described (Porporato et al., 2013). Animals were fed ad libitum and had unrestricted access to drinking water. The light/dark cycle in the room consisted of 12/12 h with artificial light. To generate dystrophic mice overexpressing the ghrelin gene, C57BL/6J hemizygous Myh6/Ghrl male mice were bred to homozygous $Dmd^{mdx/mdx}$ female mice to yield an equal proportion of male mdx^{Tg+} and mdx^{Tg-} littermate controls. Mdx mice bearing Myh6/Ghrl transgene were identified by PCR genotyping. High levels of plasmatic UnAG in mdx^{Tg+} were confirmed by EIA kit (SPIbio Bertin Pharma) according to the manufacturer's instructions. The numbers of mice estimated sufficient to detect a difference between two means as large as 1 SD unit with 80% power and a significance level of 95% at Student's T-test were calculated with the program by R.V. Lenth (www.stat.uiowa.edu/~rlenth/Power/index.html). The investigators conducting the experiments were blind to the experimental group assessed. The investigators quantifying the experimental outcomes were maintained blinded to the animal group or intervention. Finally, the statistic evaluation of the experimental data was performed by another investigator not directly involved in data collection and parameter measurement.

Reagents

Rat UnAG peptide was purchased from PolyPeptide Laboratories. Media and fetal bovine serum (FBS) were from Gibco (Thermo Fisher Scientific), Horse serum (HS) from PAA (GE Healthcare), and media supplements,

unless otherwise specified, were from Sigma-Aldrich.

CTX-induced muscle regeneration

Experiments on muscle regeneration were conducted on adult male FVB1 and FVB1-Myh6/Ghrl mice matched for age and weight. CTX from *Naja mossambica mossambica* (Latoxan) was dissolved in sterile saline to a final concentration of 10 µM. Mice were anesthetized by isofluorane inhalation and hindlimbs were shaved and cleaned with alcohol. TA muscles were injected with 45 µl of CTX with a 30-gauge needle, with 15 microinjections of 3 µl CTX each in the mid-belly of the muscle to induce a homogeneous damage. The TA muscles of the contralateral hindlimbs were injected with saline. After injection, animals were kept under a warming lamp until recovery.

For some experiments, immediately after CTX administration, a single intraperitoneal injection of 5-bromo-2'-deoxyuridine (BrdU) (6 µg/g mouse) was given, followed by BrdU administered ad libitum in drinking water (2.5 mg/ml) for 7 days.

Histological analysis

Muscles were trimmed of tendons and adhering non-muscle tissue, mounted in Killik embedding medium (Bio-optica), frozen in liquid-nitrogen-cooled isopentane, and stored at -80 C°. Transverse muscle sections (7 µm) were cryosectioned from the mid-belly of each muscle. Sections were stained with hematoxylin/eosin to reveal general muscle architecture. Images of whole muscle sections were acquired with the slide scanner Pannoramic Midi 1.14 (3D Histech) and cross-sectional areas (CSA) of centro-nucleated fibers quantified with ImageJ software (v1.49o). Muscle collagen content was assessed with Masson trichromic staining.

To quantify muscle damage and areas of focal necrosis, 1% w/v Evans blue dye (EBD) was injected intraperitoneally (5 µl/g of animal weight). Muscles were collected 20 h after EBD injection. Sections 7 µm thick were cryosectioned, and EBD uptake was detected as red epifluorescence and quantified as above.

SC isolation and culture

Primary myoblasts were isolated from the main hindlimb muscles (TA, gastrocnemius, quadriceps, EDL, soleus) and diaphragm. Muscles were cut with a lancet into small fragments (about 3 mm^3) and further inspected to eliminate, as much as possible, any remaining connective tissue. The mass was resuspended in 3 ml of 0.1% pronase and incubated for 1 h at 37°C for digestion. The suspension was then centrifuged at 400 x g for 5 min and the pellet resuspended in 10% HS medium, passed several times through a serological pipette, filtered through 40 µm strainers, and further centrifuged at 400 x g for 10 min. SCs were separated from fibroblasts and other cells using the Satellite Cell Isolation Kit (MACS Miltenyi Biotec) following the manufacturer's instructions. After isolation, SCs were either plated on gelatin-coated dishes or immediately used in muscle transplantation experiments.

Plated cells were cultured in growth medium (GM) with 20% FBS, 10% HS, 1% chicken embryo extract (CEE), and 10 ng/ml FGF-2. When cells reached 70-80% of confluence GM was shifted into differentiation medium (DM) with 5% of HS for 3 days. UnAG (100 nM) was added simultaneously to DM.

SC transplantation

To facilitate cell engraftment, one day before muscle transplantation, CTX injection was performed in the mid-belly of TA muscles of recipient mice. SCs were isolated from C57BL/6-Tg(CAG-EGFP)131Osb/LeySopJ (GFP+) mice and 100,000 cells, resuspended in serum-free DMEM, were injected in the previously injured recipient muscles. Contralateral TA muscles were injected with cell-free DMEM. Muscles were harvested 30 days after injection, fixed in 4% PFA, and analyzed.

Myofiber isolation and culture

EDL muscles were digested in 0.2% collagenase type-I in DMEM for 60–70 minutes at 37°C. Muscles were mechanically dissociated, and single fibres liberated. After extensive washing, myofibers were either

immediately fixed or cultured in low proliferation medium (LPM, DMEM supplemented with 10% HS and 0.5% CEE) in suspension. UnAG was added in LPM immediately after fiber seeding. At different time points after plating (6-72-96 h) fibers were fixed in 4% PFA for 10 min.

For experiments with the chemotherapic drug AraC (Cytosine β-D-arabinofuranoside), myofibers were cultured for 72 h in F12 medium supplemented with 15% HS and 1 nM FGF-2 in the presence or absence of 100 nM UnAG and then incubated with or without 100 µM AraC for 48 h and fixed (day 5).

Immunofluorescence

For Pax7 and BrdU detection, tissue sections were fixed in 4% PFA for 20 min, washed, permeabilized with cold methanol for 6 min, and then antigen-retrieved with sodium citrate (10 mM, 0.05% Tween in PBS) at 95°C for 30 min. For blocking the unspecific binding sites, slices were incubated in 4% BSA for 2 h at RT and then with M.O.M. blocking reagent (Vector) for 1 h at RT. Sections were stained with an anti-Pax7 antibody (1:100; Developmental Studies Hybridoma Bank) and with anti-BrdU antibody (1:300; Biorad) overnight at 4°C. After washing, sections were incubated with the appropriate Alexa Fluor Dyes-conjugated secondary antibody (488-anti-mouse/anti-rabbit or 568-anti-rabbit; Thermo Fisher Scientific) for 1 h at RT. DAPI was incubated for 5 min.

For immunofluorescence with anti-laminin (1:200; Dako), anti-GFP (1:200; Thermo Fisher Scientific) and anti-embryonic MyHC (1:20; Developmental Studies Hybridoma Bank), after fixing, slices were permeabilized with 0.2% triton in 1% BSA for 15 min and blocked with 4% BSA. One hour of incubation with primary antibodies was followed by 45 min of secondary antibody incubation at RT.

Images were acquired using the slide scanner Pannoramic Midi Scanner 1.14 (3D Histech) and quantified with Pannoramic viewer software. For immunofluorescence on isolated fibres and on cultured SCs, samples were fixed in 4% PFA for 10 min, permeabilized with 0.5% triton for 6 min and blocked with 4% BSA for 30 min. Primary antibodies to detect Pax7, MyoD (1:500; Santa Cruz Biotechnology), myogenin (1:100; Developmental Studies Hybridoma Bank), and MyHC (1:100; Developmental Studies Hybridoma Bank) were

incubated overnight at 4°C, and the secondary antibodies for 45 min at RT, followed by 5 min of DAPI. Images were acquired with a Leica CTR5500 B fluorescent microscope with the Leica Application SuiteX 1.5 software, and quantification was performed with ImageJ v1.49o software.

To evaluate the asymmetric division events of SC pairs, MyoD levels in each cell were obtained by subtracting the background from the nuclear fluorescence intensity (determined by overlap with DAPI staining). Cell pairs were scored "asymmetric" when the MyoD nuclear intensity of one daughter cell was ≤ 1% ("MyoD-") and the other one was >1% ("MyoD+") of the maximal intensity.

Asymmetric distribution of the proteins was evaluated by SC incubation with rabbit or mouse anti-phospho-p38$^{T180/Y182}$ (1:200, Cell Signaling Technology), rabbit anti-p38 (1:200, Cell Signaling Technology), rat anti-CD34 (1:200; BD Bioscience), rabbit anti-PKCλ (1:200, Santa Cruz Biotechnology), and mouse anti-Pax7 (1:100; Developmental Studies Hybridoma Bank). Nuclei were counterstained with TO-PRO-3 iodide (1:100 Thermo Fisher Scientific). The appropriate Alexa Fluor Dyes-conjugated secondary antibody (546 or 647 anti-mouse, 488 anti-rabbit, and 546 anti-rat; Thermo Fisher Scientific). Images were acquired with Leica confocal microscope TCS SP2 using a 63X objective, NA=1.32, equipped with LCS Leica confocal software. Asymmetry of phospho-p38$^{T180/Y182}$ and of PKCλ were quantified with ImageJ.

For the proximity ligation assay (PLA; Duolink from Sigma-Aldrich), myofiber-associated SCs were incubated with mouse anti-PKCλ (1:200, BD Bioscience) and rabbit anti-PAR3 (1:200, Merck Millipore) then processed according to the manufacturer's instructions.

Gene expression analysis

Total RNA from muscles was extracted by RNAzol. RNA was retro-transcribed with High-Capacity cDNA Reverse Transcription Kit (Thermo Fisher Scientific), and real-time PCR was performed with the StepOnePlus Real-Time PCR System (Thermo Fisher Scientific) using Mm00445450_m1 (Ghrl) and Mm00506384_m1 (Ppif) TaqMan assays.

Hanging test

A wire-hanging test was employed to assess whole-body muscle strength and endurance. The test was performed as previously described (Raymackers et al., 2003). Briefly, mice were subjected to a 180 sec hanging test, during which "falling" and "reaching" scores were recorded. When a mouse fell or reached one of the sides of the wire, the "falling" score or "reaching" score was diminished or increased by 1, respectively. A Kaplan-Meier-like curve was created afterward. Moreover, the longest time between two falls was taken as the latency-to-fall value (van Putten et al., 2010).

Statistical analysis

All data were expressed as mean ± SEM, absolute values, or percentages. For continuous variables, the variation between groups was compared by means of nonparametric Wilcoxon and Mann-Whitney U tests, as appropriate. When analyzing experiments acquired with different instruments, ANCOVA analysis was used to determine differences between groups by using the instrument as a covariate. Multiple logistic regression was used for trends. Statistical significance was assumed for $p<0.05$. The statistical analysis was performed with SPSS for Windows version 17.0 (SPSS; Chicago, IL).

RESULTS

UnAG upregulation in Myh6/Ghrl transgenic mice enhances muscle regeneration

Muscle damage induces the release, within the muscle, of several factors that activate SCs, triggering the expression of myogenic genes, such as Myf5 and MyoD (Crist et al., 2012; Yablonka-Reuveni and Rivera, 1994) that eventually lead to the terminal differentiation of muscle precursors and their fusion among themselves or to the existing fibers. Muscle damage also induces, within the muscle, the expression of the ghrelin gene (**Supplementary information, Figure S1**) and the preproghrelin protein (Gurriarán-Rodríguez et al., 2012), suggesting that its products – ghrelin, UnAG, and obestatin – may participate in the repair process. Accordingly, exogenously administered obestatin and UnAG enhance muscle regeneration in cardiotoxin (CTX)-injured gastrocnemii and in hindlimb ischemia, respectively (Gurriarán-Rodríguez et al., 2012; Ruozi et al., 2015; Togliatto et al., 2013).

Consistently, high levels of circulating UnAG in *Myh6/Ghrl* transgenic mice (Tg) (Porporato et al., 2013) improve muscle regeneration of tibialis anterior (TA) muscle after CTX injury (**Figure 7A-C**).

Despite no differences were evident between WT and Tg in non-injured muscle CSA distribution (**Supplementary information, Figure S2A**), at day 7 post CTX injury, improved muscle regeneration in Tg mice is evidenced by a shift towards bigger areas of centronucleated (i.e. regenerating) fibers (**Figure 7B**). This regeneration is accompanied by an increment in the number of regenerating fibers with ≥2 nuclei (**Figure 7C**), suggesting an increase in myoblast differentiation and fusion during regeneration, in agreement with the pro-differentiative activity of UnAG in C2C12 myoblasts (Filigheddu et al., 2007). The shift toward bigger areas and the increased myoblast fusion did not translate into a hypertrophic phenotype, as at 15 days post-injury fiber distributions of Tg and WT overlapped (**Supplementary information, Figure S2B**). Consistently with the hypothesis that UnAG induces faster recovery, injured Tg muscles displayed more embryonal MyHC (eMyHC)-positive

myofibers at day 3 post-CTX, although no significant differences were observed in the number of eMyHC-expressing fibers at day 7 (**Supplementary information, Figure S3A-C**). Also, transient collagen deposition during regeneration tended to disappear more rapidly in Tg muscles (**Supplementary information, Figure S3D and S3E**).

Though basal Tg muscle do not overtly differ from their WT littermates (Porporato et al., 2013), a closer examination of their not-injured muscles revealed a larger number of SCs, seen as Pax7+ nuclei, in both TA and quadriceps (QUAD) from Tg animals (**Figure 7D and 7E**). However, this higher basal number of SCs does not affect the injury-induced SC proliferation, as, during regeneration, SC number in TA muscles from Tg and WT are not different (**Supplementary information, Figure S4**). This finding suggests that a UnAG-rich environment may confer a regenerative advantage, at least partially by promoting post-natal SC pool formation. In addition, transplant of SCs from GFP donor mice in muscles of Tg or WT recipient mice resulted, 30 days later, in ~80% increase in GFP+ fibers in Tg than in WT mice (**Figure 7F and 7G**), suggesting that UnAG promotes skeletal muscle regeneration plausibly by acting on the transplanted SCs.

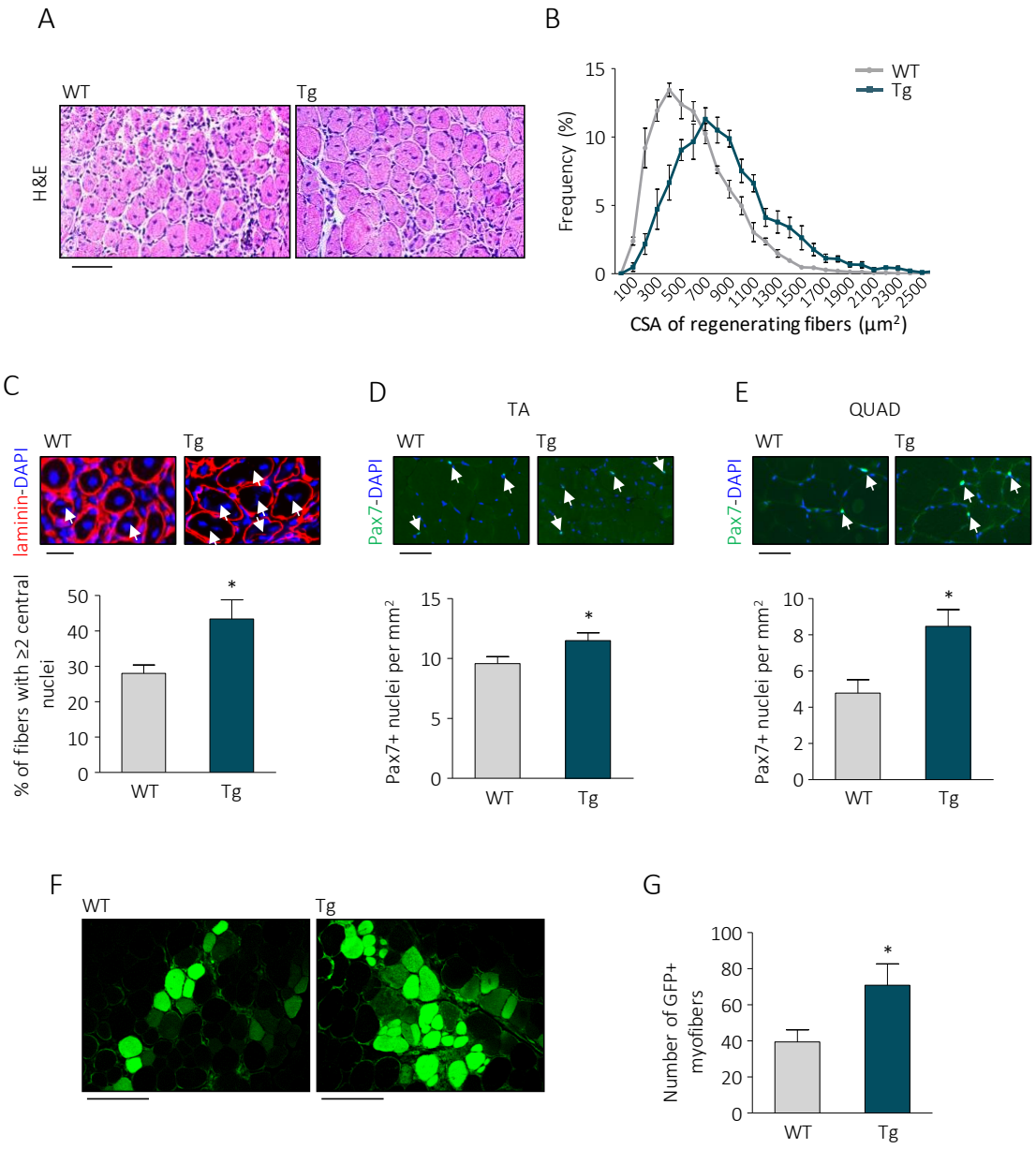

Figure 7. UnAG upregulation in Myh6/Ghrl transgenic mice enhances muscle regeneration, increases SC number in non-injured muscles, and improves SC engraftment.

*(**A**) H&E of WT and Myh6/Ghrl (Tg) TA muscle sections 7 days after CTX injury. Scale bars, 100 µm. (**B**) Cross-sectional area (CSA) frequency distribution of regenerating fibers in TA. Chi-square test was used to compare distributions. Trend P<0.01. (CSA mean µm²: Tg 837.02±55.41; WT 559.28±15.81; P<0.05). n≥4. (**C**) laminin-DAPI staining images and percentage of multinucleated fibers (≥2 nuclei) over the total of regenerating fibers. Mean±s.e.m. *P<0.05; n≥4. Scale bar, 50 µm. White arrows indicate the multinucleated fibers. (**D-E**) Images of Pax7-DAPI staining and quantification of Pax7+ SCs/mm² in non-injured TA (**D**) and quadriceps (QUAD) (**E**) of WT and Tg mice. Mean±s.e.m. *P<0.05; TA n=10; QUAD n=5. White arrows indicate Pax7+ nuclei. Scale bar, 50 µm. (**F-G**) Representative images (**F**) and quantification (**G**) of GFP+ myofibers in transplanted TA of WT and Tg mice. Scale bars, 200 µm. Mean±s.e.m. *P<0.05; n=11 (WT) and 12 (Tg).*

UnAG promotes SC activity and their asymmetric division

To explore in detail the effects of UnAG on SCs, we isolated single fibers from WT muscles, thus maintaining SCs in an original niche-like environment (Bischoff, 1975), and we cultured them in the presence or absence of 100 nM UnAG. When cultured, SCs undergo activation and turn on MyoD expression (Pax7+/MyoD+). After 72 h in culture, several clusters of myoblasts originated from a single SC are visible on myofibers. During this phase, the majority of activated SCs turns off Pax7 and commits to terminal differentiation (Pax7-/MyoD+), while a small subset undergoes self-renewal, retaining Pax7 but not MyoD expression (Pax7+/MyoD-) (Olguin and Olwin, 2004; Zammit et al., 2004). UnAG treatment within 6 h expanded the portion of activated SCs (**Figure 8A**), within 72 h it increased the number of cells in each cluster (**Figure 8B**), and within 96 h raised the portion of SCs that underwent self-renewal (**Figure 8C**). Altogether, these data indicate that UnAG enhances SC activity by promoting their activation, expansion, and self-renewal.

SCs undergo self-renewal through asymmetric division that gives rise to a proliferating daughter cell and a quiescent daughter cell (Troy et al., 2012). In culture, asymmetric division generally occurs during the first cellular division. This has been demonstrated by culturing myofibers with cytosine β-D-arabinofuranoside (AraC), a chemotherapic drug that selectively kills cycling cells and spares quiescent cells (Troy et al., 2012). Incubation of isolated myofibers with AraC during the first three days kills all myofiber-associated SCs, while the addition of AraC to the culture medium from day 3 to day 5 allows the detection of AraC-resistant Pax7+ SCs (or, in the case of differentiated SCs, Myog+) deriving from cells that divided at least once (**Figure 8D**, (Troy et al., 2012)). A higher number of Pax7+/MyoD- SCs was found in UnAG-treated myofibers after incubation with AraC from day 3 to 5 (**Figure 8E**), suggesting that UnAG acts during SC replications likely regulating SC asymmetric division. Asymmetric division can be assessed by the quantification of myofiber-associated SC doublets, bona fide derived from a single SC after the first cell division, in which only one of the two daughter cells is MyoD+ (Troy et al., 2012). UnAG treatment induced a 6-fold increase in the percentage of SC doublets in which only one cell is MyoD+ (**Figure 8F and 8G**),

indicating that UnAG actually promotes SC asymmetric division. To verify whether UnAG induces self-renewal also in vivo, we administered BrdU to WT and Tg mice during the phase of intense myoblast proliferation post-injury (**Figure 8H**). Since BrdU is incorporated in every cycling cell, when muscle regeneration is fully achieved and SC proliferation no longer occurs, any cell positive for both BrdU and Pax7 (**Figure 8I**) is a SC that cycled at least once and then underwent self-renewal (Shea et al., 2010). Fifty days post-injury the number of Pax7+/BrdU+ SCs – normalized on SC number in the contralateral, non-injured muscle – was higher in Tg than in WT muscles (**Figure 8J**), demonstrating that upregulation of UnAG enhanced SC self-renewal also in vivo. SC self-renewal is of particular importance when skeletal muscle is subjected to repeated cycles of degeneration/regeneration that could lead to the progressive depletion of the SC pool; therefore, we assessed the impact of UnAG on the compartment of Myf5- SCs, a subpopulation of SCs that undergoes depletion in an artificial model of SC pool exhaustion, obtained by multiple rounds of muscle injury (**Figure 8K**, (Buono et al., 2012)). Extensor digitorum longus (EDL) fibers isolated from injured hindlimbs of WT mice displayed a 50% loss of Myf5- SCs, while fibers from Tg mice maintained the number of Myf5- SCs (**Figure 8L**), demonstrating that UnAG helps to maintain the SC pool also upon repeated injuries.

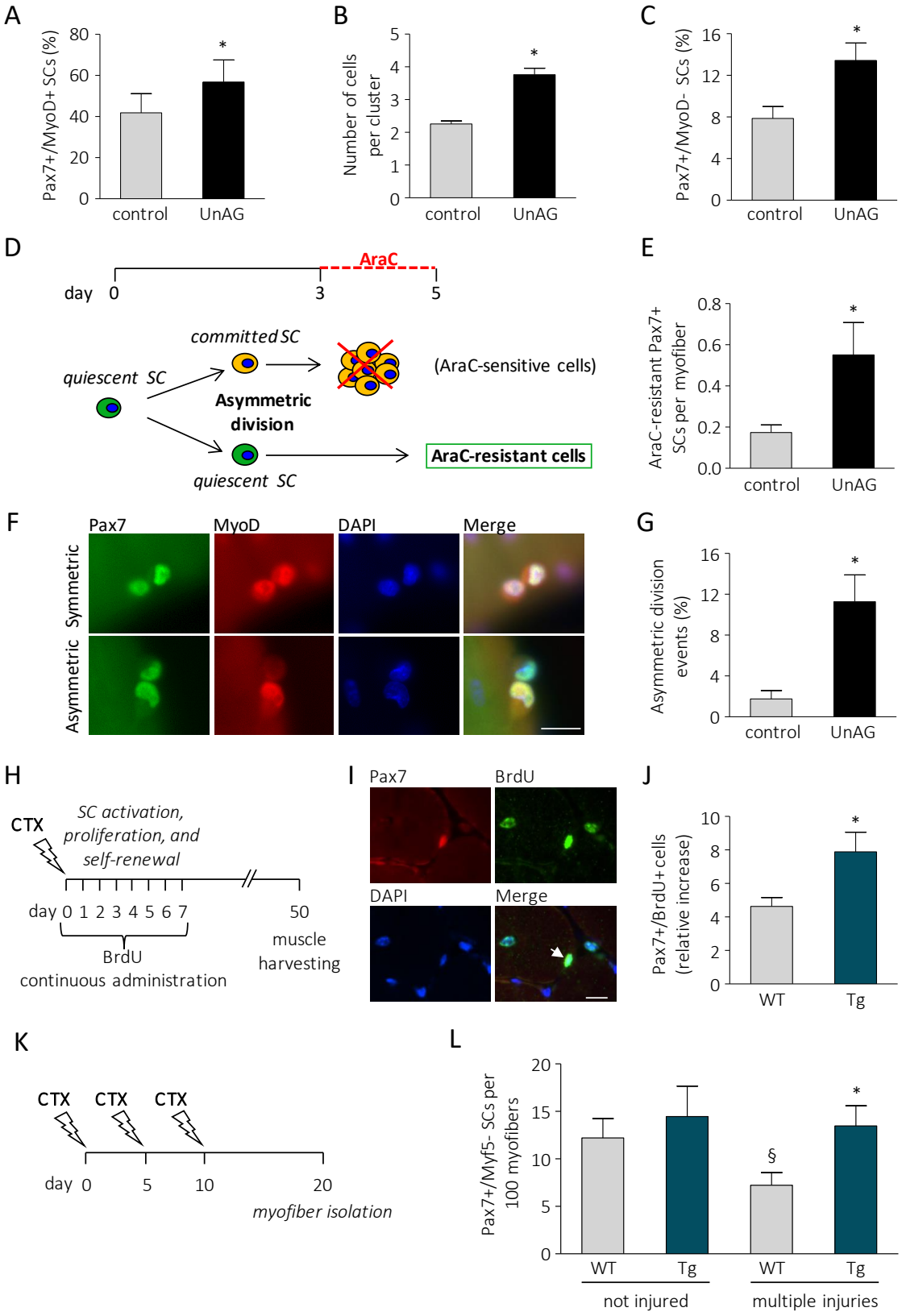
A
Pax7+/MyoD+ SCs (%)
80
60
40
20
0
control
UnAG
*
B
Number of cells per cluster
5
4
3
2
1
0
control
UnAG
*
C
Pax7+/MyoD- SCs (%)
16
12
8
4
0
control
UnAG
*
D
day 0
3
5
AraC
committed SC
quiescent SC
Asymmetric division
(AraC-sensitive cells)
AraC-resistant cells
quiescent SC
E
AraC-resistant Pax7+ SCs per myofiber
0.8
0.6
0.4
0.2
0.0
control
UnAG
*
F
Pax7
MyoD
DAPI
Merge
Symmetric
Asymmetric
G
Asymmetric division events (%)
16
12
8
4
0
control
UnAG
*
H
CTX
SC activation, proliferation, and self-renewal
day 0 1 2 3 4 5 6 7
50
muscle harvesting
BrdU
continuous administration
I
Pax7
BrdU
DAPI
Merge
J
Pax7+/BrdU+ cells (relative increase)
10
8
6
4
2
0
WT
Tg
*
K
CTX
CTX
CTX
day 0
5
10
20
myofiber isolation
L
Pax7+/Myf5- SCs per 100 myofibers
20
15
10
5
0
WT
Tg
WT
Tg
§
*
not injured
multiple injuries

Figure 8. UnAG induces activation, proliferation, and self-renewal of SCs.

*(**A**) Percentage of MyoD+ SCs after 6 h of treatment of isolated myofibers with 100 nM UnAG in low proliferation medium. (**B**) Cells per cluster after 72 h of treatment. (**C**) Percentage of Pax7+/MyoD- SCs after 96 h of treatment. Mean±s.e.m. *P<0.05. ≥25 myofibers/treatment; n=3 independent experiments. (**D**) Schematic of experiments with AraC to identify quiescent daughter SCs. (**E**) AraC-resistant Pax7+ cells. Mean±s.e.m. *P<0.05; ≥25 myofibers/treatment; n=3 independent experiments. (**F**) Representative images of SCs that underwent symmetric (top) or asymmetric (bottom) division. Scale bar, 20 µm. (**G**) Percentage of asymmetric division events in SC doublets. Mean±s.e.m. *P<0.05; ≥22 doublets/treatment; n=3 independent experiments. (**H**) Experimental design schematic: mice were daily treated with BrdU for the first 7 days after CTX injection. Muscles were harvested 50 days after injury. (**I**) Representative images of TA transverse sections, arrow: Pax7+/BrdU+ nucleus. Scale bar, 40 µm. (**J**) Pax7+/BrdU+ nuclei normalized to the contralateral SC number. Mean±s.e.m. *P<0.05; n≥8. (**K**) SC forced exhaustion design schematic: 10 days after three injections of CTX at 5-days intervals, EDL fibers were isolated from injured hindlimbs and immediately fixed. (**L**) Number of Pax7+/Myf5- SCs in 100 isolated fibers. Mean±s.e.m. *P<0.05 vs. multiple injured WT; §<0.05 vs. not injured WT; n≥8.*

UnAG induces SC self-renewal through activation of atypical PKC/p38 pathway

UnAG exerts its anti-atrophic and pro-differentiative effects on skeletal muscle through activation of p38 MAPK (Filigheddu et al., 2007; Porporato et al., 2013; Togliatto et al., 2013), a master regulator of SC activities, as its activation mediates either SC proliferation or differentiation (Jones et al., 2005; Palacios and Puri, 2006). The role of p38 MAPK is particularly relevant in SC self-renewal, since the asymmetric segregation of phosphorylated p38 MAPK in dividing SCs regulates their asymmetric division, triggering MyoD expression in only one daughter cell (Jones et al., 2005; Troy et al., 2012; **Figure 4**). Treatment of myofibers with UnAG for 36h increased the asymmetric distribution of phosphorylated p38 MAPK in SCs (**Figure 9A and 9B**), while the total p38 MAPK was mostly diffuse (**Supplementary information, Figure S5**). Since the asymmetric phosphorylated p38 MAPK colocalizes with the atypical PKCλ/ι in the dividing SC (Troy et al., 2012), we hypothesized that UnAG could enhance the asymmetric distribution of PKCλ/ι. As expected, UnAG treatment increased PKCλ/ι localization in one of the two SC halves (**Figure 9C and 9D**). Moreover, UnAG enhanced the asymmetric colocalization of PKCλ/ι and phosphorylated p38 MAPK, as UnAG treatment increased

the percentage of SCs with asymmetric distribution of the two proteins in the same side of the cell (**Figure 9E**).

Asymmetric localization of PKCλ/ι and phosphorylated p38 MAPK during SC division is closely related to the Par complex formation during SC asymmetric division (Troy et al., 2012). The increased localization of both PKCλ/ι and phosphorylated p38 MAPK observed in UnAG-treated could be a direct consequence of an enhanced Par complex formation. Thus, we performed a proximity ligation assay (PLA) to detect and quantify the complexes of the two Par complex members PKCλ/ι and PAR3 (**Figure 3**). The UnAG-treated SCs displayed an increased number of PLA dots compared to control (**Figure 9F and 9G**), suggesting that UnAG enhances Par complex assembly, thus increasing SC asymmetric localization of the polarity components and, eventually, SC asymmetric division. Accordingly, incubation with 10 µM aurothiomalate (ATM), an inhibitor of Par complex formation (Stallings-Mann et al., 2006), prevented the effect of UnAG on SC asymmetric division (**Figure 10A**).

Par complex assembly during SC division defines the segregation of active p38 MAPK, sustaining SC asymmetric division and self-renewal. Incubation of UnAG-treated myofibers with 5 µM of p38 MAPK inhibitor SB203580, completely abrogated the UnAG effect on self-renewal (**Figure 10B**), suggesting that p38 MAPK activation is required for UnAG-induced SC self-renewal.

Altogether, these data indicate that UnAG treatment enhances the formation and asymmetric localization of the Par complex – and of phosphorylated p38 – within the SC undergoing cell division, thus increasing SC asymmetric division and self-renewal.

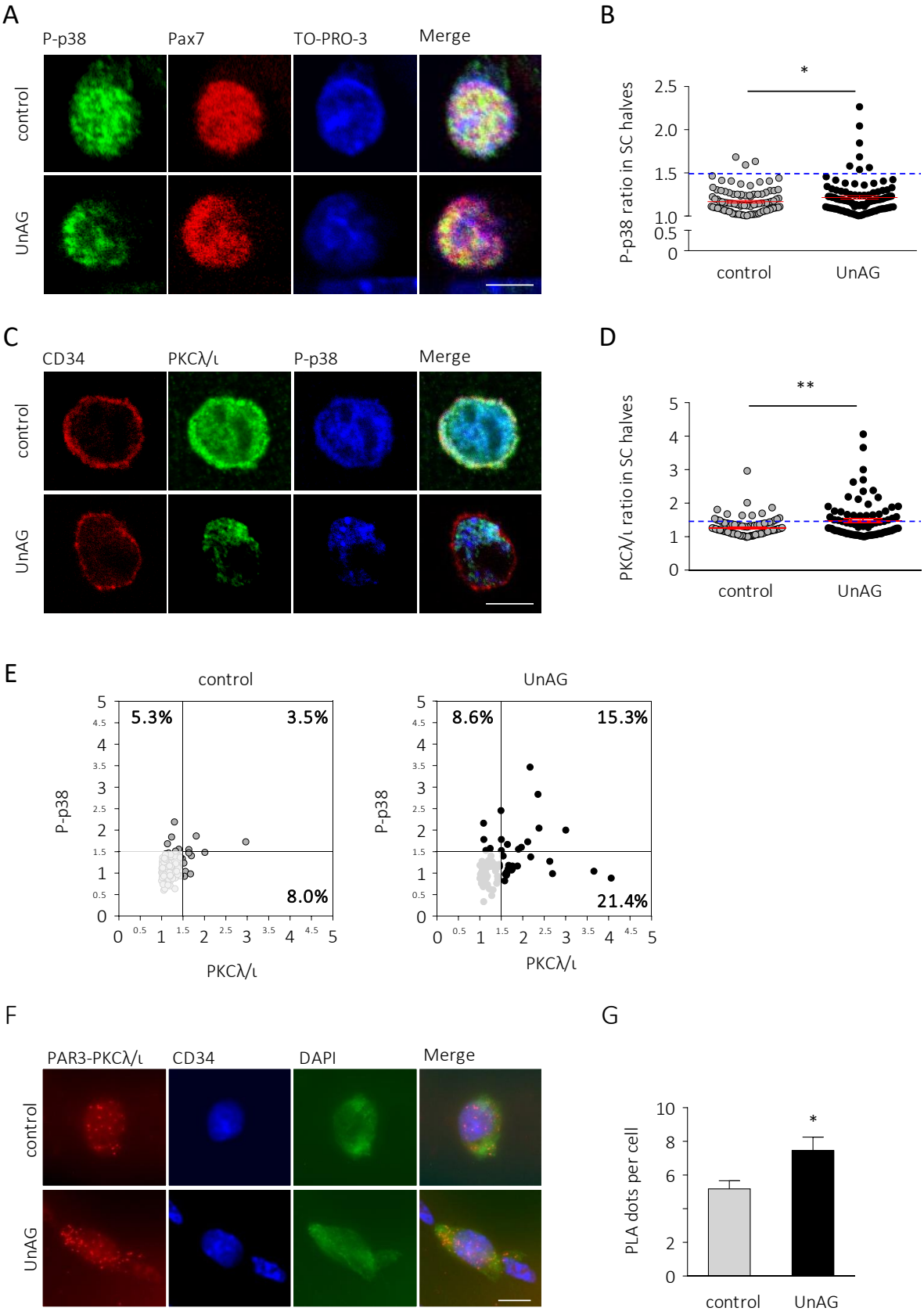
A
P-p38
Pax7
TO-PRO-3
Merge
control
UnAG
B
P-p38 ratio in SC halves
control
UnAG
C
CD34
PKCλ/ι
P-p38
Merge
control
UnAG
D
PKCλ/ι ratio in SC halves
control
UnAG
E
control
UnAG
P-p38
PKCλ/ι
5.3%
3.5%
8.0%
8.6%
15.3%
21.4%
F
PAR3-PKCλ/ι
CD34
DAPI
Merge
control
UnAG
G
PLA dots per cell
control
UnAG

Figure 9. UnAG induces asymmetric localization of active p38 MAPK and PKCλ/ι within the SC and increases PAR3-PKCλ/ι complex formation. *(**A**) Representative images and (**B**) quantification of asymmetric distribution of phospho-p38$^{T180/Y182}$ in UnAG-treated vs. untreated (control) SCs. Cells over the dashed line display at least 50% more phospho-p38$^{T180/Y182}$ in one half of the nucleus compared to the other half. Mean±s.e.m. *P<0.05; ≥30 fibers; n=3 independent experiments. Scale bar, 5 µm. (**C**) Representative images of PKCλ/ι and phospho-p38$^{T180/Y182}$ distribution in control (top) and UnAG-treated (bottom) SCs (CD34 positive). Scale bar, 5 µm. (**D**) Quantification of asymmetric distribution of PKCλ/ι in UnAG-treated vs. untreated (control) SCs. Cells over the dashed line display at least 50% more PKCλ/ι in one half of the nucleus compared to the other half. **P<0.01; ≥30 fibers; n=3 independent experiments (**E**) Correlation between the asymmetric distribution of PKCλ/ι (x axis) and phospho-p38$^{T180/Y182}$ (y axis) in control (left) vs. UnAG-treated (right) SCs. Each dot denotes a single SC. (**F**) Representative images of the proximity ligation assay (PLA)-detected complexes of PAR3 and PKCλ/ι (red) in control (top) vs. UnAG-treated (bottom) SCs (CD34 positive, green). Scale bar, 5 µm. (**G**) Quantification of the PLA dots per single SC in control vs. UnAG-treated SCs. Mean±s.e.m. *P<0.05; ≥30 fibers; n=3 independent experiments.*

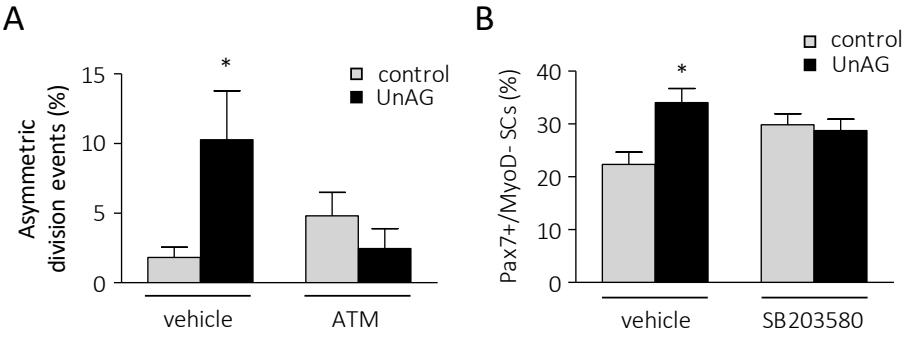

Figure 10. UnAG induces asymmetric division and self-renewal through Par complex formation and p38 MAPK activation. (A) *Percentage of asymmetric division events in SC doublets after 48h of UnAG treatment in the presence/absence of 10 µM ATM, an inhibitor of Par complex formation (see material and methods for details). Mean±s.e.m. *P<0.05; ≥22 doublets/treatment; n=4 independent experiments.* ***(B)*** *Percentage of Pax7+/MyoD- SCs after 96 h of UnAG treatment in the presence/absence of 5 µM p38 inhibitor SB203580. Mean±s.e.m. *P<0.05 vs. DMSO-treated (vehicle) control; ≥100 clusters of ≥25 myofibers/treatment; n=2 independent experiments.*

Up-regulation of UnAG protects dystrophic muscles architecture and functionality

The improved muscle regeneration in Tg mice and enhanced SC activity within the muscle of Tg mice and in response to UnAG treatment suggest that increase in UnAG may be beneficial for muscle diseases such as dystrophies, in which the lack of dystrophin impacts both on muscle fragility and on SC function, leading to chronic degeneration and impaired regeneration (Chang et al., 2016; Dumont et al., 2015). To test the hypothesis that up-regulation of UnAG circulating levels protects dystrophic muscles from deterioration, we crossed dystrophin-null mdx mice with heterozygous Myh6/Ghrl (Tg) mice, producing mdx^{Tg+} mice and mdx^{Tg-} littermate controls. Histological analysis revealed, in mdx^{Tg+} mice compared to the mdx^{Tg-} littermates, a mild shift toward bigger myofiber CSA in quadriceps of 1-month- and 3-month-old animals, while no differences were observed in 6-months-old mice (**Supplementary information, Figure S6A-C**). Analysis of the Evans blue dye (EBD) uptake in diaphragms of 1-month- and 3-month-old revealed lower fiber damage in mdx^{Tg+} mice compared to mdx^{Tg-}, while no differences were evident at 6 months of age (**Figure 11A and 11B**). During *mdx* pathology progression, the gradual collagen accumulation in diaphragms was delayed in mdx^{Tg+} mice compared to mdx^{Tg-} littermates, becoming significantly lower at 6 months of age (**Figure 11C and 11D**). Altogether these data indicate that up-regulation of UnAG ameliorates the dystrophic phenotype. Consistently, hanging-wire-test scores and latency-to-fall time, assessments of muscular functionality and endurance, were improved in mdx^{Tg+} mice starting from 4 months of age (**Figure 11E and 11F**), showing that the differences highlighted by histological analysis translated into enhanced functional performance.

To assess if these UnAG activities could have clinical relevance, as a proof of concept, we exogenously administered UnAG to dystrophic mice employing adeno-associated virus (AAV)-mediated delivery. We used the AAV9-Ghrl vector that has been demonstrated to protect the muscle from ischemic injury as the UnAG peptide does (Ruozi et al., 2015). We injected 3.5 x 10^{11} vg of either AAV9-Ghrl or AAV9-LacZ (control) in the tail vein of 3 week-old mdx mice, when the first round of muscle degeneration occurs (Grounds et al., 2008), and analyzed the effect on muscles at 3

months of age. Ghrelin up-regulation in muscles was confirmed by real-time RT-PCR (**Supplementary information, Figure S7A and S7B**). Analysis of diaphragms revealed less muscle damage (**Figure 11G and 11H**) and collagen deposition (**Figure 11I and 11L**) in AAV9-Ghrl-injected mice compared to the AAV9-LacZ-injected controls. Altogether, these data indicate that UnAG treatment is effective even after the onset of muscle degeneration, supporting the idea that UnAG administration could represent a potential treatment for muscular dystrophies.

Altogether, these data show that upregulation of circulating UnAG partially relieves the pathological condition of mdx dystrophic mice.

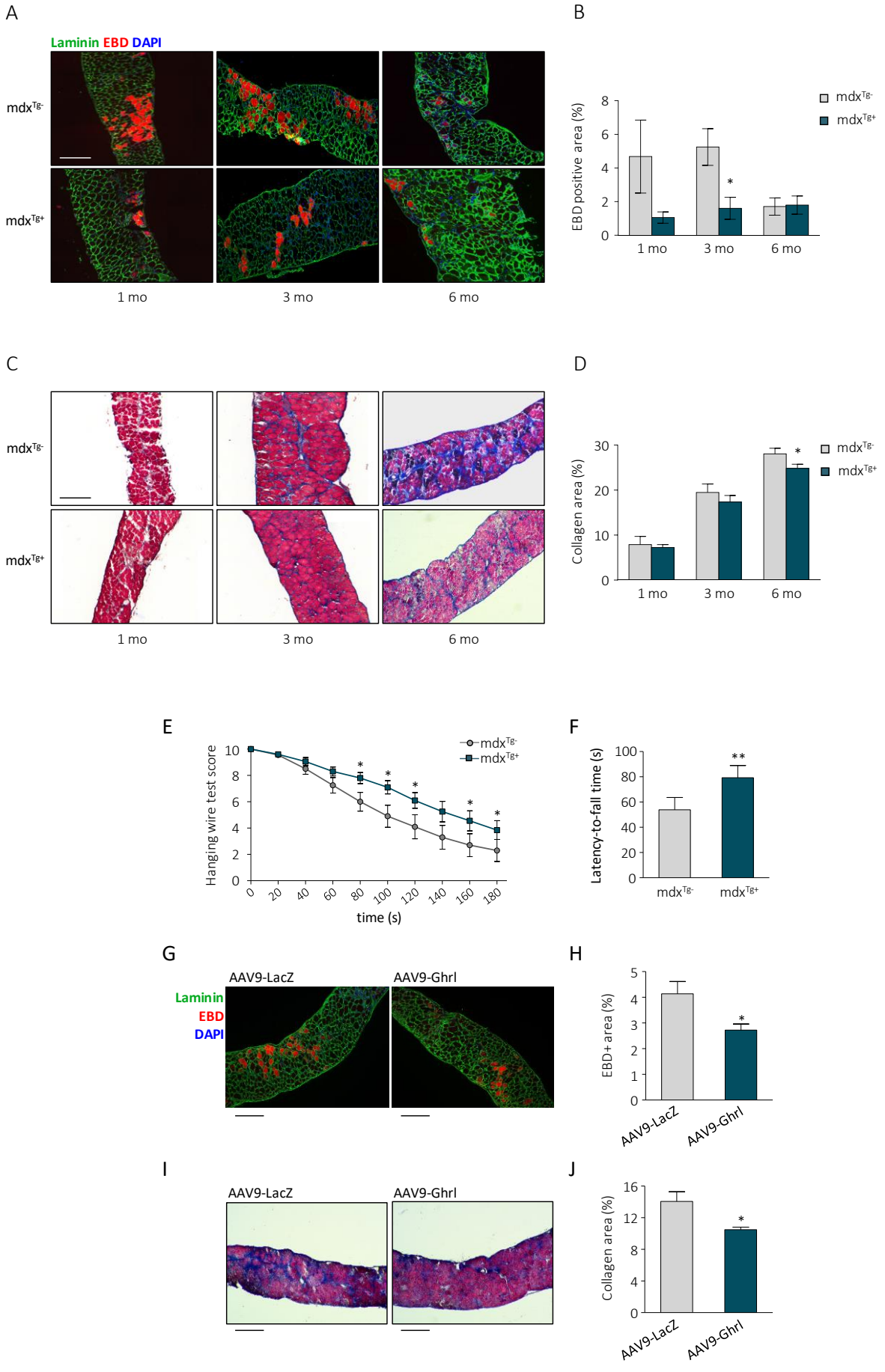
A
Laminin EBD DAPI
mdx^Tg-
mdx^Tg+
1 mo
3 mo
6 mo
B
EBD positive area (%)
mdx^Tg-
mdx^Tg+
1 mo
3 mo
6 mo
C
mdx^Tg-
mdx^Tg+
1 mo
3 mo
6 mo
D
Collagen area (%)
mdx^Tg-
mdx^Tg+
1 mo
3 mo
6 mo
E
Hanging wire test score
mdx^Tg-
mdx^Tg+
time (s)
F
Latency-to-fall time (s)
mdx^Tg-
mdx^Tg+
G
AAV9-LacZ
AAV9-Ghrl
Laminin
EBD
DAPI
H
EBD+ area (%)
AAV9-LacZ
AAV9-Ghrl
I
AAV9-LacZ
AAV9-Ghrl
J
Collagen area (%)
AAV9-LacZ
AAV9-Ghrl

***Figure 11. UnAG upregulation in mdx mice attenuates the dystrophic phenotype**. (**A**) Representative images and (**B**) quantification of Evan blue dye (EBD) uptake in diaphragms of 1, 3, and 6-month-old mdx^{Tg-} and mdx^{Tg+} mice. Scale bars, 200 µm. Mean±s.e.m. **P<0.01 vs. mdx^{Tg-}; n≥4 for each group. (**C**) Representative images of Masson trichrome staining and (**D**) quantification of collagen deposition in the diaphragm of 1, 3, and 6-month-old mdx^{Tg+} and mdx^{Tg-} mice. Scale bars, 200 µm. Mean±s.e.m. *P<0.05; n≥5 for each group. (**E-F**) Muscular functionality measured by hanging wire test scores (**E**) and average latency-to-fall time (**F**) of 4-month-old mdx^{Tg-} and mdx^{Tg+} mice. Mean±s.e.m.; *P<0.05 and **P< 0.01 vs. mdx^{Tg-}; n=20. (**G**) Representative images and (**H**) quantification of Evan Blue Dye uptake in AAV9-LacZ- or AAV9-Ghrl-transduced diaphragms of 3-month-old mdx mice. Scale bars, 200 µm. Mean±s.e.m. *P<0.05 vs. AAV9-LacZ-transduced muscles; n=5. (**I**) Representative images and (**L**) quantification of collagen deposition in AAV9-LacZ- and AAV9-Ghrl-transduced diaphragms of 3-month-old mdx mice. Scale bars, 200 µm. Mean±s.e.m. *P<0.05 vs. AAV9-LacZ-transduced muscles; n=5.*

UnAG enhances dystrophin-null SC self-renewal and myogenic commitment

To assess the direct effect of UnAG on dystrophic SCs, we isolated EDL fibers from dystrophin-null mdx and WT mice, and we cultured them in the presence or absence 100 nM UnAG for 96 h. The number of Pax7+/MyoD- SCs was 60% lower in mdx fibers compared to the WT ones, indicating an intrinsic self-renewal defect of dystrophin-deficient SCs, in agreement with previously reported data (Jiang et al., 2014); however, UnAG significantly raised the Pax7+/MyoD- SC portion in both WT and mdx fibers (**Figure 12A**). The relative increase of quiescent SCs, of about 50%, was the same in both WT and mdx fibers, indicating that UnAG promotes SC self-renewal independently from the presence of dystrophin. Also, UnAG enhances the number of myogenin-expressing SCs in mdx myofibers cultured for 72 (**Figure 12B**), indicating that the increase on quiescent SCs does not imply an unbalance between self-renewal and myogenic commitment.

Coherently with the concept that UnAG promotes SC self-renewal, we observed that the exhaustion of SC pool, characteristic of the advanced pathology (Jiang et al., 2014), was less pronounced in diaphragms of 12-month-old mdx^{Tg+} mice compared to mdx^{Tg-} mice (**Figure 12C**). Consistently, after 96 h in culture, myofibers from mdx^{Tg+} mice displayed twice as much Pax7+/MyoD- SCs, likely reflecting an initial higher content of functional SCs (i.e. able to undergo self-renewal) compared to mdx^{Tg-} mice (**Figure 12D**).

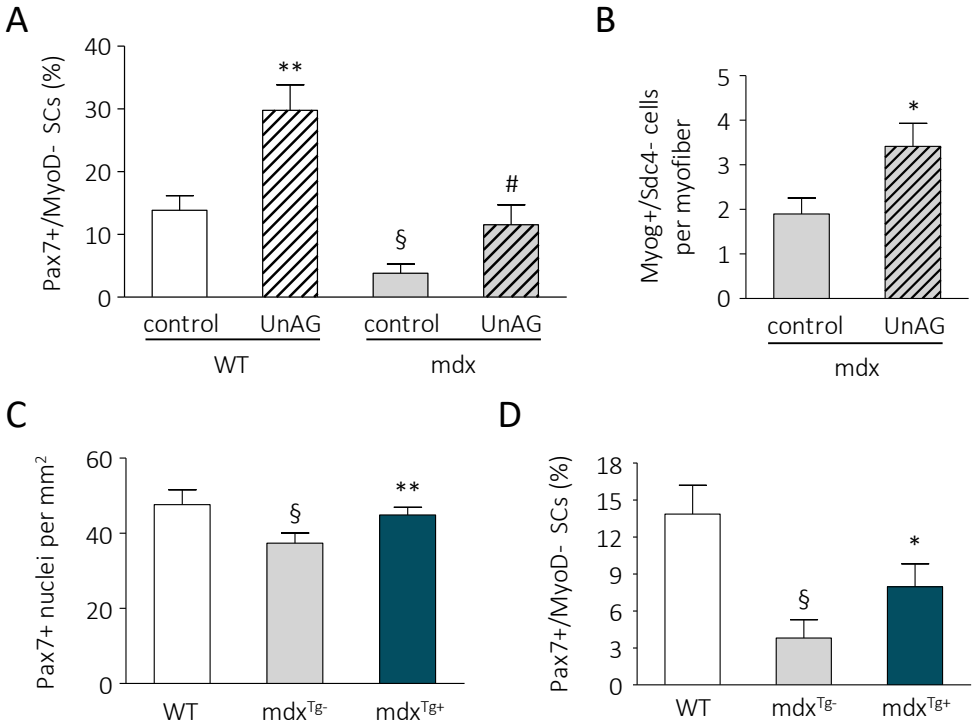

Figure 12. UnAG improves dystrophin-null SCs activity. *(**A**) Percentage of Pax7+/MyoD- SCs after 96 h of treatment of WT or mdx myofibers with 100 nM UnAG. Mean±s.e.m. **P<0.01 vs. WT control, § P<0.01 vs. WT control, and # P<0.01 vs. mdx control. ≥25 myofibers/treatment; single experiment. (**B**) Number of Myog+/Sdc4- SCs per fibers after 72 h of treatment of mdx myofibers with 100 nM UnAG. * P<0.01 vs. mdx, ≥45 myofibers/treatment; n=3 independent experiments. (**C**) Number of Pax7+ cells/mm^2 in diaphragm sections of 12-month-old mdx^{Tg+} and mdx^{Tg-} mice. Mean±s.e.m. §P<0.05 vs. WT; *P<0.05 vs. mdx^{Tg-}; n=7. (**D**) Percentage of Pax7+/MyoD- SCs on myofibers isolated from aged (12 months) WT, mdx^{Tg-} and mdx^{Tg+} cultured for 96 h in low proliferation medium. § P<0.01 vs. WT control and * P<0.05 vs. mdx^{Tg-}, ≥23 myofibers/treatment, single experiment.*

SUPPLEMENTARY INFORMATION

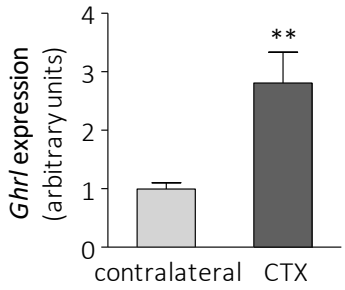

Supplementary Figure 1. CTX injury induces ghrelin gene expression in skeletal muscle. *Relative ghrelin gene expression was determined by real-time RT-PCR in tibialis anterior muscle after 18 h from CTX injection. **P<0.01 vs. non-injured contralateral muscle; n = 10.*

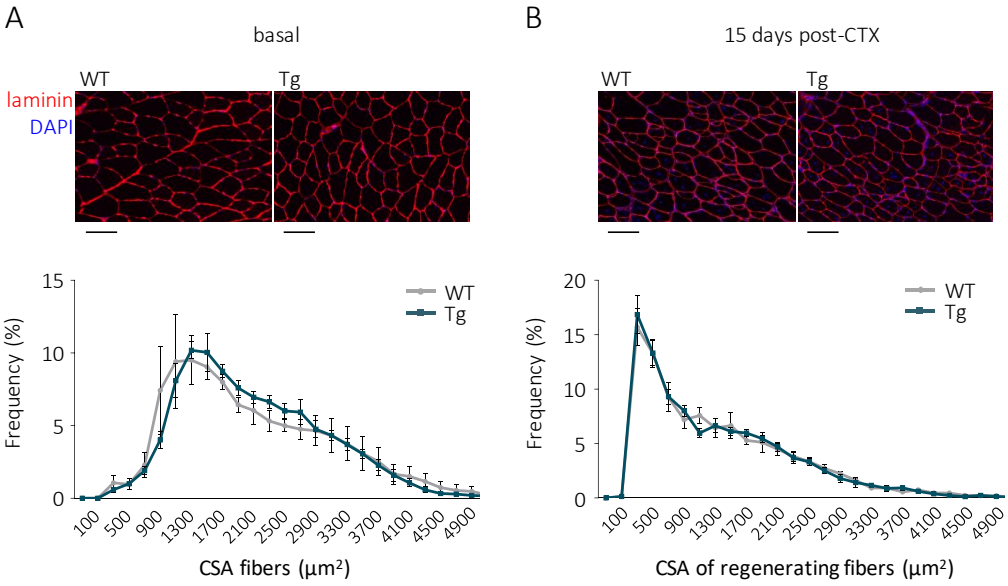

Supplementary Figure 2. Cross-sectional area in basal and regenerating muscle of WT vs. Myh6/Ghrl transgenic mice. (A-B) *Representative images of laminin and DAPI staining and quantification of cross-sectional area (CSA) frequency distribution of myofibers in basal (not-injured) conditions* ***(A)*** *and of regenerating (i.e. centronucleated) myofibers after 15 days from CTX injection* ***(B)*** *in TA muscles of WT vs Myh6/Ghrl (Tg) mice. N=5 for each group. Scale bar, 100 µm.*

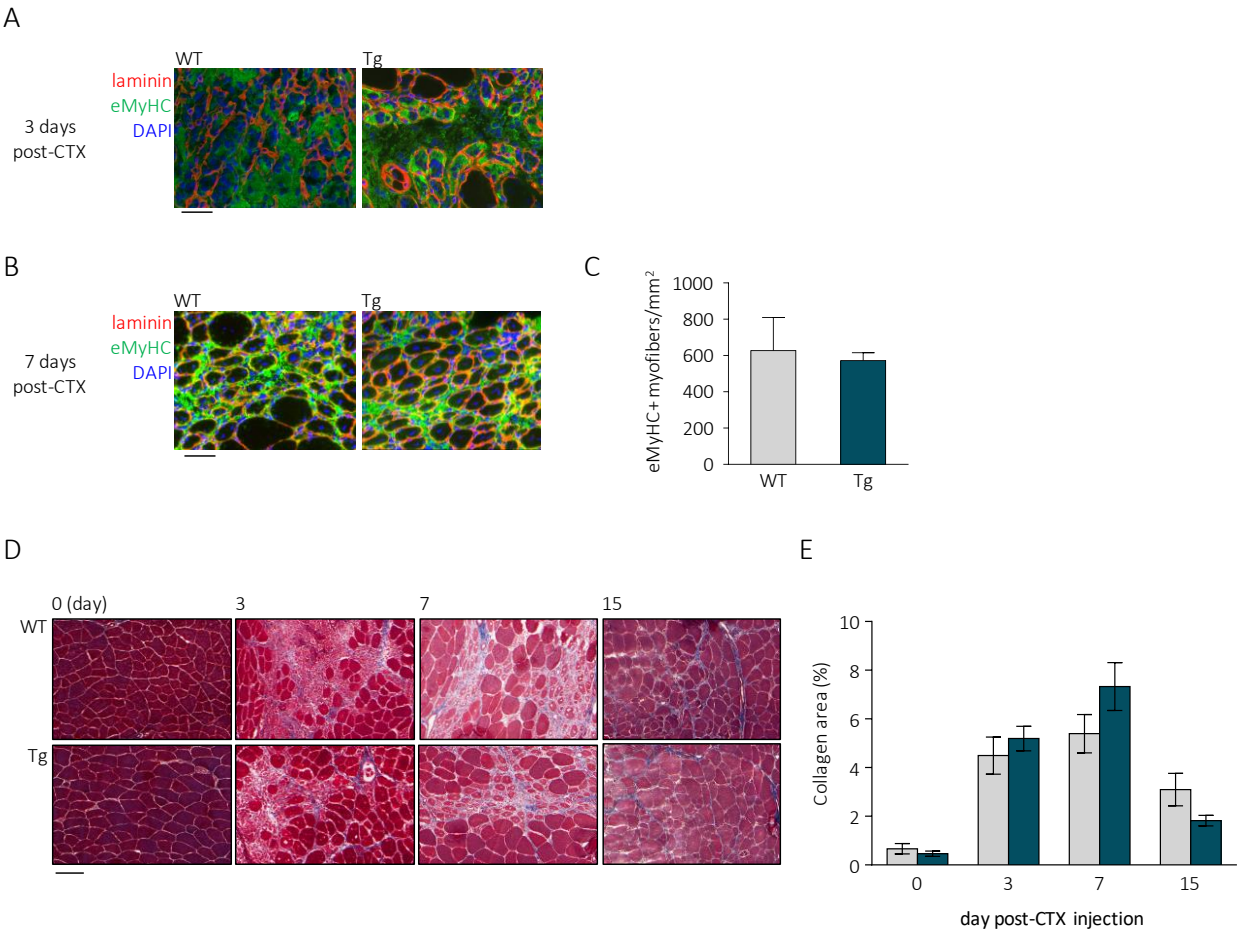

Supplementary Figure 3. Embryonic myosin heavy chain (eMyHC)-positive myofibers and transient collagen deposition during muscle regeneration in WT vs. Tg mice. (A) *laminin (red), eMyHC (green), and DAPI (blue) staining in regenerating muscle of WT and Tg mice at 3 days post-CTX injection. Scale bar, 50 µm.* ***(B-C)*** *Representative images* ***(B)*** *and quantification* ***(C)*** *of eMyHC-positive myofibers in regenerating muscle of WT and Tg mice at 7 days post-CTX. Mean±s.e.m. N=5 for each group. Scale bar, 50 µm.* ***(D-E)*** *Representative images of Masson trichrome staining* ***(D)*** *and quantification of collagen deposition* ***(E)*** *in basal condition (day 0) and in the regenerating area after 3, 7, and 15 days post CTX-injection in WT vs. Tg animals. Mean±s.e.m. N=5 for each group. Scale bar, 100 µm.*

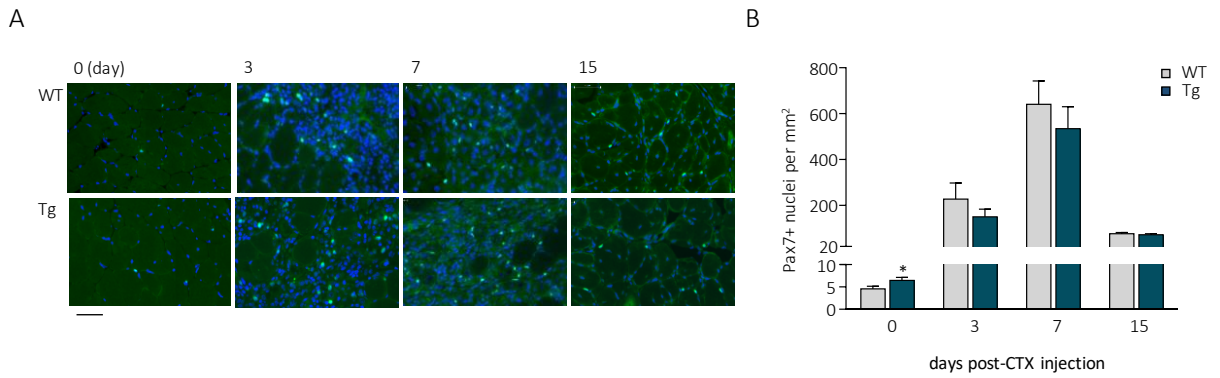

Supplementary Figure 4. Pax7 positive cells during muscle regeneration in WT vs. Myh6/Ghrl transgenic mice. *Representative images* ***(A)*** *and quantification* ***(B)*** *of Pax7 positive nuclei in basal condition (day 0) and during muscle regeneration (after 3, 7, and 15 days post-CTX) in TA of WT vs. Myh6/Ghrl (Tg) mice. Mean±s.e.m. *P<0.05 vs. WT. n=5. Scale bar, 50 µm.*

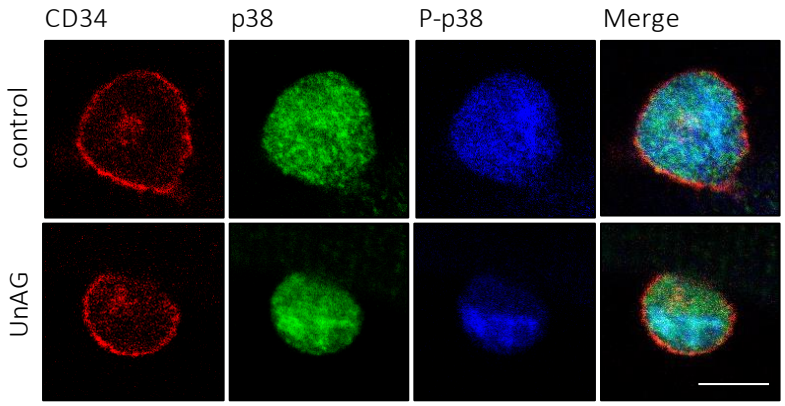

Supplementary Figure 5. Total and phosphorylated p38 MAPK in control vs. UnAG-treated SC. *UnAG treatment increases the localization of phospho-p38$^{T180/Y182}$ while maintaining unperturbed the total p38 uniform distribution. Scale bar, 5 µm.*

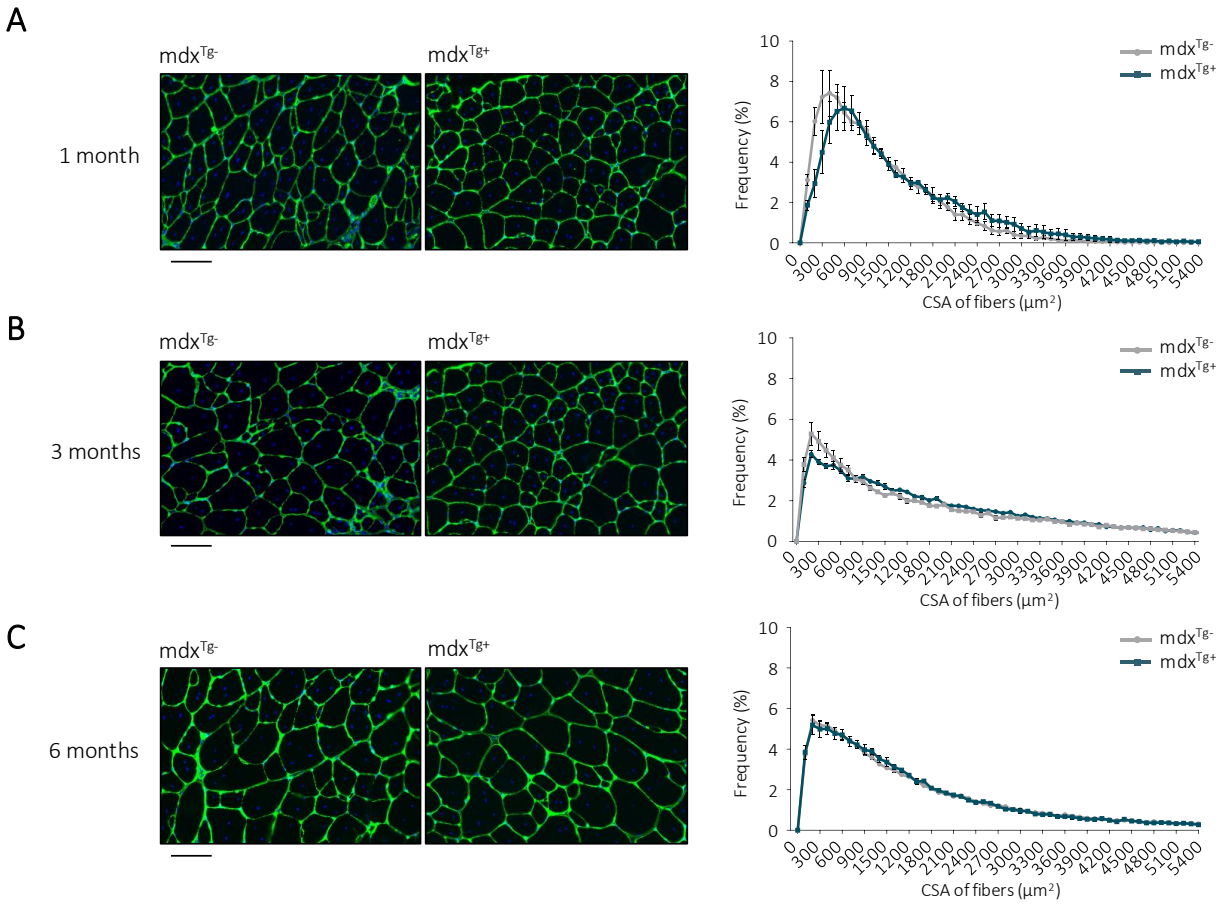

Supplementary Figure 6. Myofiber cross-sectional area in quadriceps of mdx^{Tg-} vs. mdx^{Tg+}. (A-C) *Representative images of laminin (green) and DAPI (blue) staining (**left**) and frequency distribution (**right**) of myofiber cross-sectional area (CSA) in mdx^{Tg-} vs. mdx^{Tg+} mice quadriceps at 1 **(A)**, 3 **(B)**, and 6 **(C)** months of age. N=3 for **(A)**; N=5 for **(B-C)**. Scale bar, 50 µm.*

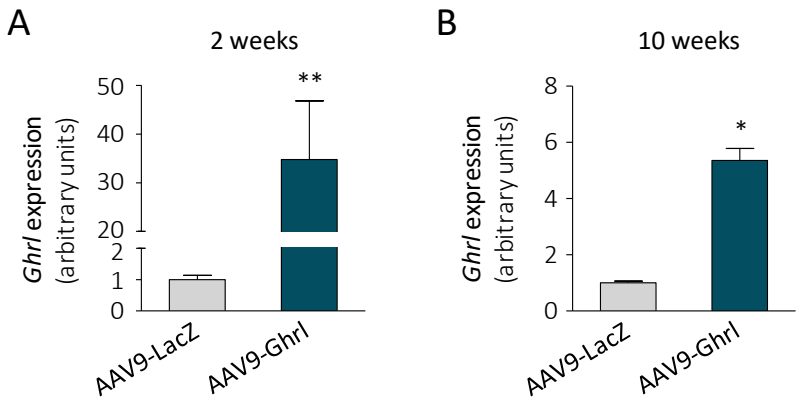

Supplementary Figure 7. AAV9-Ghrl injection induces ghrelin gene expression in skeletal muscle. *Relative ghrelin gene expression by real-time RT-PCR in mdx QUAD 2 weeks **(A)** and 10 weeks **(B)** after AVV9-Ghrl injection. Mean±s.e.m. **P<0.01, *P<0.05; N≥5.*

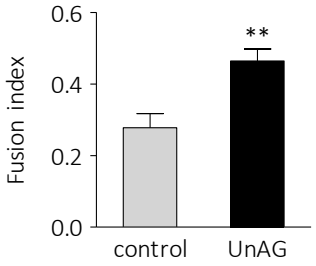

Supplementary Figure 8. UnAG treatment enhances fusion of primary myoblasts. *Fusion index calculated as MyHC+ cells with at least two nuclei above the total number of MyHC+ cells of primary myoblast-derived myotubes, treated or not with 100 nM UnAG in differentiation medium for 3 days. Mean±s.e.m. **P<0.01; n=3 independent experiments.*

CONCLUSION

The data herein presented demonstrate that UnAG acts on SCs enhancing their activation, differentiation, and self-renewal. SC self-renewal depends on either symmetric or asymmetric division of a subpopulation of non-committed progenitors. For instance, Wnt7a promotes SC self-renewal through induction of their symmetric division via a non-canonical, planar-cell-polarity pathway (Le Grand et al., 2009) and without affecting SC differentiation. On the contrary, UnAG promotes SC self-renewal enhancing at the same time their terminal differentiation, as shown by the increase of fusion index on cultured SCs (**Supplementary information, Figure S8**). This effect is likely a consequence of UnAG-induced increase on SC asymmetric division that simultaneously maintains the stem compartment of MyoD- SCs and expands the number of the committed MyoD+ myoblasts able to respond to the pro-differentiative activity of UnAG, in agreement with the effect observed on C2C12 (Filigheddu et al., 2007).

SC asymmetric division is sustained by the Par polarity complex that includes the atypical PKCλ/ι, which controls the asymmetric activation of p38 MAPK that, in turn, triggers MyoD protein expression, by inhibiting TTP-dependent MyoD mRNA decay (Hausburg et al., 2015; Troy et al., 2012). Phosphorylated p38 MAPK plays a key role in asymmetric division (Troy et al., 2012); indeed, loss or reduction of asymmetric segregation of phosphorylated p38 MAPK and its diffuse activation within the SC determines a strong decline of asymmetric division events and the consequent impairment of SC self-renewal ability in aged mice (Bernet et al., 2014).

UnAG promotes the asymmetric cosegregation of PKCλ/ι and of phospo-p38 MAPK in myofiber-associated SCs and enhances Par complex assembly. Consistently, UnAG induction of asymmetric division and self-renewal depends on PKCλ/ι-Par6 complex formation and p38 MAPK activity. These results suggest that UnAG stimulates SC asymmetric division and self-renewal by promoting the Par complex formation and, thus, the PKCλ/ι-mediated asymmetric activation of p38 MAPK.

The expansion of SCs through asymmetric division and the enhancement of their differentiation elicited by UnAG underline the ability of this hormone to enhance skeletal muscle regeneration (**Figure 7A and 7C**, (Ruozi et al., 2015; Togliatto et al., 2013)), consistently with the hypothesis that ghrelin induction in the

injured muscle contributes to the repair process. Although muscle damage induces ghrelin expression, whether this increase occurs within the muscle fibers or it is due to other cells (e.g. inflammatory infiltrate) remains to be elucidated.

The more efficient engraftment of donor SCs in Tg mice (**Figure 7F and 7G**) is consistent with a direct effect on SC functionality as well. However, the better engraftment may also depend on UnAG anti-inflammatory activity. Indeed, in skeletal muscle, UnAG inhibits TNF-α expression following either burn injury or high-fat diet (Gortan Cappellari et al., 2016; Sheriff et al., 2012). Furthermore, we cannot rule out that the increased engraftment of SCs in Tg muscle may partially be due to an anti-apoptotic effect of UnAG on transplanted SCs since UnAG inhibits apoptosis in both cardiomyocytes and myoblasts through activation of autophagy (Gortan Cappellari et al., 2016; Ruozi et al., 2015).

Altogether, these findings indicate that UnAG regulates multiple steps of muscle regeneration by stimulating asymmetric division-mediated SC self-renewal and by promoting terminal differentiation and fusion of proliferating myoblasts. The capacity of UnAG to induce SC self-renewal also in vivo translates in the ability to preserve the quiescent SC pool upon repeated cycles of injury/regeneration.

UnAG pro-regenerative effect on skeletal muscle and its activity on SCs may account for the less severe phenotype observed in dystrophic mice with high levels of circulating or local UnAG in mdx^{Tg+} or AAV-Ghrl-treated mdx mice, respectively. However, the anti-inflammatory, and, consequently, the anti-fibrotic activities of UnAG (Angelino et al., 2015; Prodam and Filigheddu, 2014) could be likewise relevant to explain the protection of tissue architecture and the amelioration of muscle performance. In addition, as defective basal autophagy contributes to the dystrophic phenotype (Pal et al., 2014; De Palma et al., 2012), UnAG-enhanced autophagy may likewise contribute to its protective activity in mdx mice.

In dystrophy, the exhaustion of the SC pool has been assumed to cause the failure of regeneration to keep up with muscle damage. However, in both human and mice SC pool exhaustion likely sets in only at late stages of the pathology as a consequence of defective SC self-renewal (Jiang et al., 2014). Furthermore, dystrophic muscles show an increased overall number of SCs, although, within this figure, the portion of quiescent SCs is reduced, reflecting an ongoing regeneration (Dumont et al., 2015; Jiang et al., 2014; Kottlors

and Kirschner, 2010). It is plausible that the defect in muscle regeneration of mdx mice resides at least in part in the defective asymmetric division of dystrophin-null SC that translates in an imbalance between SCs and committed myoblasts able to terminally differentiate and repair the damaged muscle (Chang et al., 2016; Dumont et al., 2015). The finding that UnAG, in dystrophin-null SCs, enhances their self-renewal and increases the number of committed myoblasts suggests that UnAG promotes SC asymmetric division by activating pathways that are independent of dystrophin expression. Thus, we can speculate that the increase in the absolute number of functional SCs triggered by UnAG in mdx mice may increase the number of committed progenitors, thus sustaining the better muscle regeneration and improved dystrophic phenotype observed in mdx^{Tg+} mice.

Altogether, these data suggest that increase in either circulating or local UnAG levels could delay the progression of the disease. A therapeutic approach would presumably involve the chronic administration of UnAG to dystrophic patients. Although the receptor through which UnAG exerts its biological activities remains elusive, UnAG has been recently used in clinical trials to assess its metabolic effects, and it was reported that the peptide was well-tolerated, and no serious adverse events occurred during the studies (Benso et al., 2012; Broglio et al., 2004; Kiewiet et al., 2009; Özcan et al., 2014; Tong et al., 2014); therefore, UnAG could be a realistic adjuvant treatment in the near future to help to preserve muscles of dystrophic patients.

FUTURE PERSPECTIVES

The data presented in this thesis demonstrate that UnAG increases Par complex formation and atypical PKC/active p38 MAPK localization during SC activation. However, how UnAG exerts these activities and, most importantly, the identity of the receptor that mediates its function are still to be elucidated. Several studies on different cell types, including myoblast, strongly suggest that the effects of UnAG are mediated by a Gαs protein-coupled receptor (GPCR) (**Figure 6**; Granata et al., 2007; Porporato et al., 2013; Reano et al., 2014). Uncovering the identity of this receptor will allow to define its localization in the SC, its role within the SC niche, and its expression profile in the heterogeneous quiescent SC population as well as during SC myogenic progression. Moreover, its identification could help to understand the intracellular signaling pathway underling Par complex formation and atypical PKC/P-p38 MAPK localization in the active SC.

The damage-induced upregulation of the ghrelin gene (*Ghrl*) in the skeletal muscle (**Supplementary Figure S1**) and the increased preproghrelin expression (Gurriarán-Rodríguez et al., 2012) suggest that UnAG could be physiologically implicated in the repair process of muscle. *In vivo* genetic ablation of the ghrelin gene and, possibly, of the UnAG receptor will finally define the contribution of UnAG in the physiological response to muscle injury. Moreover, the UnAG protective effects on skeletal muscle extend also to cardiac muscle. Indeed, after heart ischaemic damage, the *in vivo* functional selection of protective factors from a library of 100 different AAV-delivered cDNA, identified ghrelin as the unique protective factor against ischaemia-induced heart damage, exerting both structural and functional recovery (Ruozi et al., 2015). This suggests that UnAG could be a strong protective factor also for DMD-related cardiomyopathies, mainly dependent on cardiomyocyte necrosis and apoptosis. A relevant future perspective could imply the investigation of the cardioprotective effects of UnAG in dystrophic mice, by the assessment of structural and functional changes during the pathology progression. The UnAG effects on cardioprotection could synergize with its positive activities on muscle regeneration and SC functionality observed in dystrophic mice (reported in this thesis), and this could strengthening its therapeutic potential.

Moreover, the recent finding of a cell-autonomous defect in dystrophin-null SCs (Dumont et al., 2015) indicates that the functional recovery of SC asymmetric division and self-renewal exerted by UnAG could impact on the dystrophic phenotype, although the relevance of this effect on the structural and functional muscle recovery in *mdx* dystrophic mice remains to be elucidated. More in general, further studies are required to assess the involvement of SC intrinsic and extrinsic defects - and the consequent rescue possibility - in the progression of muscle wasting-related conditions, such as cancer cachexia, sarcopenia, and dystrophies.

ACKNOWLEDGMENTS

This study was supported by research grants from the Muscular Dystrophy Association (grant n. MDA294617 to Nicoletta Filigheddu and Andrea Graziani), Association Française contre les Myopathies (to Andrea Graziani) and Compagnia di San Paolo (to Andrea Graziani and Nicoletta Filigheddu).

I'm very grateful to my supervisor Andrea Graziani and my tutor Nicoletta Filigheddu for supporting me and this work during my PhD course.

I would like to thank the co-first author of this work Simone Reano, and the other member of my lab, co-authors of this work: Michele Ferrara, Valeria Malacarne, Hana Sustova, Emanuela Agosti, and Sara Clerici.

REFERENCES

Adkin, C.F., Meloni, P.L., Fletcher, S., Adams, A.M., Muntoni, F., Wong, B., and Wilton, S.D. (2012). Multiple exon skipping strategies to by-pass dystrophin mutations. Neuromuscul. Disord. 22, 297–305.

Almada, A.E., and Wagers, A.J. (2016). Molecular circuitry of stem cell fate in skeletal muscle regeneration, ageing and disease. Nat. Rev. Mol. Cell Biol. 17(5):267-79.

Almeida, C.F., Fernandes, S.A., Ribeiro Junior, A.F., Keith Okamoto, O., Vainzof, M., Almeida, C.F., Fernandes, S.A., Ribeiro Junior, A.F., Keith Okamoto, O., and Vainzof, M. (2016). Muscle Satellite Cells: Exploring the Basic Biology to Rule Them. Stem Cells Int. 2016:1078686.

Angelini, C. (2015). Prevention of cardiomyopathy in Duchenne muscular dystrophy. Lancet Neurol. 14, 127–128.

Angelini, C., and Peterle, E. (2012). Old and new therapeutic developments in steroid treatment in Duchenne muscular dystrophy. Acta Myol. 31, 9–15.

Angelini, C., Pegoraro, E., Turella, E., Intino, M.T., Pini, A., and Costa, C. (1994). Deflazacort in Duchenne dystrophy: Study of long-term effect. Muscle Nerve 17, 386–391.

Angelino, E., Reano, S., Ferrara, M., Agosti, E., Graziani, A., and Filigheddu, N. (2015). Antifibrotic Activity of Acylated and Unacylated Ghrelin. Int J Endocrinol. 2015:38568.

Baldanzi, G., Filigheddu, N., Cutrupi, S., Catapano, F., Bonissoni, S., Fubini, A., Malan, D., Baj, G., Granata, R., Broglio, F., et al. (2002). Ghrelin and des-acyl ghrelin inhibit cell death in cardiomyocytes and endothelial cells through ERK1/2 and PI 3-kinase/AKT. J. Cell Biol. 159, 1029–1037.

Benedetti, S., Hoshiya, H., and Tedesco, F.S. (2013). Repair or replace? Exploiting novel gene and cell therapy strategies for muscular dystrophies. FEBS J. 280, 4263–4280.

Benso, A., St-Pierre, D.H., Prodam, F., Gramaglia, E., Granata, R., Van Der Lely, A.J., Ghigo, E., and Broglio, F. (2012). Metabolic effects of overnight continuous infusion of unacylated ghrelin in humans. Eur. J. Endocrinol. 166, 911–916.

Bentzinger, C.F., Wang, Y.X., and Rudnicki, M. A. (2012). Building muscle: molecular regulation of myogenesis. Cold Spring Harb. Perspect. Biol. 4(2).

Bentzinger, C.F., Wang, Y.X., von Maltzahn, J., Soleimani, V.D., Yin, H., and Rudnicki, M. A. (2013). Fibronectin regulates Wnt7a signaling and satellite cell expansion. Cell Stem Cell. 12, 75–87.

Bernet, J.D., Doles, J.D., Hall, J.K., Kelly Tanaka, K., Carter, T. A., and Olwin, B.B. (2014). p38 MAPK signaling underlies a cell-autonomous loss of stem cell self-renewal in skeletal muscle of aged mice. Nat. Med. 20, 265–271.

Bertoni, C., Jarrahian, S., Wheeler, T.M., Li, Y., Olivares, E.C., Calos, M.P., and Rando, T. A. (2006). Enhancement of plasmid-mediated gene therapy for muscular dystrophy by directed plasmid integration. Proc. Natl. Acad. Sci. U. S. A. 103, 419–424.

Beytía, M. de los A., Vry, J., and Kirschner, J. (2012). Drug treatment of Duchenne muscular dystrophy: available evidence and perspectives. Acta Myol. Myopathies Cardiomyopathies Off. J. Mediterr. Soc. Myol. 31, 4–8.

Bischoff, R. (1975). Regeneration of single skeletal muscle fibers in vitro. Anat. Rec. 182, 215–235.

Bladen, C.L., Salgado, D., Monges, S., Foncuberta, M.E., Kekou, K., Kosma, K., Dawkins, H., Lamont, L., Roy, A.J., Chamova, T., et al. (2015). The TREAT-NMD DMD global database: Analysis of more than 7,000 duchenne muscular dystrophy mutations. Hum. Mutat. 36, 395–402.

Broglio, F., Gottero, C., Prodam, F., Gauna, C., Muccioli, G., Papotti, M., Abribat, T., Van Der Lely, A. J., and Ghigo, E. (2004). Non-acylated ghrelin counteracts the metabolic but not the neuroendocrine response to acylated ghrelin in humans. J. Clin. Endocrinol. Metab. 89, 3062–3065.

Buono, R., Vantaggiato, C., Pisa, V., Azzoni, E., Bassi, M.T., Brunelli, S., Sciorati, C., and Clementi, E. (2012). Nitric oxide sustains long-term skeletal muscle regeneration by regulating fate of satellite cells via signaling pathways requiring Vangl2 and cyclic GMP. Stem Cells. 30, 197–209.

Cairns, J. (1975). Mutation selection and the natural history of cancer. Nature. 255, cp1.

Chang, N.C., Chevalier, F.P., and Rudnicki, M.A. (2016). Satellite Cells in Muscular Dystrophy – Lost in Polarity. Trends Mol. Med. 22(6):479-96.

Chen, C., Asakawa, A., Fujimiya, M., Lee, S., and Inui, A. (2009). Ghrelin Gene Products and the Regulation of Food Intake and Gut Motility. 61, 430–481.

Chen, J., Splenser, A., Guillory, B., Luo, J., Mendiratta, M., Belinova, B., Halder, T., Zhang, G., Li, Y.-P., and Garcia, J.M. (2015). Ghrelin prevents tumour- and cisplatin-induced muscle wasting: characterization of multiple mechanisms involved. J. Cachexia. Sarcopenia Muscle. 6(2):132-43.

Cirak, S., Feng, L., Anthony, K., Arechavala-Gomeza, V., Torelli, S., Sewry, C., Morgan, J.E., and Muntoni, F. (2012). Restoration of the dystrophin-associated glycoprotein complex after exon skipping therapy in Duchenne muscular dystrophy. Mol. Ther. 20, 462–467.

Collins, C. A., Olsen, I., Zammit, P.S., Heslop, L., Petrie, A., Partridge, T. A., and Morgan, J.E. (2005). Stem cell function, self-renewal, and behavioral heterogeneity of cells from the adult muscle satellite cell niche. Cell. 122, 289–301.

Consalvi, S., Mozzetta, C., Bettica, P., Germani, M., Fiorentini, F., Del Bene, F., Rocchetti, M., Leoni, F., Monzani, V., Mascagni, P., et al. (2013). Preclinical studies in the mdx mouse model of duchenne muscular dystrophy with the histone deacetylase inhibitor givinostat. Mol. Med. 19, 79–87.

Cornelison, D.D.W., Filla, M.S., Stanley, H.M., Rapraeger, A.C., and Olwin, B.B. (2001). Syndecan-3 and syndecan-4 specifically mark skeletal muscle satellite cells and are implicated in satellite cell maintenance and muscle regeneration. Dev. Biol. 239, 79–94.

Cornelison, D.D.W., Wilcox-adelman, S. A., Goetinck, P.F., Rauvala, H., Rapraeger, A.C., and Olwin, B.B. (2004). Essential and separable roles for Syndecan-3 and Syndecan-4 in skeletal muscle development and regeneration Essential and separable roles for Syndecan-3 and Syndecan-4 in skeletal muscle development and regeneration. Genes Dev. 18, 2231–2236.

Cosgrove, B.D., Gilbert, P.M., Porpiglia, E., Mourkioti, F., Lee, S.P., Corbel, S.Y., Llewellyn, M.E., Delp, S.L., and Blau, H.M. (2014). Rejuvenation of the muscle stem cell population restores strength to injured aged muscles. Nat. Med. 20, 255–264.

Cossu, G., Previtali, S.C., Napolitano, S., Cicalese, M.P., Tedesco, F.S., Nicastro, F., Noviello, M., Roostalu, U., Natali Sora, M.G., Scarlato, M., et al. (2015). Intra-arterial transplantation of HLA-matched donor mesoangioblasts in Duchenne muscular dystrophy. EMBO Mol. Med. 7, 1513–1528.

Crist, C.G., Montarras, D., and Buckingham, M. (2012). Muscle Satellite Cells Are Primed for Myogenesis but Maintain Quiescence with Sequestration of Myf5 mRNA Targeted by microRNA-31 in mRNP Granules. Cell Stem Cell. 11, 118–126.

Cummings, D.E., Frayo, R.S., Marmonier, C., Aubert, R., and Chapelot, D. (2004). Plasma ghrelin levels and hunger scores in humans initiating meals voluntarily without time- and food-related cues. Am. J. Physiol. Endocrinol. Metab. 287, E297-304.

De Palma, C., Morisi, F., Cheli, S., Pambianco, S., Cappello, V., Vezzoli, M., Rovere-Querini, P., Moggio, M., Ripolone, M., Francolini, M., et al. (2012). Autophagy as a new therapeutic target in Duchenne muscular dystrophy. Cell Death Dis. 3, e418.

DeBoer, M.D. (2011). Ghrelin and cachexia: Will treatment with GHSR-1a agonists make a difference for patients suffering from chronic wasting syndromes? Mol. Cell. Endocrinol. 340, 97–105.

Dezaki, K., Sone, H., and Yada, T. (2008). Ghrelin is a physiological regulator of insulin release in pancreatic islets and glucose homeostasis. Pharmacol. Ther. 118, 239–249.

Dixit, V.D., Schaffer, E.M., Pyle, R.S., Collins, G.D., Sakthivel, S.K., Palaniappan, R., Lillard, J.W., and Taub, D.D. (2004). Ghrelin inhibits leptin- and activation-induced proinflammatory cytokine expression by human monocytes and T cells. J. Clin. Invest. 114, 57–66.

Dowling, J.J. (2016). Eteplirsen therapy for Duchenne muscular dystrophy: skipping to the front of the line. Nat. Rev. Neurol. 12(12):675-676.

Dumont, N.A., and Rudnicki, M.A. (2016). Targeting muscle stem cell intrinsic defects to treat Duchenne muscular dystrophy. Npj Regen. Med. 1, 16006.

Dumont, N.A., Wang, Y.X., von Maltzahn, J., Pasut, A., Bentzinger, C.F., Brun, C.E., and Rudnicki, M.A. (2015). Dystrophin expression in muscle stem cells regulates their polarity and asymmetric division. Nat. Med. 21(12):1455-63.

Evans, W.J., and Campbell, W.W. (1993). Sarcopenia and Age-Related Changes in Body Composition and Functional Capacity. J. Nutr. 123, 465–468.

Fenichel, G.M., Florence, J.M., Pestronk, A., Mendell, J.R., Moxley 3rd, R.T., Griggs, R.C., Brooke, M.H., Miller, J.P., Robison, J., King, W., et al. (1991). Long-term benefit from prednisone therapy in Duchenne muscular dystrophy. Neurology. 41, 1874–1877.

Filigheddu, N., Gnocchi, V.F., Coscia, M., Cappelli, M., Porporato, P.E., Taulli, R., Traini, S., Baldanzi, G., Chianale, F., Cutrupi, S., et al. (2007). Ghrelin and Des-Acyl Ghrelin Promote Differentiation and Fusion of C2C12 Skeletal Muscle Cells. Mol Biol. 18, 986–994.

Frontera, W.R., and Ochala, J. (2015). Skeletal muscle: a brief review of structure and function. Calcif. Tissue Int. 96, 183–195.

Garcia, J.M., Jatoi, A., and Del Fabbro, E. (2013). The Potential of Ghrelin in Cancer Anorexia – Cachexia. European Oncology & Haematology. 9(2):77–83.

Gauna, C., van de Zande, B., van Kerkwijk, A., Themmen, A.P.N., van der Lely, A.J., and Delhanty, P.J.D. (2007). Unacylated ghrelin is not a functional antagonist but a full agonist of the type 1a growth hormone secretagogue receptor (GHS-R). Mol. Cell. Endocrinol. 274, 30–34.

Gortan Cappellari, G., Zanetti, M., Semolic, A., Vinci, P., Ruozi, G., Falcione, A., Filigheddu, N., Guarnieri, G., Graziani, A., Giacca, M., et al. (2016). Unacylated ghrelin reduces skeletal muscle reactive oxygen species generation and inflammation and prevents high-fat diet induced hyperglycemia and whole-body insulin resistance in rodents. Diabetes. 65(4):874-86.

Goulas, S., Conder, R., and Knoblich, J.A. (2012). The par complex and integrins direct asymmetric cell division in adult intestinal stem cells. Cell Stem Cell. 11, 529–540.

Granata, R., Settanni, F., Biancone, L., Trovato, L., Nano, R., Bertuzzi, F., Destefanis, S., Annunziata, M., Martinetti, M., Catapano, F., et al. (2007). Acylated and unacylated ghrelin promote proliferation and inhibit

apoptosis of pancreatic beta-cells and human islets: involvement of 3',5'-cyclic adenosine monophosphate/protein kinase A, extracellular signal-regulated kinase 1/2, and phosphatidyl inosit. Endocrinology. 148, 512–529.

Grounds, M.D. (1998). Age-associated changes in the response of skeletal muscle cells to exercise and regeneration. Ann. N Y Acad. Sci. 854:78-91.

Grounds, M.D., Radley, H.G., Lynch, G.S., Nagaraju, K., and De Luca, A. (2008). Towards developing standard operating procedures for pre-clinical testing in the mdx mouse model of Duchenne muscular dystrophy. Neurobiol. Dis. 31, 1–19.

Guiraud, S., Chen, H., Burns, D.T., and Davies, K.E. (2015). Advances in genetic therapeutic strategies for Duchenne muscular dystrophy. Exp. Physiol. 100(12):1458-67.

Gumerson, J.D., and Michele, D.E. (2011). The dystrophin-glycoprotein complex in the prevention of muscle damage. J. Biomed. Biotechnol. 2011:210797.

Gurriarán-Rodríguez, U., Santos-Zas, I., Al-Massadi, O., Mosteiro, C.S., Beiroa, D., Nogueiras, R., Crujeiras, A.B., Seoane, L.M., Señarís, J., García-Caballero, T., et al. (2012). The obestatin/GPR39 system is up-regulated by muscle injury and functions as an autocrine regenerative system. J. Biol. Chem. 287, 38379–38389.

Gussoni, E., Soneoka, Y., Strickland, C.D., Buzney, E.A., Khan, M.K., Flint, A.F., Kunkel, L.M., and Mulligan, R.C. (1999). Dystrophin expression in the mdx mouse restored by stem cell transplantation. Nature. 401, 390–394.

Gutierrez, J. A., Solenberg, P.J., Perkins, D.R., Willency, J. A., Knierman, M.D., Jin, Z., Witcher, D.R., Luo, S., Onyia, J.E., and Hale, J.E. (2008). Ghrelin octanoylation mediated by an orphan lipid transferase. Proc. Natl. Acad. Sci. U. S. A. 105, 6320–6325.

Hataya, Y., Akamizu, T., Hosoda, H., Kanamoto, N., Moriyama, K., Kangawa, K., Takaya, K., and Nakao, K. (2003). Alterations of plasma ghrelin levels in rats with lipopolysaccharide-induced wasting syndrome and effects of ghrelin treatment on the syndrome. Endocrinology. 144, 5365–5371.

Hausburg, M.A., Doles, J.D., Clement, S.L., Cadwallader, A.B., Hall, M.N., Blackshear, P.J., Lykke-Andersen, J., and Olwin, B.B. (2015). Post-transcriptional regulation of satellite cell quiescence by TTP-mediated mRNA decay. Elife. 4:e03390.

Hoffman, E.P., Brown, R.H., and Kunkel, L.M. (1987). Dystrophin: The protein product of the duchenne muscular dystrophy locus. Cell. 51, 919–928.

Ibraghimov-Beskrovnaya, O., Ervasti, J.M., Leveille, C.J., Slaughter, C.A., Sernett, S.W., and Campbell, K.P. (1992). Primary structure of dystrophin-associated glycoproteins linking dystrophin to the extracellular matrix. Nature. 355, 696–702.

Inaba, M., and Yamashita, Y.M. (2012). Asymmetric stem cell division: Precision for robustness. Cell Stem Cell. 11, 461–469.

Jensen, J., Rustad, P.I., Kolnes, A.J., and Lai, Y.C. (2011). The role of skeletal muscle glycogen breakdown for regulation of insulin sensitivity by exercise. Front. Physiol. 2:112.

Jiang, C., Wen, Y., Kuroda, K., Hannon, K., Rudnicki, M. A., and Kuang, S. (2014). Notch signaling deficiency underlies age-dependent depletion of satellite cells in muscular dystrophy. Dis. Model. Mech. 7(8):997-1004.

Joe, A.W., Yi, L., Natarajan, A., Le Grand, F., So, L., Wang, J., Rudnicki, M.A., and Rossi, F.M. (2010). Muscle injury activates resident fibro/adipogenic progenitors that facilitate myogenesis. Nat Cell Biol. 12, 153–163.

Jones, N.C., Tyner, K.J., Nibarger, L., Stanley, H.M., Cornelison, D.D.W., Fedorov, Y. V, and Olwin, B.B. (2005). The p38alpha/beta MAPK functions as a molecular switch to activate the quiescent satellite cell. J. Cell Biol. 169, 105–116.

Karakelides, H., and Nair, K.S. (2005). Sarcopenia of Aging and Its Metabolic Impact. Curr. Top. Dev. Biol. 68, 123–148.

Karpowicz, P., Morshead, C., Kam, A., Jervis, E., Ramuns, J., Cheng, V., and Van Der Kooy, D. (2005). Support for the immortal strand hypothesis: Neural stem cells partition DNA asymmetrically in vitro. J. Cell Biol. 170, 721–732.

Kharraz, Y., Guerra, J., Pessina, P., Serrano, A.L., and Muñoz-Cánoves P. (2014). Understanding the process of fibrosis in duchenne muscular dystrophy. Biomed Res. Int. 2014:965631.

Kiewiet, R.M., Van Aken, M.O., Van Der Weerd, K., Uitterlinden, P., Themmen, A.P.N., Hofland, L.J., De Rijke, Y.B., Delhanty, P.J.D., Ghigo, E., Abribat, T., et al. (2009). Effects of acute administration of acylated and unacylated ghrelin on glucose and insulin concentrations in morbidly obese subjects without overt diabetes. Eur. J. Endocrinol. 161, 567–573.

Knoblich, J. A. (2010). Asymmetric cell division: recent developments and their implications for tumour biology. Nat. Rev. Mol. Cell Biol. 11, 849–860.

Kojima, M., Hosoda, H., Date, Y., Nakazato, M., Matsuo, H., and Kangawa, K. (1999). Ghrelin is a growth-hormone-releasing acylated peptide from stomach. Nature. 402, 656–660.

Kole, R., and Leppert, B.J. (2012). Targeting mRNA splicing as a potential treatment for Duchenne muscular dystrophy. Discov. Med. 14, 59–69.

Konieczny, P., Swiderski, K., and Chamberlain, J.S. (2013). Gene and cell-mediated therapies for muscular dystrophy. Muscle Nerve. 47, 649–663.

Konigsberg, U.R., Lipton, B.H., and Konigsberg, I.R. (1975). The regenerative response of single mature muscle fibers isolated in vitro. Dev. Biol. 45, 260–275.

Kottlors, M., and Kirschner, J. (2010). Elevated satellite cell number in Duchenne muscular dystrophy. Cell Tissue Res. 340, 541–548.

Kuang, S., Gillespie, M. A., and Rudnicki, M. A. (2008). Niche regulation of muscle satellite cell self-renewal and differentiation. Cell Stem Cell. 2, 22–31.

Kuang, S., Kuroda, K., Le Grand, F., and Rudnicki, M. A. (2007). Asymmetric self-renewal and commitment of satellite stem cells in muscle. Cell. 129, 999–1010.

Le Grand, F., Jones, A.E., Seale, V., Scimè, A., and Rudnicki, M. A. (2009). Wnt7a activates the planar cell polarity pathway to drive the symmetric expansion of satellite stem cells. Cell Stem Cell. 4, 535–547.

Lepper, C., Partridge, T. A., and Fan, C.M. (2011). An absolute requirement for Pax7-positive satellite cells in acute injury-induced skeletal muscle regeneration. Development. 138, 3639–3646.

Li, W.G., Gavrila, D., Liu, X., Wang, L., Gunnlaugsson, S., Stoll, L.L., McCormick, M.L., Sigmund, C.D., Tang, C., and Weintraub, N.L. (2004). Ghrelin Inhibits Proinflammatory Responses and Nuclear Factor-kB Activation in Human Endothelial Cells. Circulation. 109, 2221–2226.

Lin, L., Lee, J.H., Buras, E.D., Yu, K., Wang, R., Smith, C.W., Wu, H., Sheikh-Hamad, D., and Sun, Y. (2016). Ghrelin receptor regulates adipose tissue inflammation in aging. Aging (Albany. NY). 8(1):178-91.

Liu, F., Nishikawa, M., Clemens, P.R., and Huang, L. (2001). Transfer of full-length Dmd to the diaphragm muscle of Dmd(mdx/mdx) mice through systemic administration of plasmid DNA. Mol. Ther. 4, 45–51.

Liu, N., Garry, G.A., Li, S., Bezprozvannaya, S., Sanchez-ortiz, E., Chen, B., Shelton, J.M., Jaichander, P., Bassel-duby, R., and Olson, E.N. (2017). A Twist2-dependent progenitor cell contributes to adult skeletal muscle. Nat. Cell Biol. 19(3):202-213.

Liu, Z., Wang, W., Li, Q., Tang, M., Li, J., Wu, W., Wan, Y., and Wang, Z. (2015). Growth hormone secretagogue receptor is important in the development of experimental colitis. Cell Biosci. 5:12.

Longo, K. A., Charoenthongtrakul, S., Giuliana, D.J., Govek, E.K., McDonagh, T., Qi, Y., DiStefano, P.S., and Geddes, B.J. (2008). Improved insulin sensitivity and metabolic flexibility in ghrelin receptor knockout mice. Regul. Pept. 150, 55–61.

Ma, X., Lin, L., Yue, J., Pradhan, G., Qin, G., Minze, L.J., Wu, H., Sheikh-Hamad, D., Smith, C.W., and Sun, Y. (2013). Ghrelin receptor regulates HFCS-induced adipose inflammation and insulin resistance. Nutr. Diabetes. 3, e99.

Maffioletti, S.M., Noviello, M., English, K., and Tedesco, F.S. (2014). Review Article Stem Cell Transplantation for Muscular Dystrophy : The Challenge of Immune Response. Biomed Res. Int. 2014:964010.

Mauro, A. (1961). Satellite cell of skeletal muscle fibers. J. Biophys. Biochem. Cytol. 9, 493–495.

McKinnell, I.W., Ishibashi, J., Le Grand, F., Punch, V.G.J., Addicks, G.C., Greenblatt, J.F., Dilworth, F.J., and Rudnicki, M.A. (2008). Pax7 activates myogenic genes by recruitment of a histone methyltransferase complex. Nat. Cell Biol. 10, 77–84.

Mendell, J.R., Campbell, K., Rodino-Klapac, L., Sahenk, Z., Shilling, C., Lewis, S., Bowles, D., Gray, S., Li, C., Galloway, G., et al. (2010). Dystrophin Immunity in Duchenne's Muscular Dystrophy. N. Engl. J. Med. 363, 1429–1437.

Mendell, J.R., Kissel, J.T., Amato, A.A., King, W., Signore, L., Prior, T.W., Sahenk, Z., Benson, S., McAndrew, P.E., and Rice, R. (1995). Myoblast transfer in the treatment of Duchenne's muscular dystrophy. N. Engl. J. Med. 333, 832–838.

Mercuri, E., and Muntoni, F. (2013). Muscular dystrophies. Lancet. 381, 845–860.

Molnar, M.J., Gilbert, R., Lu, Y., Liu, A.B., Guo, A., Larochelle, N., Lochmuller, H., Petrof, B.J., Nalbantoglu, J., and Karpati, G. (2004). Factors influencing the efficacy, longevity, and safety of electroporation-assisted plasmid-based gene transfer into mouse muscles. Mol. Ther. 10, 447–455.

Monteleone, P., Martiadis, V., Fabrazzo, M., Serritella, C., and Maj, M. (2003). Ghrelin and leptin responses to food ingestion in bulimia nervosa: implications for binge-eating and compensatory behaviours. Psychol. Med. 33, 1387–1394.

Moreno, M., Chaves, J.F., Sancho-Bru, P., Ramalho, F., Ramalho, L.N., Mansego, M.L., Ivorra, C., Dominguez, M., Conde, L., Milĺan, C., et al. (2010). Ghrelin attenuates hepatocellular injury and liver fibrogenesis in rodents and influences fibrosis progression in humans. Hepatology. 51, 974–985.

Müller, T.D., Nogueiras, R., Andermann, M.L., Andrews, Z.B., Anker, S.D., Argente, J., Batterham, R.L., Benoit, S.C., Bowers, C.Y., Broglio, F., et al. (2015). Ghrelin. Mol. Metab. 4, 437–460.

Nishi, Y., Yoh, J., Hiejima, H., and Kojima, M. (2011). Structures and molecular forms of the ghrelin-family peptides. Peptides. 32, 2175–2182.

Olguin, H.C., and Olwin, B.B. (2004). Pax-7 up-regulation inhibits myogenesis and cell cycle progression in satellite cells: a potential mechanism for self-renewal. Dev. Biol. 275, 375–388.

Özcan, B., Neggers, S.J.C.M.M., Miller, A.R., Yang, H.C., Lucaites, V., Abribat, T., Allas, S., Huisman, M., Visser, J., Themmen, A.N., et al. (2014). Does des-acyl ghrelin improve glycemic control in obese diabetic subjects by decreasing acylated ghrelin levels? Eur. J. Endocrinol. 170, 799–807.

Pal, R., Palmieri, M., Loehr, J. A., Li, S., Abo-Zahrah, R., Monroe, T.O., Thakur, P.B., Sardiello, M., and Rodney, G.G. (2014). Src-dependent impairment of autophagy by oxidative stress in a mouse model of Duchenne muscular dystrophy. Nat. Commun. 5, 4425.

Palacios, D., and Puri, P.L. (2006). The epigenetic network regulating muscle development and regeneration. J. Cell. Physiol. 207, 1–11.

Partridge, T. (1978). Evidence of fusion between host and donor myoblasts in skeletal muscle grafts. Nature. 273, 306–308.

Partridge, T.A., Morgan, J.E., Coulton, G.R., Hoffman, E.P., and Kunkel, L.M. (1989). Conversion of mdx myofibres from dystrophin-negative to -positive by injection of normal myoblasts. Nature. 337, 176–179.

Plant, P.J., Fawcett, J.P., Lin, D.C.C., Holdorf, A.D., Binns, K., Kulkarni, S., and Pawson, T. (2003). A polarity complex of mPar-6 and atypical PKC binds, phosphorylates and regulates mammalian Lgl. Nat. Cell Biol. 5, 301–308.

Porporato, P.E., Filigheddu, N., Reano, S., Ferrara, M., Angelino, E., Gnocchi, V.F., Prodam, F., Ronchi, G., Fagoonee, S., Fornaro, M., et al. (2013). Acylated and unacylated ghrelin impair skeletal muscle atrophy in mice. J. Clin. Invest. 123(2):611-22.

Price, F.D., Kuroda, K., and Rudnicki, M.A. (2007). Stem cell based therapies to treat muscular dystrophy. Biochim. Biophys. Acta - Mol. Basis Dis. 1772, 272–283.

Prodam, F., and Filigheddu, N. (2014). Ghrelin gene products in acute and chronic inflammation. Arch. Immunol. Ther. Exp. (Warsz). 62, 369–384.

Qi, Y., Longo, K. a, Giuliana, D.J., Gagne, S., McDonagh, T., Govek, E., Nolan, A., Zou, C., Morgan, K., Hixon, J., et al. (2011). Characterization of the insulin sensitivity of ghrelin receptor KO mice using glycemic clamps. BMC Physiol. 11:1.

Rahimov, F., and Kunkel, L.M. (2013). The cell biology of disease: cellular and molecular mechanisms underlying muscular dystrophy. J. Cell Biol. 201, 499–510.

Rapraeger, A.C. (2000). Syndecan-regulated Receptor Signaling. 149, 995–997.

Raymackers, J.M., Debaix, H., Colson-Van Schoor, M., De Backer, F., Tajeddine, N., Schwaller, B., Gailly, P., and Gillis, J.M. (2003). Consequence of parvalbumin deficiency in the mdx mouse: Histological, biochemical and mechanical phenotype of a new double mutant. Neuromuscul. Disord. 13, 376–387.

Reano, S., Graziani, A., and Filigheddu, N. (2014). Acylated and unacylated ghrelin administration to blunt muscle wasting. Curr. Opin. Clin. Nutr. Metab. Care. 17, 236–240.

Relaix, F., and Zammit, P.S. (2012). Satellite cells are essential for skeletal muscle regeneration: the cell on the edge returns centre stage. Development. 139, 2845–2856.

Rocheteau, P., Gayraud-Morel, B., Siegl-Cachedenier, I., Blasco, M. A., and Tajbakhsh, S. (2012). A subpopulation of adult skeletal muscle stem cells retains all template DNA strands after cell division. Cell. 148, 112–125.

Ruozi, G., Bortolotti, F., Falcione, A., Dal Ferro, M., Ukovich, L., Macedo, A., Zentilin, L., Filigheddu, N., Cappellari, G.G., Baldini, G., et al. (2015). AAV-mediated in vivo functional selection of tissue-protective factors against ischaemia. Nat. Commun. 6, 7388.

Rybakova, I.N., Patel, J.R., and Ervasti, J.M. (2000). The dystrophin complex forms a mechanically strong link between the sarcolemma and costameric actin. J. Cell Biol. 150, 1209–1214.

Sacco, A., and Puri, P.L. (2015). Regulation of Muscle Satellite Cell Function in Tissue Homeostasis and Aging. Cell Stem Cell. 16, 585–587.

Sacco, A., Doyonnas, R., Kraft, P., Vitorovic, S., and Blau, H.M. (2008). Self-renewal and expansion of single transplanted muscle stem cells. Nature. 456, 502–506.

Sampaolesi, M., Blot, S., D'Antona, G., Granger, N., Tonlorenzi, R., Innocenzi, A., Mognol, P., Thibaud, J.-L., Galvez, B.G., Barthélémy, I., et al. (2006). Mesoangioblast stem cells ameliorate muscle function in dystrophic dogs. Nature. 444, 574–579.

Sangiao-Alvarellos, S., and Cordido, F. (2010). Effect of ghrelin on glucose-insulin homeostasis: therapeutic implications. Int. J. Pept. pii: 234709.

Seale, P., Sabourin, L.A., Girgis-Gabardo, A., Mansouri, A., Gruss, P., and Rudnicki, M.A. (2000). Pax7 is required for the specification of myogenic satellite cells. Cell. 102, 777–786.

Shea, K.L., Xiang, W., LaPorta, V.S., Licht, J.D., Keller, C., Basson, M.A., and Brack, A.S. (2010). Sprouty1 regulates reversible quiescence of a self-renewing adult muscle stem cell pool during regeneration. Cell Stem Cell. 6, 117–129.

Sheriff, S., Kadeer, N., Joshi, R., Friend, L.A., James, J.H., and Balasubramaniam, A. (2012). Des-acyl ghrelin exhibits pro-anabolic and anti-catabolic effects on C2C12 myotubes exposed to cytokines and reduces burn-induced muscle proteolysis in rats. Mol. Cell. Endocrinol. 351, 286–295.

Shinin, V., Gayraud-Morel, B., Gomès, D., and Tajbakhsh, S. (2006). Asymmetric division and cosegregation of template DNA strands in adult muscle satellite cells. Nat. Cell Biol. 8, 677–687.

Singh, K., and Dilworth, F.J. (2013). Differential modulation of cell cycle progression distinguishes members of the myogenic regulatory factor family of transcription factors. FEBS J. 280, 3991–4003.

Skuk, D. (2013). Cell Transplantation and "Stem Cell Therapy" in the Treatment of Myopathies: Many Promises in Mice, Few Realities in Humans. ISRN Transplant. 2013, 1–25.

Sousa-Victor, P., Gutarra, S., García-Prat, L., Rodriguez-Ubreva, J., Ortet, L., Ruiz-Bonilla, V., Jardí, M., Ballestar, E., González, S., Serrano, A.L., et al. (2014). Geriatric muscle stem cells switch reversible quiescence into senescence. Nature. 506, 316–321.

Spuler, S., and Engel, A.G. (1998). Unexpected sarcolemmal complement membrane attack complex deposits on nonnecrotic muscle fibers in muscular dystrophies. Neurology. 50, 41–46.

Stallings-Mann, M., Jamieson, L., Regala, R.P., Weems, C., Murray, N.R., and Fields, A.P. (2006). A Novel Small-Molecule Inhibitor of Protein Kinase Cι Blocks Transformed Growth of Non–Small-Cell Lung Cancer Cells. Cancer Res. 66, 1767–1774.

Straub, V., Balabanov, P., Bushby, K., Ensini, M., Goemans, N., De Luca, A., Pereda, A., Hemmings, R., Campion, G., Kaye, E., et al. (2016). Stakeholder cooperation to overcome challenges in orphan medicine development: The example of Duchenne muscular dystrophy. Lancet Neurol. 15, 882–890.

Sun, Y., Butte, N.F., Garcia, J.M., and Smith, R.G. (2008). Characterization of adult ghrelin and ghrelin receptor knockout mice under positive and negative energy balance. Endocrinology. 149, 843–850.

Tam BT1, Pei XM1, Yung BY1, Yip SP1, Chan LW1, Wong CS1, Siu PM2. (2015). Unacylated ghrelin restores insulin and autophagic signaling in skeletal muscle of diabetic mice. Pflugers Arch. 467(12):2555-69.

Tierney, M.T., and Sacco, A. (2016). Satellite Cell Heterogeneity in Skeletal Muscle Homeostasis. Trends Cell Biol. 26, 434–444.

Togliatto, G., Trombetta, A., Dentelli, P., Cotogni, P., Rosso, A., Tschöp, M.H., Granata, R., Ghigo, E., and Brizzi, M.F. (2013). Unacylated ghrelin promotes skeletal muscle regeneration following hindlimb ischemia via SOD-2-mediated miR-221/222 expression. J. Am. Heart Assoc. 2, e000376.

Tong, J., Davis, H.W., Summer, S., Benoit, S.C., Haque, A., Bidlingmaier, M., Tschöp, M.H., and D'Alessio, D. (2014). Acute administration of unacylated ghrelin has no effect on basal or stimulated insulin secretion in healthy humans. Diabetes. 63, 2309–2319.

Tong, J., Prigeon, R.L., Davis, H.W., Bidlingmaier, M., Kahn, S.E., Cummings, D.E., Tschöp, M.H., and D'Alessio, D. (2010). Ghrelin suppresses glucose-stimulated insulin secretion and deteriorates glucose tolerance in healthy humans. Diabetes. 59, 2145–2151.

Troy, A., Cadwallader, A.B., Fedorov, Y., Tyner, K., Tanaka, K.K., and Olwin, B.B. (2012). Coordination of satellite cell activation and self-renewal by Par-complex-dependent asymmetric activation of p38α/β MAPK. Cell Stem Cell. 11, 541–553.

Tschöp, M.H., Smiley, D.L., and Heiman, M.L. (2000). Ghrelin induces adiposity in rodents. Nature. 407, 908–913.

van Putten, M., de Winter, C., van Roon-Mom, W., van Ommen, G.J., 't Hoen, P.A.C., and Aartsma-Rus, A. (2010). A 3 months mild functional test regime does not affect disease parameters in young mdx mice. Neuromuscul. Disord. 20, 273–280.

Vestergaard, P., Glerup, H., Steffensen, B.F., Rejnmark, L., Rahbek, J., and Moseklide, L. (2001). Fracture risk in patients with muscular dystrophy and spinal muscular atrophy. J. Rehabil. Med. 33, 150–155.

Wallace, G.Q., and McNally, E.M. (2009). Mechanisms of muscle degeneration, regeneration, and repair in the muscular dystrophies. Annu. Rev. Physiol. 71, 37–57.

Wang, Y.X., Dumont, N. A., and Rudnicki, M. A. (2014). Muscle stem cells at a glance. J. Cell Sci. 127, 4543–4548.

Wang Y.X. and Rudnicki M.A. (2011). Satellite cells, the engines of muscle repair. Nat. Rev. Mol. Cell Biol. 13(2):127-33.

Waseem, T., Duxbury, M., Ito, H., Ashley, S.W., and Robinson, M.K. (2008). Exogenous ghrelin modulates release of pro-inflammatory and anti-inflammatory cytokines in LPS-stimulated macrophages through distinct signaling pathways. Surgery. 143, 334–342.

Wen, Y., Bi, P., Liu, W., Asakura, A., Keller, C., and Kuang, S. (2012). Constitutive Notch activation upregulates Pax7 and promotes the self-renewal of skeletal muscle satellite cells. Mol. Cell. Biol. 32, 2300–2311.

Wilton, S.D., Dye, D.E., Blechynden, L.M., and Laing, N.G. (1997). Revertant fibres: A possible genetic therapy for Duchenne muscular dystrophy? Neuromuscul. Disord. 7, 329–335.

Wirtz-Peitz, F., Nishimura, T., and Knoblich, J.A. (2008). Linking Cell Cycle to Asymmetric Division: Aurora-A Phosphorylates the Par Complex to Regulate Numb Localization. Cell. 135, 161–173.

Wolfe, R.R. (2006). The underappreciated role of muscle in health and disease. Am. J. Clin. Nutr. 84(3):475-82.

Wren, A.M., Small, C.J., Abbott, C.R., Dhillo, W.S., Seal, L.J., Cohen, M.A., Batterham, R.L., Taheri, S., Stanley, S.A., Ghatei, M.A., et al. (2001). Ghrelin Causes Hyperphagia and Obesity in Rats. Diabetes. 50, 2540–2547.

Yablonka-Reuveni, Z., and Rivera, A.J. (1994). Temporal expression of regulatory and structural muscle proteins during myogenesis of satellite cells on isolated adult rat fibers. Dev. Biol. 164, 588–603.

Yang, J., Brown, M.S., Liang, G., Grishin, N. V., and Goldstein, J.L. (2008). Identification of the Acyltransferase that Octanoylates Ghrelin, an Appetite-Stimulating Peptide Hormone. Cell. 132, 387–396.

Yin, H., Price, F., and Rudnicki, M. A. (2013). Satellite cells and the muscle stem cell niche. Physiol. Rev. 93, 23–67.

Zammit, P.S., Golding, J.P., Nagata, Y., Hudon, V., Partridge, T. A., and Beauchamp, J.R. (2004). Muscle satellite cells adopt divergent fates: a mechanism for self-renewal? J. Cell Biol. 166, 347–357.

Hindawi Publishing Corporation
International Journal of Endocrinology
Volume 2015, Article ID 385682, 9 pages
http://dx.doi.org/10.1155/2015/385682

Review Article

Antifibrotic Activity of Acylated and Unacylated Ghrelin

Elia Angelino, Simone Reano, Michele Ferrara, Emanuela Agosti, Andrea Graziani, and Nicoletta Filigheddu

Department of Translational Medicine, University of Piemonte Orientale, Via Solaroli 17, 28100 Novara, Italy

Correspondence should be addressed to Nicoletta Filigheddu; nicoletta.filigheddu@med.uniupo.it

Received 16 December 2014; Accepted 1 April 2015

Academic Editor: Ludwik K. Malendowicz

Fibrosis can affect almost all tissues and organs, it often represents the terminal stage of chronic diseases, and it is regarded as a major health issue for which efficient therapies are needed. Tissue injury, by inducing necrosis/apoptosis, triggers inflammatory response that, in turn, promotes fibroblast activation and pathological deposition of extracellular matrix. Acylated and unacylated ghrelin are the main products of the ghrelin gene. The acylated form, through its receptor GHSR-1a, stimulates appetite and growth hormone (GH) release. Although unacylated ghrelin does not bind or activate GHSR-1a, it shares with the acylated form several biological activities. Ghrelin peptides exhibit anti-inflammatory, antioxidative, and antiapoptotic activities, suggesting that they might represent an efficient approach to prevent or reduce fibrosis. The aim of this review is to summarize the available evidence regarding the effects of acylated and unacylated ghrelin on different pathologies and experimental models in which fibrosis is a predominant characteristic.

1. Introduction

Repair of damaged tissues is a complex physiological process that results in the deposition of extracellular matrix (ECM) components by resident fibroblasts [1]. Although the deposition of ECM proteins is normally a transient event, repeated tissue injuries in chronic pathologies or dysregulation of this process can lead to fibrosis and, eventually, to organ dysfunction [2]. Fibrosis can affect almost all tissues and organs, including heart, liver, kidney, lungs, and skin, therefore representing a major health issue for which efficient therapies are needed.

Regardless of the specific fibrotic disease and organs affected, the mechanisms involved in the progression of this pathology are very similar. Indeed, damaged tissue repair can be recapitulated in four overlapping phases, hemostasis, inflammation, proliferation, and remodeling in which several cell types, closely interconnected to each other, play an important role [3]. During the phases of hemostasis and inflammation, platelets secrete cytokines, including platelet-derived growth factor (PDGF) and transforming growth factor-β (TGF-β) that, in turn, recruit macrophages, neutrophils, and natural-killer cells to the site of injury. These cells, besides removing dead cells, debris, and pathogens, release cytokines that trigger activation and proliferation of resident fibroblasts, thus affecting ECM production [4]. For example, macrophages release TGF-β1 that controls a wide spectrum of activities, such as promoting fibroblast differentiation into active myofibroblasts, inducing ECM protein expression [5, 6], and repressing the expression of matrix metalloproteinases (MMPs), key proteins able to degrade several ECM components [7]. In addition, macrophages release tumor necrosis factor-α (TNF-α) and interleukin-1β (IL-1β) that promote fibroblast activation and fibrotic tissue deposition [2]. Tissue damage and inflammation increase reactive oxygen species (ROS) production, which, in turn, contributes to fibrosis, enhancing the secretion of fibrogenic factors [8].

Acylated and unacylated ghrelin are circulating peptide hormones encoded by the ghrelin gene which are mainly released from the stomach during fasting [9]. The 117-amino acid preproghrelin undergoes proteolytic cleavages leading to the mature ghrelin peptides and to another biological active peptide named obestatin [10]. The acylated form, through high affinity binding to the growth hormone secretagogue receptor type 1a (GHSR-1a), induces GH release and promotes food intake, adiposity, and positive energy balance [11–13]. Alongside its role in feeding and energy homeostasis,

Table 1: Changes of acylated ghrelin, unacylated ghrelin, and obestatin blood concentrations in human pathological conditions leading to organ fibrosis.

Pathological condition	Acylated ghrelin	Unacylated ghrelin	Obestatin	Notes	Reference
Chronic heart failure (CHF)	↑	nd	nd		[46]
	↓	nd	nd	Acylated ghrelin levels positively correlate with favorable prognosis	[47]
Chronic hepatitis C	↓	nd	nd	Acylated ghrelin levels negatively correlate with fibrosis severity	[48]
Alcoholic hepatitis	↓	nd	nd	Acylated ghrelin levels negatively correlate with fibrosis severity	[48]
Nonalcoholic fatty liver disease (NAFLD)	nd	nd	=		[90]
Nonalcoholic steatohepatitis (NASH)	=	↑	=	NASH versus non-NASH (among NAFLD patients)	[50]
	↑	=	↑	Severe NASH (fibrosis index ≥2) versus not severe NASH (fibrosis index <2)	
Chronic obstructive pulmonary disease (COPD)	↑	nd	nd	Acylated ghrelin levels positively correlate with inflammation	[51]
Systemic sclerosis	↓	↓	nd		[52]

ghrelin exerts also many other biological activities, including cardioprotection and enhancement of cardiac function [14], a strong anti-inflammatory activity [15], antioxidant activity on several cell types and tissues such as liver, heart, and lung [16–19], and neuroprotective activities [20]. The acylated ghrelin anti-inflammatory function mainly depends on its direct effect on T lymphocytes and monocytes, in which it inhibits the expression of proinflammatory cytokines such as IL-1β, IL-6, and TNF-α [21].

Acylation of ghrelin is essential for its binding to GHSR-1a, since the unacylated form does not activate this receptor, unless administered at very high concentrations, in which case it acts as a functional agonist [22–25]. However, both acylated and unacylated ghrelin share high affinity binding sites in a number of cell lines and tissues, where they mediate several activities, such as protection from apoptosis and oxidative injury [26–32], stimulation of cell differentiation [33–36], induction of proliferation [30, 37–39], and protection of skeletal muscles from wasting [40–42]. These effects suggest the presence of a not yet identified common receptor of both acylated and unacylated ghrelin. In addition, some biological activities are elicited only by the unacylated but not the acylated form of ghrelin, suggesting the existence of a specific receptor for unacylated ghrelin [39, 43–45].

Circulating levels of acylated and unacylated ghrelin are often altered in pathological states associated with fibrosis and this suggests a role for these hormones in tissue homeostasis and/or in etiology of these conditions ([46–52], Table 1).

2. Acylated and Unacylated Ghrelin as Antifibrotic Factors

2.1. Heart. The massive deposition of collagen in the heart that occurs upon several stimuli, such as cardiomyocyte death, inflammation, hypertension-induced enhanced workload, hypertrophy, or chemotherapy with doxorubicin, plays a crucial role in cardiac remodeling after heart injury and may contribute to ventricular arrhythmias, left ventricular dysfunction, heart failure, and sudden cardiac death [53].

Together with inflammation, cardiac fibroblasts, the most abundant cells in the heart, are the main players in cardiac remodeling: upon injury they undergo proliferation and synthesize collagen to replace the necrotic or apoptotic cardiomyocytes [53].

Due to the antiapoptotic and anti-inflammatory activity of ghrelin, several researchers investigated the antifibrotic effect of acylated and unacylated ghrelin in different models of cardiac injury. Doxorubicin, an antibiotic used in chemotherapy, alters cardiomyocytes energy metabolism and induces their apoptosis, thus determining myocardial fibrosis, which eventually results in cardiomyopathy and congestive heart failure [54]. Accordingly with the in vitro data on the cardioprotective effect of acylated and unacylated ghrelin against doxorubicin-induced apoptosis of cardiomyocytes [26], it has been recently demonstrated that both peptides are effective in inhibiting the cardiotoxicity of this drug also in vivo [55, 56]. Unacylated ghrelin displays antiapoptotic effects on cardiomyocytes through the activation of the prosurvival ERK1/2 and PI3K/Akt signaling pathways ([26, 55], Figure 1). Acylated ghrelin seems to play an important role in the regulation of autophagy, a cellular pathway involved in protein and organelle degradation. Although this cellular pathway is normally a protective mechanism, excessive autophagy can destroy essential cellular components and eventually induce apoptosis [57]. Doxorubicin treatment induces oxidative stress, autophagy, apoptosis, and, finally, cardiac dysfunction and collagen deposition in the heart [56, 57]. In this experimental model of cardiac injury, acylated ghrelin inhibits ROS-induced autophagy and cardiomyocyte death through the inhibition of AMPK and activation of p38-MAPK pathway ([56], Figure 1), thus leading to a decrease of doxorubicin-induced fibrosis and cardiac dysfunction.

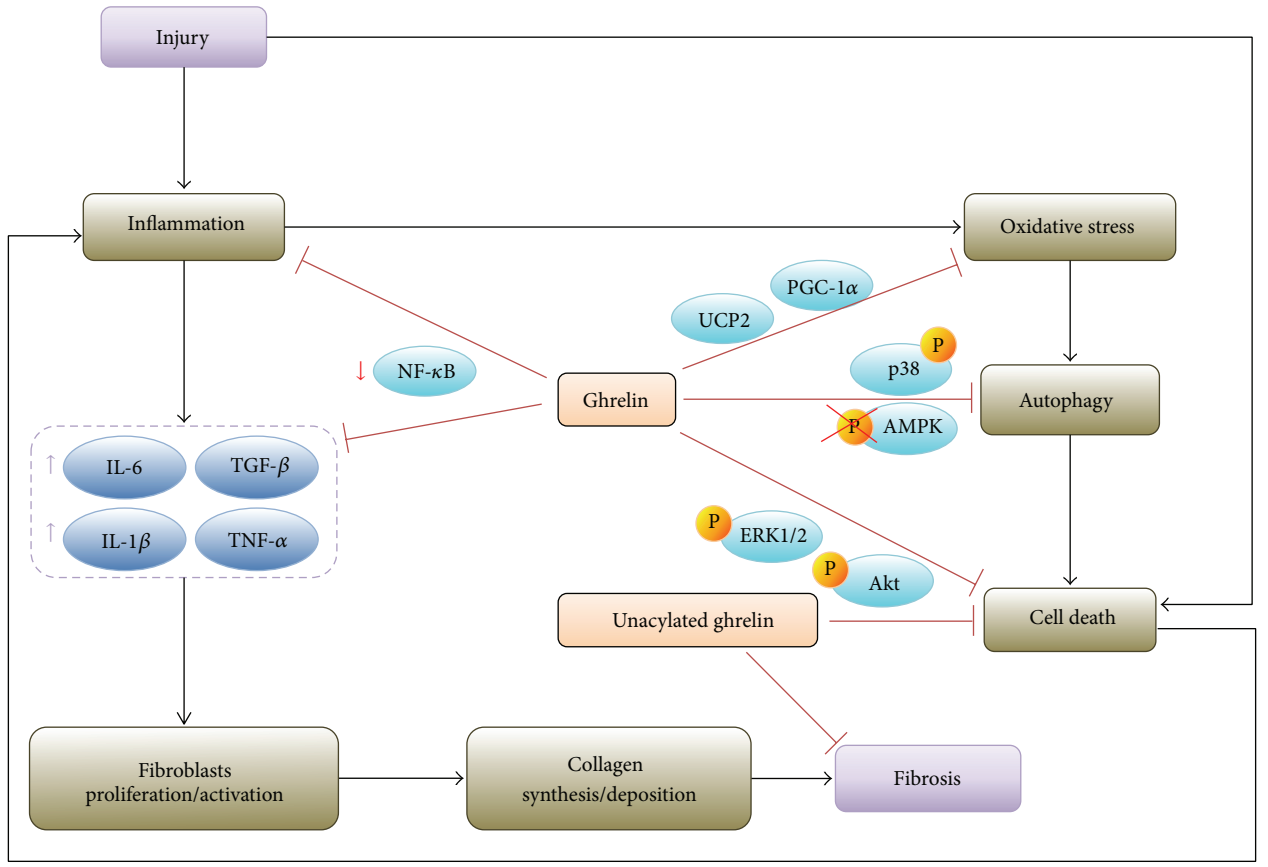

Figure 1: Schematic representation of the molecular pathways involved in the antifibrotic activity of ghrelin and unacylated ghrelin. See text for details.

The antifibrotic effects of acylated and unacylated ghrelin have been demonstrated in other experimental models of cardiac injury, such as isoproterenol administration, myocardial infarction (MI), and spontaneous or diabetes-associated hypertension [58–62]. The subacute injection in rats of the β-adrenergic agonist isoproterenol induces myocardial injury and fibrosis and increases myocardial ghrelin expression and plasmatic acylated ghrelin levels [58, 59]. In this model, acylated ghrelin treatment ameliorates myocardial function and reduces fibrosis, although the mechanisms of such a protection have not been elucidated [59]. The unacylated form of the peptide displays similar effects, suggesting that the antifibrotic activity of ghrelin is mediated by both GHSR-dependent and GHSR-independent pathways [59].

Ghrelin has a positive effect on cardiac remodeling and cardiac function also in rats undergoing MI by coronary artery ligation. MI induces a strong increase in tissutal IL-1β and TNF-α that is inhibited by the chronic administration of ghrelin [60]. Ghrelin also blunts the induction of MMP-2 and MMP-9 that could be viewed as an inhibition of overall fibroblasts activity [60]. However, in spontaneously hypertensive rats, the synthetic GH-secretagogue hexarelin prevents cardiac fibrosis by inducing, rather than by inhibiting, MMP-2 and MMP-9 activity [61]. Notably, unacylated ghrelin, despite reducing cardiac fibrosis in diabetic mice, has no effect on other MMPs involved in cardiac fibrosis development such as MMP-8 and MMP-13 [62]. The effect of unacylated ghrelin treatment was in fact investigated also in db/db diabetic mice compared to nondiabetic mice [62], since cardiac fibrosis is also observed in diabetic patients without hypertension [63]. In this model of diabetic mice, unacylated ghrelin impairs collagen accumulation by upregulating adiponectin cardiac expression [62], which is known to prevent myocardial hypertrophy and fibrosis [64, 65].

2.2. Liver. In liver, hepatitis C or B viral infections, autoimmune diseases, alcohol abuse, and nonalcoholic fatty liver disease (NAFLD) can progress to a severe fibrotic disease in which parenchymal tissue is replaced by nonfunctional fibrotic tissue, a condition defined as cirrhosis [66]. Removal of the causative agent, such as viral infections, could revert liver fibrosis, but in the case of autoimmune diseases and NAFLD the causative agent is not clearly defined and the identification of new agents that could modulate this process is of pivotal importance [67].

In patients with alcoholic hepatitis and chronic hepatitis C, plasmatic ghrelin levels are lower than in healthy subjects and negatively correlate with the severity of fibrosis ([48], Table 1). Circulating ghrelin levels also correlate with other hepatic fibrotic diseases; however, in the case of patients with NAFLD, a worsening of the fibrotic stage is associated

with high plasmatic concentration of both acylated and unacylated ghrelin ([50], Table 1). Interestingly, a screening of miRNAs expression in visceral adipose tissue of NAFLD patients revealed that miR-132, of which the ghrelin gene is a predicted target, is downregulated in nonalcoholic steatohepatitis (NASH) compared to non-NASH patients [68], although a biological validation of this relationship still needs to be performed.

Although the causative relationship between ghrelin circulating levels and NAFLD is not defined, ghrelin might have a therapeutic potential in this and other hepatic pathologies, as demonstrated in several experimental models. The most used models to induce hepatic fibrosis include CCl_4 or thioacetamide (TAA) administration to rodents, which lead to oxidative stress-mediated liver cirrhosis [69]. Another model to induce liver fibrosis consists in bile duct ligation (BDL), which causes accumulation of hydrophobic bile acids in the liver, leading to ROS formation, oxidative damage, inflammatory cell accumulation, and the increase of serum proinflammatory cytokines [70]. In addition, NAFLD may be reproduced in rats by feeding animals with a high-fat diet, thus inducing liver fat accumulation, inflammation, and cellular necrosis [71]. In this model, ghrelin treatment blunts the induction of TNF-α and IL-6 expression, counteracts hepatic oxidative stress, and inhibits hepatic cell apoptosis [72]. The beneficial effects of ghrelin on liver injury and fibrosis have been pointed out by other studies as well. Indeed, in rats with chronic hepatic fibrosis caused by BDL, ghrelin administration prevents hepatic damage by blunting the BDL-induced increase of TNF-α, IL-1β, and IL-6 plasma levels [73]. Moreover, ghrelin treatment impairs neutrophil infiltration and diminishes the amount of myofibroblast accumulation in the injured liver [48, 73]. Accordingly, ghrelin downregulates the expression of collagen-α1 and TGF-β1 in primary hepatic stellate cells (HSC), the main hepatic fibrogenic cells [48], resulting in a diminished collagen deposition [48, 73]. Ghrelin features anti-inflammatory and antifibrotic effects also in TAA-induced hepatic injury in rats where it attenuates liver injury and collagen deposition through inhibition of hepatic cell apoptosis and antioxidative activity, in a way partially mediated by the induction of nitric oxide (NO) [49].

Finally, the physiological role of the ghrelin gene in the establishment of liver fibrosis was investigated exploiting ghrelin knock-out mice that display much more severe CCl_4-induced liver injury and fibrosis compared to wild type animals, suggesting that endogenous ghrelin is required for a proper response to liver damage [48].

2.3. Kidneys. Ghrelin is expressed in kidneys and its expression is altered in pathological conditions such as glomerulopathies, in particular in the proliferative form, in which the immunoexpression of ghrelin is abated [74]. Moreover, the expression of ghrelin negatively correlates with the profibrotic protein endothelin-1 and interstitial inflammatory cell infiltration, suggesting that the loss of ghrelin could contribute to the development of renal interstitial fibrosis, which is the common feature of different end-stage renal diseases [74].

The renin-angiotensin system (RAS) is a well-known regulator of blood pressure and contributes to the development of target organ damage due to hypertension. Angiotensin-II (AngII) is the main mediator of RAS-induced chronic kidney damage through multiple mechanisms, including promotion of inflammation, fibrosis, oxidative stress, and senescence [75]. Indeed, in the experimental model of chronic kidney disease induced by AngII infusion, the kidneys display increased ROS and an accelerated tissue senescence [76, 77]. In addition, treated mice express higher levels of TGF-β and plasminogen activator inhibitor-1 (PAI-1) than saline-infused animals [78]. In this model, ghrelin impairs renal tubular damage, fibrosis development, and senescence by both reducing the oxidative stress and maintaining the redox state. This is mediated by the induction of UCP2 and PGC1α that affect ROS production and mitochondriogenesis, respectively ([78], Figure 1).

The antifibrogenic activity of ghrelin was demonstrated also in a rat model of renal damage obtained by unilateral ureteral obstruction (UUO), which results in tubular injury and cell death, with interstitial macrophage infiltration [79]. In this model, ghrelin protects renal tubular cells from apoptosis, impairs macrophage infiltration, and reduces the induction of the proinflammatory cytokines IL-1β, TNF-α, and monocyte chemoattractant protein-1 (MCP-1) [80]. Moreover, this work demonstrates that ghrelin attenuates renal fibrosis by inhibiting fibroblast differentiation and by blocking epithelial mesenchymal transition (EMT), thus stabilizing the epithelial phenotype [80]. The mechanisms through which ghrelin elicits its antifibrotic activity involve the reduction of collagen I/III, fibronectin, and α-SMA expression via inhibition of the TGF-β1/Smad3 signaling pathway [80].

2.4. Lungs. Lung fibrosis occurs as a consequence of acute lung injury leading to persistent respiratory failure. Lung fibrosis is usually differentiated into distinct types, including diffuse fibrosing alveolitis, diffuse interstitial fibrosis, and idiopathic pulmonary fibrosis, which is considered the most common and severe form of pulmonary fibrosis [81]. Currently, there are no therapies to counteract acute lung injury progression and lung transplantation remains the only possible intervention in end-stage disease [81].

Acute lung injury is characterized by the damage of the alveolar capillary barrier, neutrophil accumulation, and the induction of proinflammatory cytokines, followed by devastating lung fibrosis [82, 83]. In particular, the exfoliation of alveolar epithelial cells from alveolar septa leads to the activation of fibroblasts and the subsequent massive ECM deposition [82].

Cecal ligation and puncture (CLP), the most used technique to induce peritonitis and sepsis, also induces lung injury and fibrosis as direct consequence of hypoxemia, neutrophilic inflammation, and alveolar edema [83].

In CLP-treated rats, ghrelin attenuates acute lung injury and mortality through inhibition of nuclear factor- (NF-)κB activity ([84], Figure 1). NF-κB is a transcription factor that regulates gene expression of several cytokines, including

TNF-α, IL-6, IL-1, and IL-8 [85]. Accordingly, treatment with ghrelin reduces pulmonary levels of TNF-α and IL-6 in CLP-treated rats [84].

Another experimental model used to induce acute lung injury in rodents is the intratracheal injection of bleomycin that promotes massive cell death, neutrophil and lymphocyte infiltration, cytokine production, and fibrosis [83, 86]. In bleomycin-treated mice, ghrelin administration improves animal survival in a dose-dependent manner and maintains lung architecture by reducing fibrosis [86]. This antifibrotic activity is due to the impairment of neutrophil infiltration and accumulation in bronchoalveolar lavage fluid and through the inhibition of proinflammatory cytokines and of IGF-1 release, which promotes collagen production by fibroblasts [86]. In addition, the inhibition of alveolar epithelial cell death, observed in ghrelin-treated mice, represents another mechanism that contributes to ghrelin antifibrotic effects, since the prevention of the denudation of alveolar membranes impairs the subsequent fibrosis establishment [86].

In the same model of lung fibrosis, the traditional Japanese herbal medicine rikkunshito, known to stimulate a strong secretion of ghrelin, reduces lung fibrosis and ameliorates the systemic cachectic condition [87]. However, rikkunshito effects are only partially due to the associated ghrelin increase, since it maintains its protective effects also in mice devoid of the ghrelin gene [88].

2.5. Systemic Sclerosis. Systemic sclerosis, or scleroderma, is an autoimmune chronic connective tissue disease characterized by extensive fibrosis of the skin and internal organs, including lungs, gastrointestinal tract, kidneys, and heart [52]. Plasmatic levels of acylated and unacylated ghrelin are lower in systemic sclerosis patients than in healthy controls and even lower in patients with interstitial lung disease, suggesting that acylated ghrelin levels inversely correlate with tissue fibrosis ([52], Table 1). Consistently, acylated ghrelin treatment of fibroblasts isolated from systemic sclerosis patients reduces TGF-β1 expression and collagen production [52].

Skin scleroderma might be experimentally induced in mice by subcutaneous injections of bleomycin that result in increased dermal thickness, a higher number of α-SMA-positive myofibroblasts, and greater infiltration of inflammatory cells. All these effects are prevented by both acylated and unacylated ghrelin [89]. Taken together, these data suggest that restoring normal circulating acylated and unacylated levels might efficiently contrast the fibrosis induced by systemic sclerosis.

3. Conclusions

Fibrosis is an intrinsic response to chronic injury, maintaining organ integrity when extensive necrosis or apoptosis occurs. With protracted damage, fibrosis can progress towards excessive scarring and organ failure. To date, no satisfactory treatments are available. Anti-inflammation strategies are one of the possible therapeutic approaches to fibrosis. Acylated ghrelin has a potent anti-inflammatory activity and its ability to inhibit proinflammatory cytokines expression and release has been demonstrated by a large number of studies, both in vitro and in vivo [15]. Most of the studies on the antifibrotic effects of acylated and unacylated ghrelin agree that the mechanism of action includes the reduction of inflammation. However, also their effect on oxidative stress reduction plays a crucial role in repressing the formation of fibrosis, and their broad antiapoptotic activity surely contributes in maintaining organ structure and function. This has, however, raised a doubt that if they inhibit apoptosis also in myofibroblasts, this could help, instead of hinder, fibrosis [67].

Circulating levels of ghrelin are often altered in pathologies characterized by the presence of fibrosis; however, it is difficult to discern a causative effect between ghrelin levels and fibrosis, as it is plausible that alterations in ghrelin levels reflect body mass and/or body energy metabolism. This is particularly possible in pathologies co-occurring with cachexia, such as heart and renal failure, in which the increase of ghrelin may represent a compensatory mechanism of the organism in the attempt at re-establishing optimal energetic balance or the establishment of ghrelin resistance [42]. However, in pathologies such as scleroderma, in which fibrosis affects the gastrointestinal tract, it cannot be excluded that the altered levels of ghrelin are a direct consequence of the altered gut condition.

Based on the studies reviewed herein, ghrelin, both in its acylated and unacylated forms, acts at least at two different levels. On one side, ghrelin peptides reduce the infiltration of inflammatory cells in the injured tissue and the subsequent release of cytokines responsible for fibroblast activation. On the other side, they directly affect fibroblast activity by reducing collagen production through the inhibition of TGF-β signaling pathway.

In conclusion, ghrelin peptides and their analogues appear to be promising in the treatment of fibrosis, although their safety and efficacy in long-term use still need to be elucidated.

Abbreviations

AMPK:	Adenosine monophosphate-activated protein kinase
AngII:	Angiotensin-II
BDL:	Bile duct ligation
CLP:	Cecal ligation and puncture
CTGF:	Connective tissue growth factor
ECM:	Extracellular matrix
EMT:	Epithelial mesenchymal transition
ERK1/2:	Extracellular signal-regulated kinase 1/2
GH:	Growth hormone
GHSR-1a:	Growth hormone secretagogue receptor type 1a
HSC:	Hepatic stellate cells
IGF-1:	Insulin-like growth factor 1
IL-1β:	Interleukin-1 beta
IL-6:	Interleukin-6
MCP-1:	Monocyte chemoattractant protein-1
MI:	Myocardial infarction

MMPs: Matrix metalloproteinases
NAFLD: Nonalcoholic fatty liver disease
NASH: Nonalcoholic steatohepatitis
NO: Nitric oxide
PAI-1: Plasminogen activator inhibitor-1
PDGF: Platelet-derived growth factor
PGC1α: Peroxisome proliferator-activated receptor gamma coactivator 1-alpha
PI3K: Phosphatidylinositol 3-kinase
RAS: Renin-angiotensin system
ROS: Reactive oxygen species
TAA: Thioacetamide
TGF-β: Transforming growth factor beta
TNF-α: Tumor necrosis factor-alpha
UCP2: Uncoupling protein 2
UUO: Unilateral ureteral obstruction
α-SMA: Alpha smooth muscle actin.

Conflict of Interests

The authors declare that no conflict of interests exists.

Acknowledgments

The authors thank Dr. Gillian Walker for her careful English editing. Nicoletta Filigheddu is recipient of a Muscular Dystrophy Association Grant (no. MDA294617).

References

[1] A. Meneghin and C. M. Hogaboam, "Infectious disease, the innate immune response, and fibrosis," *Journal of Clinical Investigation*, vol. 117, no. 3, pp. 530–538, 2007.

[2] T. A. Wynn and T. R. Ramalingam, "Mechanisms of fibrosis: therapeutic translation for fibrotic disease," *Nature Medicine*, vol. 18, no. 7, pp. 1028–1040, 2012.

[3] S. Guo and L. A. DiPietro, "Factors affecting wound healing," *Journal of Dental Research*, vol. 89, no. 3, pp. 219–229, 2010.

[4] T. J. Koh and L. A. DiPietro, "Inflammation and wound healing: the role of the macrophage," *Expert Reviews in Molecular Medicine*, vol. 13, article e23, 2011.

[5] A. C. Midgley, M. Rogers, M. B. Hallett et al., "Transforming growth factor-β1 (TGF-β1)-stimulated fibroblast to myofibroblast differentiation is mediated by hyaluronan (HA)-facilitated epidermal growth factor receptor (EGFR) and CD44 co-localization in lipid rafts," *Journal of Biological Chemistry*, vol. 288, no. 21, pp. 14824–14838, 2013.

[6] V. V. Petrov, R. H. Fagard, and P. J. Lijnen, "Stimulation of collagen production by transforming growth factor-β1 during differentiation of cardiac fibroblasts to myofibroblasts," *Hypertension*, vol. 39, no. 2, pp. 258–263, 2002.

[7] M.-C. Hall, D. A. Young, J. G. Waters et al., "The comparative role of activator protein 1 and Smad factors in the regulation of Timp-1 and MMP-1 gene expression by transforming growth factor-β1," *Journal of Biological Chemistry*, vol. 278, no. 12, pp. 10304–10313, 2003.

[8] A. Shroff, A. Mamalis, and J. Jagdeo, "Oxidative stress and skin fibrosis," *Current Pathobiology Reports*, vol. 2, no. 4, pp. 257–267, 2014.

[9] M. Kojima, H. Hosoda, Y. Date, M. Nakazato, H. Matsuo, and K. Kangawa, "Ghrelin is a growth-hormone-releasing acylated peptide from stomach," *Nature*, vol. 402, no. 6762, pp. 656–660, 1999.

[10] J. V. Zhang, P.-G. Ren, O. Avsian-Kretchmer et al., "Obestatin, a peptide encoded by the ghrelin gene, opposes ghrelin's effects on food intake," *Science*, vol. 310, no. 5750, pp. 996–999, 2005.

[11] M. Tschöp, D. L. Smiley, and M. L. Heiman, "Ghrelin induces adiposity in rodents," *Nature*, vol. 407, no. 6806, pp. 908–913, 2000.

[12] H. Ariyasu, K. Takaya, T. Tagami et al., "Stomach is a major source of circulating ghrelin, and feeding state determines plasma ghrelin-like immunoreactivity levels in humans," *Journal of Clinical Endocrinology and Metabolism*, vol. 86, no. 10, pp. 4753–4758, 2001.

[13] A. M. Wren, L. J. Seal, M. A. Cohen et al., "Ghrelin enhances appetite and increases food intake in humans," *The Journal of Clinical Endocrinology & Metabolism*, vol. 86, no. 12, pp. 5992–5995, 2001.

[14] T. Tokudome, I. Kishimoto, M. Miyazato, and K. Kangawa, "Ghrelin and the cardiovascular system," *Frontiers of Hormone Research*, vol. 43, pp. 125–133, 2014.

[15] F. Prodam and N. Filigheddu, "Ghrelin gene products in acute and chronic inflammation," *Archivum Immunologiae et Therapiae Experimentalis*, vol. 62, no. 5, pp. 369–384, 2014.

[16] B. Dobutovic, E. Sudar, S. Tepavcevic et al., "Experimental research Effects of ghrelin on protein expression of antioxidative enzymes and iNOS in the rat liver," *Archives of Medical Science*, vol. 10, no. 4, pp. 806–816, 2014.

[17] R. Barazzoni, A. Semolic, M. R. Cattin, M. Zanetti, and G. Guarnieri, "Acylated ghrelin limits fat accumulation and improves redox state and inflammation markers in the liver of high-fat-fed rats," *Obesity*, vol. 22, no. 1, pp. 170–177, 2014.

[18] X.-X. Tong, D. Wu, X. Wang et al., "Ghrelin protects against cobalt chloride-induced hypoxic injury in cardiac H9c2 cells by inhibiting oxidative stress and inducing autophagy," *Peptides*, vol. 38, no. 2, pp. 217–227, 2012.

[19] D. Yang, Z. Liu, H. Zhang, and Q. Luo, "Ghrelin protects human pulmonary artery endothelial cells against hypoxia-induced injury via PI3-kinase/Akt," *Peptides*, vol. 42, pp. 112–117, 2013.

[20] S. Raimondo, G. Ronchi, S. Geuna et al., "Ghrelin: a novel neuromuscular recovery promoting factor?" *International Review of Neurobiology*, vol. 108, pp. 207–221, 2013.

[21] V. D. Dixit, E. M. Schaffer, R. S. Pyle et al., "Ghrelin inhibits leptin- and activation-induced proinflammatory cytokine expression by human monocytes and T cells," *Journal of Clinical Investigation*, vol. 114, no. 1, pp. 57–66, 2004.

[22] M. A. Bednarek, S. D. Feighner, S.-S. Pong et al., "Structure—function studies on the new growth hormone-releasing peptide, ghrelin: minimal sequence of ghrelin necessary for activation of growth hormone secretagogue receptor 1a," *Journal of Medicinal Chemistry*, vol. 43, no. 23, pp. 4370–4376, 2000.

[23] M. Matsumoto, H. Hosoda, Y. Kitajima et al., "Structure-activity relationship of ghrelin: pharmacological study of ghrelin peptides," *Biochemical and Biophysical Research Communications*, vol. 287, no. 1, pp. 142–146, 2001.

[24] C. Gauna, B. van de Zande, A. van Kerkwijk, A. P. N. Themmen, A. J. van der Lely, and P. J. D. Delhanty, "Unacylated ghrelin is not a functional antagonist but a full agonist of the type 1a growth hormone secretagogue receptor (GHS-R)," *Molecular and Cellular Endocrinology*, vol. 274, no. 1-2, pp. 30–34, 2007.

[25] K. M. Heppner, C. L. Piechowski, A. Müller et al., "Both acyl and des-acyl ghrelin regulate adiposity and glucose metabolism via central nervous system ghrelin receptors," *Diabetes*, vol. 63, no. 1, pp. 122–131, 2014.

[26] G. Baldanzi, N. Filigheddu, S. Cutrupi et al., "Ghrelin and des-acyl ghrelin inhibit cell death in cardiomyocytes and endothelial cells through ERK1/2 and PI 3-kinase/AKT," *Journal of Cell Biology*, vol. 159, no. 6, pp. 1029–1037, 2002.

[27] T. Shimada, H. Furuta, A. Doi et al., "Des-acyl ghrelin protects microvascular endothelial cells from oxidative stress-induced apoptosis through sirtuin 1 signaling pathway," *Metabolism: Clinical and Experimental*, vol. 63, no. 4, pp. 469–474, 2014.

[28] R. Granata, F. Settanni, L. Trovato et al., "Unacylated as well as acylated ghrelin promotes cell survival and inhibit apoptosis in HIT-T15 pancretic β-cells," *Journal of Endocrinological Investigation*, vol. 29, no. 9, pp. RC19–RC22, 2006.

[29] H. Chung, S. Seo, M. Moon, and S. Park, "Phosphatidylinositol-3-kinase/Akt/glycogen synthase kinase-3 beta and ERK1/2 pathways mediate protective effects of acylated and unacylated ghrelin against oxygen-glucose deprivation-induced apoptosis in primary rat cortical neuronal cells," *Journal of Endocrinology*, vol. 198, no. 3, pp. 511–521, 2008.

[30] P. J. D. Delhanty, P. M. van Koetsveld, C. Gauna et al., "Ghrelin and its unacylated isoform stimulate the growth of adrenocortical tumor cells via an anti-apoptotic pathway," *American Journal of Physiology—Endocrinology and Metabolism*, vol. 293, no. 1, pp. E302–E309, 2007.

[31] A. P. Yu, X. M. Pei, T. K. Sin et al., "Acylated and unacylated ghrelin inhibit doxorubicin-induced apoptosis in skeletal muscle," *Acta Physiologica*, vol. 211, no. 1, pp. 201–213, 2014.

[32] E. Dieci, L. Casati, F. Pagani, F. Celotti, and V. Sibilia, "Acylated and unacylated ghrelin protect MC3T3-E1 cells against tert-butyl hydroperoxide-induced oxidative injury: pharmacological characterization of ghrelin receptor and possible epigenetic involvement," *Amino Acids*, vol. 46, no. 7, pp. 1715–1725, 2014.

[33] N. Filigheddu, V. F. Gnocchi, M. Coscia et al., "Ghrelin and des-acyl ghrelin promote differentiation and fusion of C2C12 skeletal muscle cells," *Molecular Biology of the Cell*, vol. 18, no. 3, pp. 986–994, 2007.

[34] A. Giovambattista, R. C. Gaillard, and E. Spinedi, "Ghrelin gene-related peptides modulate rat white adiposity," *Vitamins and Hormones*, vol. 77, pp. 171–205, 2007.

[35] P. Miegueu, D. St Pierre, F. Broglio, and K. Cianflone, "Effect of desacyl ghrelin, obestatin and related peptides on triglyceride storage, metabolism and GHSR signaling in 3T3-L1 adipocytes," *Journal of Cellular Biochemistry*, vol. 112, no. 2, pp. 704–714, 2011.

[36] M. Gao, J. Yang, R. Wei et al., "Ghrelin induces cardiac lineage differentiation of human embryonic stem cells through ERK1/2 pathway," *International Journal of Cardiology*, vol. 167, no. 6, pp. 2724–2733, 2013.

[37] P. J. Delhanty, B. C. van der Eerden, M. van der Velde et al., "Ghrelin and unacylated ghrelin stimulate human osteoblast growth via mitogen-activated protein kinase (MAPK)/phosphoinositide 3-kinase (PI3K) pathways in the absence of GHS-R1a," *Journal of Endocrinology*, vol. 188, no. 1, pp. 37–47, 2006.

[38] R. Granata, F. Settanni, L. Biancone et al., "Acylated and unacylated ghrelin promote proliferation and inhibit apoptosis of pancreatic β-cells and human islets: Involvement of $3',5'$-cyclic adenosine monophosphate/protein kinase A, extracellular signal-regulated kinase 1/2, and phosphatidyl inositol 3-kinase/Akt signaling," *Endocrinology*, vol. 148, no. 2, pp. 512–529, 2007.

[39] G. Togliatto, A. Trombetta, P. Dentelli et al., "Unacylated ghrelin promotes skeletal muscle regeneration following hindlimb ischemia via SOD-2-mediated miR-221/222 expression," *Journal of the American Heart Association*, vol. 2, no. 6, Article ID e000376, 2013.

[40] S. Sheriff, N. Kadeer, R. Joshi, L. A. Friend, J. H. James, and A. Balasubramaniam, "Des-acyl ghrelin exhibits pro-anabolic and anti-catabolic effects on C2C12 myotubes exposed to cytokines and reduces burn-induced muscle proteolysis in rats," *Molecular and Cellular Endocrinology*, vol. 351, no. 2, pp. 286–295, 2012.

[41] P. E. Porporato, N. Filigheddu, S. Reano et al., "Acylated and unacylated ghrelin impair skeletal muscle atrophy in mice," *Journal of Clinical Investigation*, vol. 123, no. 2, pp. 611–622, 2013.

[42] S. Reano, A. Graziani, and N. Filigheddu, "Acylated and unacylated ghrelin administration to blunt muscle wasting," *Current Opinion in Clinical Nutrition and Metabolic Care*, vol. 17, no. 3, pp. 236–240, 2014.

[43] C. Gauna, P. J. D. Delhanty, L. J. Hofland et al., "Ghrelin stimulates, whereas des-octanoyl ghrelin inhibits, glucose output by primary hepatocytes," *Journal of Clinical Endocrinology and Metabolism*, vol. 90, no. 2, pp. 1055–1060, 2005.

[44] G. Togliatto, A. Trombetta, P. Dentelli et al., "Unacylated ghrelin rescues endothelial progenitor cell function in individuals with type 2 diabetes," *Diabetes*, vol. 59, no. 4, pp. 1016–1025, 2010.

[45] A. Benso, D. H. St-Pierre, F. Prodam et al., "Metabolic effects of overnight continuous infusion of unacylated ghrelin in humans," *European Journal of Endocrinology*, vol. 166, no. 5, pp. 911–916, 2012.

[46] N. Nagaya, M. Uematsu, M. Kojima et al., "Elevated circulating level of ghrelin in cachexia associated with chronic heart failure: relationships between ghrelin and anabolic/catabolic factors," *Circulation*, vol. 104, no. 17, pp. 2034–2038, 2001.

[47] Y. Chen, X.-W. Ji, A.-Y. Zhang, J.-C. Lv, J.-G. Zhang, and C.-H. Zhao, "Prognostic value of plasma ghrelin in predicting the outcome of patients with chronic heart failure," *Archives of Medical Research*, vol. 45, no. 3, pp. 263–269, 2014.

[48] M. Moreno, J. F. Chaves, P. Sancho-Bru et al., "Ghrelin attenuates hepatocellular injury and liver fibrogenesis in rodents and influences fibrosis progression in humans," *Hepatology*, vol. 51, no. 3, pp. 974–985, 2010.

[49] N. N. Kabil, H. A. Seddiek, N. A. Yassin, and M. M. Gamal-Eldin, "Effect of ghrelin on chronic liver injury and fibrogenesis in male rats: possible role of nitric oxide," *Peptides*, vol. 52, pp. 90–97, 2014.

[50] M. Estep, M. Abawi, M. Jarrar et al., "Association of obestatin, ghrelin, and inflammatory cytokines in obese patients with non-alcoholic fatty liver disease," *Obesity Surgery*, vol. 21, no. 11, pp. 1750–1757, 2011.

[51] T. Itoh, N. Nagaya, M. Yoshikawa et al., "Elevated plasma ghrelin level in underweight patients with chronic obstructive pulmonary disease," *American Journal of Respiratory and Critical Care Medicine*, vol. 170, no. 8, pp. 879–882, 2004.

[52] Y. Ota, Y. Kawaguchi, K. Takagi et al., "Ghrelin attenuates collagen production in lesional fibroblasts from patients with systemic sclerosis," *Clinical Immunology*, vol. 147, no. 2, pp. 71–78, 2013.

[53] D. Fan, A. Takawale, J. Lee, and Z. Kassiri, "Cardiac fibroblasts, fibrosis and extracellular matrix remodeling in heart disease," *Fibrogenesis and Tissue Repair*, vol. 5, no. 1, article 15, 2012.

[54] Y. Octavia, C. G. Tocchetti, K. L. Gabrielson, S. Janssens, H. J. Crijns, and A. L. Moens, "Doxorubicin-induced cardiomyopathy: from molecular mechanisms to therapeutic strategies," *Journal of Molecular and Cellular Cardiology*, vol. 52, no. 6, pp. 1213–1225, 2012.

[55] X. M. Pei, B. Y. Yung, S. P. Yip, M. Ying, I. F. Benzie, and P. M. Siu, "Desacyl ghrelin prevents doxorubicin-induced myocardial fibrosis and apoptosis via the GHSR-independent pathway," *The American Journal of Physiology—Endocrinology and Metabolism*, vol. 306, no. 3, pp. E311–E323, 2014.

[56] X. Wang, X.-L. Wang, H.-L. Chen et al., "Ghrelin inhibits doxorubicin cardiotoxicity by inhibiting excessive autophagy through AMPK and p38-MAPK," *Biochemical Pharmacology*, vol. 88, no. 3, pp. 334–350, 2014.

[57] Y.-W. Zhang, J. Shi, Y.-J. Li, and L. Wei, "Cardiomyocyte death in doxorubicin-induced cardiotoxicity," *Archivum Immunologiae et Therapiae Experimentalis*, vol. 57, no. 6, pp. 435–445, 2009.

[58] Z. Nichtova, M. Novotova, E. Kralova, and T. Stankovicova, "Morphological and functional characteristics of models of experimental myocardial injury induced by isoproterenol," *General Physiology and Biophysics*, vol. 31, no. 2, pp. 141–151, 2012.

[59] L. Li, L.-K. Zhang, Y.-Z. Pang et al., "Cardioprotective effects of ghrelin and des-octanoyl ghrelin on myocardial injury induced by isoproterenol in rats," *Acta Pharmacologica Sinica*, vol. 27, no. 5, pp. 527–535, 2006.

[60] C. X. Huang, M. J. Yuan, H. Huang et al., "Ghrelin inhibits post-infarct myocardial remodeling and improves cardiac function through anti-inflammation effect," *Peptides*, vol. 30, no. 12, pp. 2286–2291, 2009.

[61] X. Xu, F. Ding, J. Pang et al., "Chronic administration of hexarelin attenuates cardiac fibrosis in the spontaneously hypertensive rat," *American Journal of Physiology—Heart and Circulatory Physiology*, vol. 303, no. 6, pp. H703–H711, 2012.

[62] X. M. Pei, B. Y. Yung, S. P. Yip et al., "Protective effects of desacyl ghrelin on diabetic cardiomyopathy," *Acta Diabetologica*, vol. 52, no. 2, pp. 293–306, 2014.

[63] C. Voulgari, D. Papadogiannis, and N. Tentolouris, "Diabetic cardiomyopathy: From the pathophysiology of the cardiac myocytes to current diagnosis and management strategies," *Vascular Health and Risk Management*, vol. 6, no. 1, pp. 883–903, 2010.

[64] E. E. Essick, N. Ouchi, R. M. Wilson et al., "Adiponectin mediates cardioprotection in oxidative stress-induced cardiac myocyte remodeling," *The American Journal of Physiology—Heart and Circulatory Physiology*, vol. 301, no. 3, pp. H984–H993, 2011.

[65] R. Shibata, N. Ouchi, M. Ito et al., "Adiponectin-mediated modulation of hypertrophic signals in the heart," *Nature Medicine*, vol. 10, no. 12, pp. 1384–1389, 2004.

[66] D. Schuppan and Y. O. Kim, "Evolving therapies for liver fibrosis," *Journal of Clinical Investigation*, vol. 123, no. 5, pp. 1887–1901, 2013.

[67] S. L. Friedman, D. Sheppard, J. S. Duffield, and S. Violette, "Therapy for fibrotic diseases: nearing the starting line," *Science Translational Medicine*, vol. 5, no. 167, Article ID 167sr1, 2013.

[68] M. Estep, D. Armistead, N. Hossain et al., "Differential expression of miRNAs in the visceral adipose tissue of patients with non-alcoholic fatty liver disease," *Alimentary Pharmacology & Therapeutics*, vol. 32, no. 3, pp. 487–497, 2010.

[69] S. K. Natarajan, S. Thomas, P. Ramamoorthy et al., "Oxidative stress in the development of liver cirrhosis: a comparison of two different experimental models," *Journal of Gastroenterology and Hepatology*, vol. 21, no. 6, pp. 947–957, 2006.

[70] Y. Takahashi, Y. Soejima, and T. Fukusato, "Animal models of nonalcoholic fatty liver disease/nonalcoholic steatohepatitis," *World Journal of Gastroenterology*, vol. 18, no. 19, pp. 2300–2308, 2012.

[71] A. Nakamura and Y. Terauchi, "Lessons from mouse models of high-fat diet-induced NAFLD," *International Journal of Molecular Sciences*, vol. 14, no. 11, pp. 21240–21257, 2013.

[72] Y. Li, J. Hai, L. Li et al., "Administration of ghrelin improves inflammation, oxidative stress, and apoptosis during and after non-alcoholic fatty liver disease development," *Endocrine*, vol. 43, no. 2, pp. 376–386, 2013.

[73] S. Ö. Işeri, G. Şener, B. Saglam, F. Ercan, N. Gedik, and B. Ç. Yeğen, "Ghrelin alleviates biliary obstruction-induced chronic hepatic injury in rats," *Regulatory Peptides*, vol. 146, no. 1–3, pp. 73–79, 2008.

[74] M. Danilewicz and M. Wagrowska-Danilewicz, "Renal immunoexpression of ghrelin is attenuated in human proliferative glomerulopathies," *Nefrologia*, vol. 30, no. 6, pp. 633–638, 2010.

[75] L. M. Harrison-Bernard, "The renal renin-angiotensin system," *Advances in Physiology Education*, vol. 33, no. 4, pp. 270–274, 2009.

[76] A. Benigni, P. Cassis, and G. Remuzzi, "Angiotensin II revisited: new roles in inflammation, immunology and aging," *EMBO Molecular Medicine*, vol. 2, no. 7, pp. 247–257, 2010.

[77] K.-H. Krause, "Aging: a revisited theory based on free radicals generated by NOX family NADPH oxidases," *Experimental Gerontology*, vol. 42, no. 4, pp. 256–262, 2007.

[78] K. Fujimura, S. Wakino, H. Minakuchi et al., "Ghrelin protects against renal damages induced by angiotensin-II via an antioxidative stress mechanism in mice," *PLoS ONE*, vol. 9, no. 4, Article ID e94373, 2014.

[79] R. L. Chevalier, M. S. Forbes, and B. A. Thornhill, "Ureteral obstruction as a model of renal interstitial fibrosis and obstructive nephropathy," *Kidney International*, vol. 75, no. 11, pp. 1145–1152, 2009.

[80] G. X. Sun, R. Ding, M. Li et al., "Ghrelin attenuates renal fibrosis and inflammation of obstructive nephropathy," *The Journal of Urology*, 2014.

[81] G. Raghu, H. R. Collard, J. J. Egan et al., "An Official ATS/ERS/JRS/ALAT Statement: idiopathic pulmonary fibrosis: evidence-based guidelines for diagnosis and management," *The American Journal of Respiratory and Critical Care Medicine*, vol. 183, no. 6, pp. 788–824, 2011.

[82] L. B. Ware and M. A. Matthay, "The acute respiratory distress syndrome," *The New England Journal of Medicine*, vol. 342, no. 18, pp. 1334–1349, 2000.

[83] G. Matute-Bello, C. W. Frevert, and T. R. Martin, "Animal models of acute lung injury," *The American Journal of Physiology—Lung Cellular and Molecular Physiology*, vol. 295, no. 3, pp. L379–L399, 2008.

[84] R. Wu, W. Dong, M. Zhou et al., "Ghrelin attenuates sepsis-induced acute lung injury and mortality in rats," *The American Journal of Respiratory and Critical Care Medicine*, vol. 176, no. 8, pp. 805–813, 2007.

[85] T. S. Blackwell and J. W. Christman, "The role of nuclear factor-κ B in cytokine gene regulation," *American Journal of Respiratory Cell and Molecular Biology*, vol. 17, no. 1, pp. 3–9, 1997.

[86] Y. Imazu, S. Yanagi, K. Miyoshi et al., "Ghrelin ameliorates bleomycin-induced acute lung injury by protecting alveolar epithelial cells and suppressing lung inflammation," *European Journal of Pharmacology*, vol. 672, no. 1–3, pp. 153–158, 2011.

[87] H. Tsubouchi, S. Yanagi, A. Miura et al., "Rikkunshito ameliorates cachexia associated with bleomycin-induced lung fibrosis in mice by stimulating ghrelin secretion," *Nutrition Research*, vol. 34, no. 10, pp. 876–885, 2014.

[88] H. Tsubouchi, S. Yanagi, A. Miura et al., "Rikkunshito ameliorates bleomycin-induced acute lung injury in a ghrelin-independent manner," *The American Journal of Physiology—Lung Cellular and Molecular Physiology*, vol. 306, no. 3, pp. L233–L245, 2014.

[89] S. S. Koca, M. Ozgen, M. Sarikaya, F. Dagli, B. Ustundag, and A. Isik, "Ghrelin prevents the development of dermal fibrosis in bleomycin-induced scleroderma," *Clinical and Experimental Dermatology*, vol. 39, no. 2, pp. 176–181, 2014.

[90] B. Aktas, Y. Yilmaz, F. Eren et al., "Serum levels of vaspin, obestatin, and apelin-36 in patients with nonalcoholic fatty liver disease," *Metabolism*, vol. 60, no. 4, pp. 544–549, 2011.

Acylated and unacylated ghrelin impair skeletal muscle atrophy in mice

Paolo E. Porporato,[1] Nicoletta Filigheddu,[1] Simone Reano,[1] Michele Ferrara,[1] Elia Angelino,[1] Viola F. Gnocchi,[1] Flavia Prodam,[2] Giulia Ronchi,[3] Sharmila Fagoonee,[4] Michele Fornaro,[3] Federica Chianale,[1] Gianluca Baldanzi,[1] Nicola Surico,[1] Fabiola Sinigaglia,[1] Isabelle Perroteau,[5] Roy G. Smith,[6] Yuxiang Sun,[7] Stefano Geuna,[3] and Andrea Graziani[1]

[1]Department of Translational Medicine, Interdisciplinary Research Center of Autoimmune Diseases (IRCAD), and Biotechnology Center for Applied Medical Research (BRMA), Università del Piemonte Orientale "Amedeo Avogadro" — Alessandria, Novara, Vercelli, Italy. [2]Department of Health Sciences, Università del Piemonte Orientale "Amedeo Avogadro" — Alessandria, Novara, Vercelli, Italy. [3]Neuroscience Institute "Cavalieri Ottolenghi" (NICO) and Department of Clinical and Biological Sciences, University of Torino, Orbassano (TO), Italy. [4]Molecular Biotechnology Center and Department of Genetics, Biology and Biochemistry, and [5]Department of Life Sciences and Systems Biology, University of Torino, Torino, Italy. [6]Department of Metabolism and Aging, The Scripps Research Institute, Scripps, Florida, USA. [7]USDA ARS Children's Nutrition Research Center, Departments of Pediatrics and Molecular and Cellular Biology, Baylor College of Medicine, Houston, Texas, USA.

Cachexia is a wasting syndrome associated with cancer, AIDS, multiple sclerosis, and several other disease states. It is characterized by weight loss, fatigue, loss of appetite, and skeletal muscle atrophy and is associated with poor patient prognosis, making it an important treatment target. Ghrelin is a peptide hormone that stimulates growth hormone (GH) release and positive energy balance through binding to the receptor GHSR-1a. Only acylated ghrelin (AG), but not the unacylated form (UnAG), can bind GHSR-1a; however, UnAG and AG share several GHSR-1a–independent biological activities. Here we investigated whether UnAG and AG could protect against skeletal muscle atrophy in a GHSR-1a–independent manner. We found that both AG and UnAG inhibited dexamethasone-induced skeletal muscle atrophy and atrogene expression through PI3Kβ-, mTORC2-, and p38-mediated pathways in myotubes. Upregulation of circulating UnAG in mice impaired skeletal muscle atrophy induced by either fasting or denervation without stimulating muscle hypertrophy and GHSR-1a–mediated activation of the GH/IGF-1 axis. In *Ghsr*-deficient mice, both AG and UnAG induced phosphorylation of Akt in skeletal muscle and impaired fasting-induced atrophy. These results demonstrate that AG and UnAG act on a common, unidentified receptor to block skeletal muscle atrophy in a GH-independent manner.

Introduction

Skeletal muscle atrophy involves massive loss of muscle structural proteins, which leads to muscle weight decrease and progressive loss of muscle function. Skeletal muscle atrophy is induced by muscle denervation and disuse, and it is also the key component of cachexia, a catabolic, debilitating response to several diseases. Cachectic patients not only sustain a decreased quality of life, but also face a worse prognosis of the underlying pathology, making cachexia an important target for treatment (1). Ghrelin is a circulating peptide hormone, octanoylated on Ser3, that is mainly produced by the stomach, which, by acting on the hypothalamus and the pituitary, induces GH secretion and stimulates food intake and adiposity through binding to its receptor, GHSR-1a (2–5). In addition to its endocrine activities, ghrelin protects cardiac function after heart damage (6, 7). In vitro, ghrelin inhibits the apoptosis of cardiomyocytes and other cell types by activating PI3K/Akt and ERK-1/2 pathways (8–10). Acylated ghrelin (AG) and unacylated ghrelin (UnAG) are generated from the same precursor, which can be acylated by the specific intracellular ghrelin-O-acyltransferase GOAT (11, 12). UnAG, which is far more abundant in plasma than AG, does not bind to GHSR-1a, lacks any GH-releasing activity (13), and has been considered for many years to be the inactive product of ghrelin catabolism. However, UnAG shares with AG common high-affinity binding sites on several cell types lacking GHSR-1a, including myocardial and skeletal myocytes, where they stimulate survival and differentiation, respectively (8, 9, 14–16). Furthermore, UnAG regulates gene expression in fat, muscle, and liver independently of GHSR-1a (17).

In both human patients and experimental models, AG ameliorates cachexia induced by several pathological conditions (6, 7, 13, 18–21). Although AG may inhibit cachexia by stimulating food intake, positive energy balance, and release of GH and IGF-1, the mechanisms underlying its anticachectic activity have not been fully elucidated.

Since we have previously shown that AG and UnAG, independently of GHSR-1a, inhibit apoptosis of cardiomyocytes by activating PI3K/Akt (8), a major antiatrophic signaling pathway (22, 23), and stimulate C2C12 skeletal myoblast differentiation (16), we investigated whether AG and UnAG could protect skeletal muscle from atrophy. Here, we provided evidence in vitro and in vivo that AG and UnAG, independently of GHSR-1a and activation of the GH/IGF-1 axis, trigger an antiatrophic signaling pathway by acting directly on the skeletal muscle, thereby protecting it from experimentally induced atrophy.

Results

AG and UnAG prevent dexamethasone-induced atrophy in C2C12-derived myotubes via mTORC2. C2C12 myotubes are a widely used model to study in vitro skeletal muscle atrophy induced by the synthetic glucocorticoid dexamethasone (24–26). Muscle atrophy was measured

Authorship note: Paolo E. Porporato and Nicoletta Filigheddu contributed equally to this work.

Conflict of interest: The authors have declared that no conflict of interest exists.

Citation for this article: *J Clin Invest.* 2013;123(2):611–622. doi:10.1172/JCI39920.

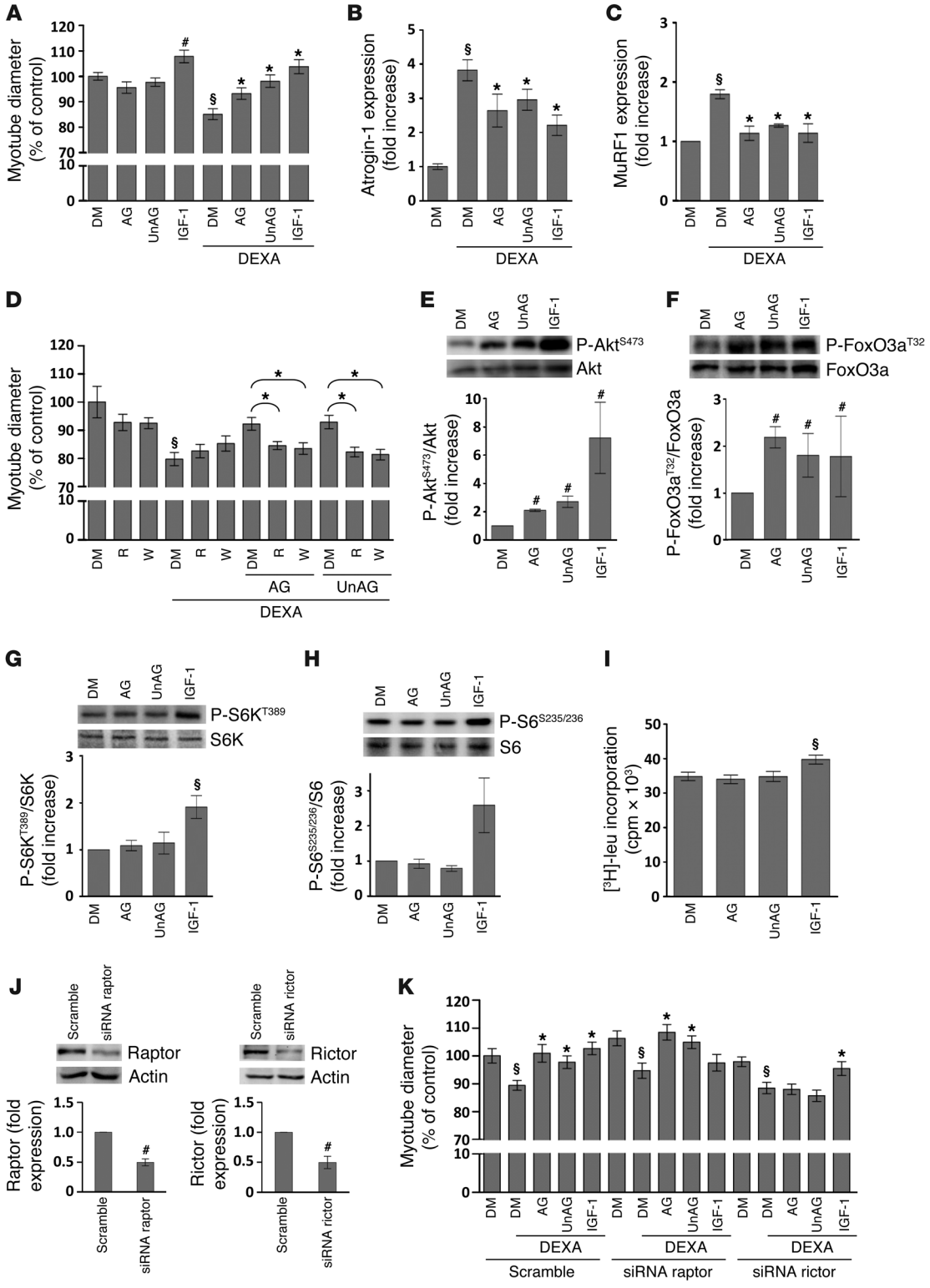

Figure 1
AG and UnAG protect C2C12 myotubes from dexamethasone-induced atrophy without induction of protein synthesis or hypertrophy. (**A**) Myotube diameters were measured after 24-hour treatment in differentiation medium (DM) with 10 nM AG, 10 nM UnAG, and/or 1 μM dexamethasone (DEXA). In every experiment, 10 ng/ml IGF-1 was used as positive control for antiatrophic/hypertrophic activity. (**B** and **C**) Atrogin-1 and MuRF1 expression analysis upon dexamethasone treatment with or without AG and UnAG. (**D**) Treatment with 100 nM wortmannin (W) or 20 ng/ml rapamycin (R) reverted the antiatrophic activity of AG and UnAG on myotube diameter. Control myotubes in differentiation medium were treated with DMSO, a vehicle for both wortmannin and rapamycin. (**E** and **F**) Phosphorylation of Akt^{S473} and $FoxO3a^{T32}$, detected by Western blotting, upon treatment for 20 minutes with 1 μM AG or UnAG. Shown are representative blots and quantification of 3 independent experiments. (**G**–**I**) IGF-1, but not AG and UnAG, induced protein synthesis, as determined by phosphorylation of $S6K^{T389}$ (**G**) or $S6^{S235/236}$ (**H**) and by incorporation of [^{3}H]-leucine (**I**). (**J**) Effect of raptor and rictor silencing on protein levels, detected by Western blotting. (**K**) Silencing of rictor, but not of raptor, reverted the antiatrophic activity of AG and UnAG on the diameter of myotubes treated as in **A**. $^{\#}P < 0.05$, $^{\S}P < 0.01$ vs. DM control; $^{*}P < 0.01$ vs. DEXA treatment.

both as reduction of myotube diameter and as expression of the muscle-specific ubiquitin ligases Atrogin-1 (also known as MAFbx) and MuRF1, which drive muscle protein degradation in several models of muscle atrophy (24–27). Myotubes were treated with 1 μM dexamethasone for 24 hours in the presence or absence of 10 nM AG or UnAG, or with 10 ng/ml IGF-1 as a positive control of atrophy protection. Treatment with dexamethasone reduced myotube diameters by 20% and induced Atrogin-1 and MuRF1 expression. AG and UnAG impaired both these effects (Figure 1, A–C).

Skeletal muscle atrophy and atrogene expression can be opposed by the activation of mammalian target of rapamycin (mTOR), which, by forming 2 distinct protein complexes, mTORC1 and mTORC2, triggers distinct pathways that lead, respectively, to increased protein synthesis and to inhibited protein degradation (28, 29). To assess whether mTOR mediates the signaling triggered by AG/UnAG, myotubes were incubated with rapamycin, an inhibitor of mTORC1, which, upon prolonged treatment, also impairs the assembly of mTORC2 in several cell types, including C2C12 cells (refs. 30–32 and Supplemental Figure 1, A and B; supplemental material available online with this article; doi:10.1172/JCI39920DS1).

Upon 24-hour treatment of atrophying myotubes with 20 ng/ml rapamycin, the antiatrophic activity of AG/UnAG on myotube diameter was fully reverted (Figure 1D), which indicates that activation of mTOR is indeed required for the antiatrophic activity of AG and UnAG. Moreover, in the same assay, the antiatrophic activity of AG/UnAG was inhibited by 100 nM wortmannin, an inhibitor of PI3K, whose product $PI(3,4,5)P_3$ is essential for the activity of Akt, a substrate of mTORC2 that also mediates the activation of mTORC1 (29). These findings indicate that AG/UnAG antiatrophic activity requires both mTOR and Akt. Thus, we assayed the activity of both mTOR complexes. We evaluated mTORC2 activity as phosphorylation of Akt^{S473}, which, in turn, phosphorylates $FoxO3a^{T32}$, thus preventing Atrogin-1 transcription (24, 25). AG/UnAG, as well as IGF-1, induced phosphorylation of Akt^{S473} and $FoxO3a^{T32}$ (Figure 1, E and F), which indicates that they activate mTORC2-mediated pathways.

The activity of mTORC1 was assayed as phosphorylation of $S6K^{T389}$, a direct substrate of mTORC1, and of its substrate $S6^{S235/236}$, a ribosomal protein whose phosphorylation mediates protein synthesis (29). AG and UnAG did not induce phosphorylation of $S6K^{T389}$ and $S6^{S235/236}$ (Figure 1, G and H), nor protein synthesis (as measured by [^{3}H]-leucine incorporation; Figure 1I) or myotube hypertrophy (Figure 1A). Conversely, IGF-1 induced $S6K^{T389}$ and $S6^{S235/236}$ phosphorylation, [^{3}H]-leucine incorporation, and myotube diameter increase, as expected.

By silencing raptor and rictor, specific components of mTORC1 and mTORC2, respectively (Figure 1J), we observed that downregulation of rictor abrogated the protective effect of both peptides on dexamethasone-induced muscle atrophy, measured as myotube diameter, while it did not affect the antiatrophic activity of IGF-1 (Figure 1K). Conversely, raptor silencing impaired IGF-1 antiatrophic activity without affecting that of AG/UnAG. These results indicate that mTORC2 pathway mediates AG/UnAG antiatrophic activity in C2C12 myotubes, without involving mTORC1-mediated protein synthesis.

To identify the signaling pathways differently activated by AG/UnAG and IGF-1, we investigated the role of p38 serine kinase, whose activation by AG/UnAG mediates C2C12 myoblast differentiation (16). In C2C12 myotubes, AG/UnAG, as well as IGF-1, induced phosphorylation of $p38^{T180/Y182}$ (Figure 2A), and its pharmacological inhibition impaired the antiatrophic activity of AG/UnAG, but not of IGF-1 (Figure 2B).

Activation of p38 has been reported to downregulate Atrogin-1, thereby contributing to the protection of skeletal muscle from atrophy (33). On the other hand, p38 mediates induction of Atrogin-1 by TNF-α and oxidative stress and of MuRF1 by serum starvation (34–37). Inhibition of p38 with SB203580 reduced dexamethasone-induced expression of both Atrogin-1 and MuRF1; nevertheless, induction of Atrogin-1, but not MuRF1, was still significant (Figure 2, C and D). In the presence of SB203580, AG and UnAG, but not IGF-1, failed to further reduce the residual induction of Atrogin-1, which indicates that p38 mediates AG/UnAG signaling in regulating Atrogin-1 expression.

To further characterize AG/UnAG antiatrophic activity, we treated C2C12 myotubes with NF449, a compound uncoupling $G\alpha_s$ from GPCRs, which inhibits antiapoptotic activity of AG and UnAG in pancreatic β cells (9, 38). NF449 completely abrogated Akt^{S473} phosphorylation and antiatrophic activity of AG/UnAG without affecting IGF-1 activities (Figure 2, E and F), which supports the hypothesis that AG and UnAG act through a GPCR, as previously suggested (9).

PI3K α and β isoforms mediate Akt activation upon stimulation of tyrosine kinase receptors and GPCRs, respectively (39, 40). We dissected the contribution of PI3Kα and PI3Kβ to IGF-1 and AG/UnAG antiatrophic activity using isoform-specific PI3K inhibitors. Whereas inhibition of PI3Kα by PIK-75 abolished IGF-1 antiatrophic activity, it did not affect AG/UnAG protection. Conversely, inhibition of PI3Kβ by TGX-221 impaired AG/UnAG antiatrophic activity while not affecting IGF-1 protection (Figure 2G). The involvement of PI3Kβ in AG/UnAG antiatrophic activity was further supported by the finding that TGX-221 prevented AG/UnAG from reducing dexamethasone-induced Atrogin-1 expression (Figure 2H). Together, these data strongly suggest that AG/UnAG acts through GPCR-dependent signaling pathways involving a PI3K isoform distinct from that of IGF-1.

Glucocorticoids induce muscle mass reduction by also upregulating the expression of myostatin, a TGF-β family member that acts as a negative regulator of muscle mass. Myostatin reduces the

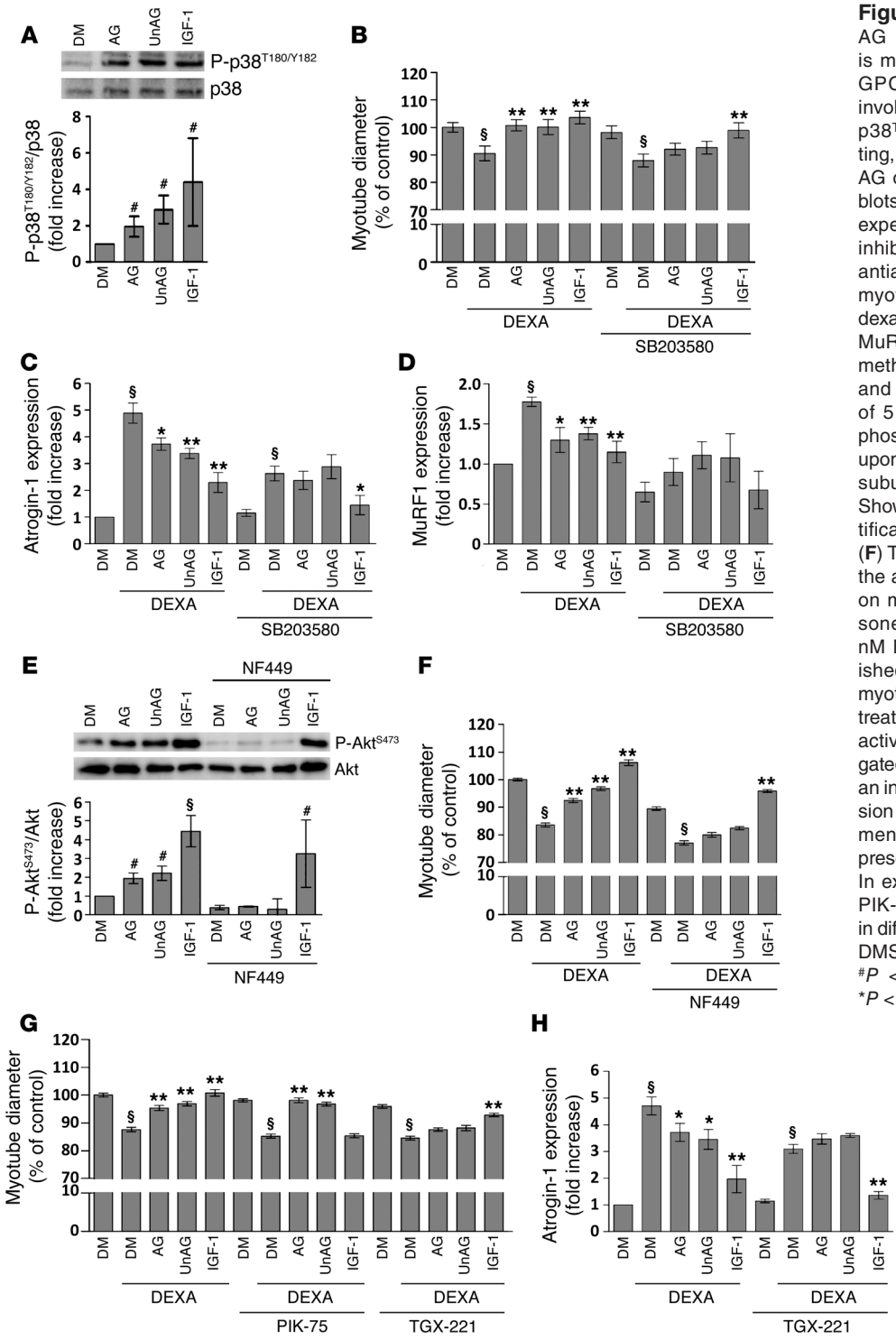

Figure 2

AG and UnAG antiatrophic signaling is mediated by p38 and acts through a GPCR-dependent signaling pathway involving PI3Kβ. (**A**) Phosphorylation of $p38^{T180/Y182}$, detected by Western blotting, after 20-minute treatment with 1 μM AG or UnAG. Shown are representative blots and quantification of 3 independent experiments. (**B**) Treatment with the p38 inhibitor SB203580 (5 μM) reverted the antiatrophic activity of AG and UnAG on myotube diameter upon treatment with dexamethasone. (**C** and **D**) Atrogin-1 and MuRF1 expression analysis upon dexamethasone treatment with or without AG and UnAG in the presence or absence of 5 μM SB203580. (**E**) AG and UnAG phosphorylation of Akt^{S473} was abolished upon treatment with 10 μM NF449, a $G\alpha_s$ subunit–selective G protein antagonist. Shown are representative blots and quantification of 3 independent experiments. (**F**) Treatment with 10 μM NF449 reverted the antiatrophic activity of AG and UnAG on myotube diameter upon dexamethasone treatment. (**G**) Treatment with 25 nM PIK-75, an inhibitor of PI3Kα, abolished the antiatrophic effect of IGF-1 on myotube diameter upon dexamethasone treatment, without affecting AG and UnAG activity. The antiatrophic effect was abrogated by treatment with 200 nM TGX-221, an inhibitor of PI3Kβ. (**H**) Atrogin-1 expression analysis upon dexamethasone treatment with AG, UnAG, and IGF-1 in the presence or absence of 200 nM TGX-221. In experiments with SB203580, NF449, PIK-75, and TGX-221, control myotubes in differentiation medium were treated with DMSO, a vehicle for all these compounds. $^{\#}P < 0.05$, $^{\S}P < 0.01$ vs. DM control; $^{*}P < 0.05$, $^{**}P < 0.01$ vs. DEXA treatment.

size of human skeletal muscle cell–derived myotubes by reducing mTOR/Akt/p70S6K signaling, while simultaneous treatment with IGF-1 restores myotube size, Akt phosphorylation, and protein synthesis (41, 42). In C2C12 myotubes, dexamethasone treatment actually induced the expression of myostatin, which was significantly reduced by IGF-1. However, AG/UnAG had no effect on myostatin expression (Supplemental Figure 1C), providing further evidence that ghrelin and IGF-1 inhibit muscle atrophy through distinct, partially overlapping, mechanisms.

Tg mice with high levels of circulating UnAG are protected from fasting- and denervation-induced atrophy. To verify in vivo the relevance of the findings described above, we used a strain of Tg mice with cardiac-specific ghrelin gene (*Ghrl*) expression. In these mice (referred to herein as *Myh6/Ghrl*), *Ghrl* overexpression in the heart results in

Table 1
Phenotypical characterization of *Myh6/Ghrl* mice

	WT	*Myh6/Ghrl*
UnAG (pg/ml)	445.4 ± 155	25,000.5 ± 360[A]
AG, fed (pg/ml)	41.7 ± 1.6	39.3 ± 1.5
AG, fasted (pg/ml)	75.7 ± 8.8	68.2 ± 9.5
IGF-1, fed (ng/ml)	748.5 ± 56	765.5 ± 120
IGF-1, fasted (ng/ml)	398 ± 93	328 ± 37
Insulin (pg/ml)	571 ± 58	631 ± 129
Tibial length (mm)	19.65 ± 0.11	19.62 ± 0.22
Nasoanal length (mm)	91.59 ± 0.51	90.61 ± 0.95
BMI, fed (g/cm^2)	3.32 ± 0.12	3.33 ± 0.08
BMI, fasted (g/cm^2)	2.93 ± 0.06	2.92 ± 0.09
Gastrocnemius weight, fed (mg)	134.86 ± 4.6	137.2 ± 5.62
Gastrocnemius weight, fasted (mg)	118 ± 4	124 ± 3.1
Gastrocnemius weight/tibial length, fed (mg/mm)	6.86 ± 0.22	6.99 ± 0.25
Gastrocnemius weight/tibial length, fasted (mg/mm)	5.89 ± 0.14	6.36 ± 0.15[B]
Heart weight, fed (mg)	117.5 ± 11.8	122 ± 6.8
Heart weight, fasted (mg)	103.0 ± 7.1	105 ± 3.3
Heart weight/nasoanal length, fed (mg/mm)	1.22 ± 0.12	1.28 ± 0.08
Heart weight/nasoanal length, fasted (mg/mm)	1.16 ± 0.07	1.16 ± 0.03
Daily food intake (g)	4.66 ± 0.17	4.73 ± 0.07
Daily food intake, denervated (g)	4.60 ± 0.17	4.60 ± 0.18

Measurements were performed as described in Methods. Muscle mass and tibial length were calculated as the mean of right and left hindlimbs. $n = 7$ per group (fed); 4 per group (fasted 48 hours); 5 per group (denervated). Data are mean ± SEM. [A]$P < 0.01$ vs. WT. [B]$P < 0.05$ vs. WT.

a 50-fold increase of circulating UnAG, without affecting AG levels (Table 1), as previously observed in other *Ghrl*-overexpressing Tg mice (43–45). *Ghrl* mRNA overexpression was restricted to the myocardium of *Myh6/Ghrl* mice, without leakage in the skeletal muscle (Supplemental Figure 2A). Moreover, consistent with the inability of UnAG to activate GHSR-1a and to promote GH release and adiposity, *Myh6/Ghrl* mice did not feature any change in circulating IGF-1 concentration, tibial and nasoanal length, BMI, or food intake compared with their WT littermates. In addition, fasting decreased IGF-1 and increased ghrelin circulating concentrations to the same extent in WT and *Myh6/Ghrl* mice (Table 1). These data strongly indicate that the upregulation of circulating UnAG in *Myh6/Ghrl* mice does not activate GHSR-1a in the pituitary and hypothalamus, stimulate the GH/IGF-1 axis, or affect endogenous ghrelin regulation. Moreover, tissue expression of IGF-1, which in skeletal muscle may act locally in a paracrine/autocrine manner (46), was not altered in *Myh6/Ghrl* mice, either in fed or in fasted animals (Supplemental Figure 2B).

Although AG and UnAG differently regulate insulin release and sensitivity (47), basal insulin level, glucose uptake, and insulin sensitivity were not affected in *Myh6/Ghrl* mice (Table 1 and Supplemental Figure 2, C and D).

Notably, compared with WT animals, fed *Myh6/Ghrl* mice did not feature any difference in heart and gastrocnemius muscle weight (Table 1), fiber cross-sectional area (CSA) distribution, or hindlimb force (as measured by grasping test; Supplemental Figure 2, E and F), which indicates that high levels of circulating UnAG do not induce skeletal muscle hypertrophy in vivo, consistent with the inability of UnAG to induce hypertrophy in C2C12-derived myotubes.

To investigate whether UnAG might protect from muscle wasting, we induced skeletal muscle atrophy by food deprivation. After 48 hours of fasting, gastrocnemius weight was decreased by approximately 14% in WT mice, and by approximately 9% in *Myh6/Ghrl* mice, compared with fed animals (Figure 3A), which indicates that increased circulating UnAG results in 30% protection from fasting-induced loss in gastrocnemius mass. Accordingly, gastrocnemii CSA was reduced by 29% in WT mice and by 19% in *Myh6/Ghrl* mice compared with fed animals (Figure 3B), indicative of 34% protection. Similarly, extensor digitorum longus (EDL) muscle weight and mean fiber area of *Myh6/Ghrl* mice was reduced to a lesser extent than in WT animals (Figure 3, D and E). This protection was reflected by shift in CSA distributions of gastrocnemii and EDL — toward fibers with wider area — in *Myh6/Ghrl* compared with WT mice under fasting conditions (Figure 3, C and F).

After 48 hours of fasting, Atrogin-1 and MuRF1 expression in gastrocnemii of WT animals dramatically increased. In *Myh6/Ghrl* mice, the induction of Atrogin-1 was significantly reduced by one-third, while MuRF1 was only slightly, not significantly, decreased (Figure 3, G and H).

Plasma levels of glycerol and FFAs did not change in fasted *Myh6/Ghrl* and WT mice (Supplemental Figure 2, G and H), which indicates that fasting did not significantly affect either glycerol or FFA concentrations, consistent with previous reports in the FVB mouse background (48, 49). Moreover, hepatic phosphoenolpyruvate carboxykinase (PEPCK) expression was induced to the same extent in fasted *Myh6/Ghrl* and WT littermates (Supplemental Figure 2I). Together, these data suggest that muscle wasting–resistant properties of *Myh6/Ghrl* mice do not depend on effects of UnAG on energy balance.

Furthermore, *Myh6/Ghrl* mice were protected from denervation-induced muscle atrophy, an experimental procedure that does not affect animal daily food intake (Table 1). At 7 and 14 days after denervation, gastrocnemii weight of WT animals was reduced by 21% and 27%, respectively, while the loss of muscle weight in *Myh6/Ghrl* animals was significantly lower (Figure 4A). Consistently, gastrocnemii mean fiber CSA of WT animals was remarkably reduced at both 7 and 14 days after denervation, whereas CSA in *Myh6/Ghrl* animals was reduced to a lesser extent (Figure 4B). At 7 days after denervation, *Myh6/Ghrl* mice featured a mild shift of gastrocnemii CSA distribution that became impressive after 14 days (Figure 4, C and D). A strong inhibition of atrophy at 7 days after denervation was also evident in EDL (Figure 4, E and F) and tibialis anterior (TA) muscles (Figure 4, G and H).

Moreover, in gastrocnemii of *Myh6/Ghrl* mice, the induction of Atrogin-1 was reduced by 40% (Figure 4I). Conversely, MuRF1 was only slightly, not significantly, reduced (Figure 4J), consistent with the fasting-induced atrophy data. Together, these observations indicated that constitutive high levels of UnAG impair experimentally induced atrophy in vivo, likely through a mechanism independent of GHSR-1a and activation of the GH/IGF-1 axis.

UnAG pharmacological treatment induces antiatrophic signaling in muscle and inhibits fasting- and denervation-induced atrophy. Acute

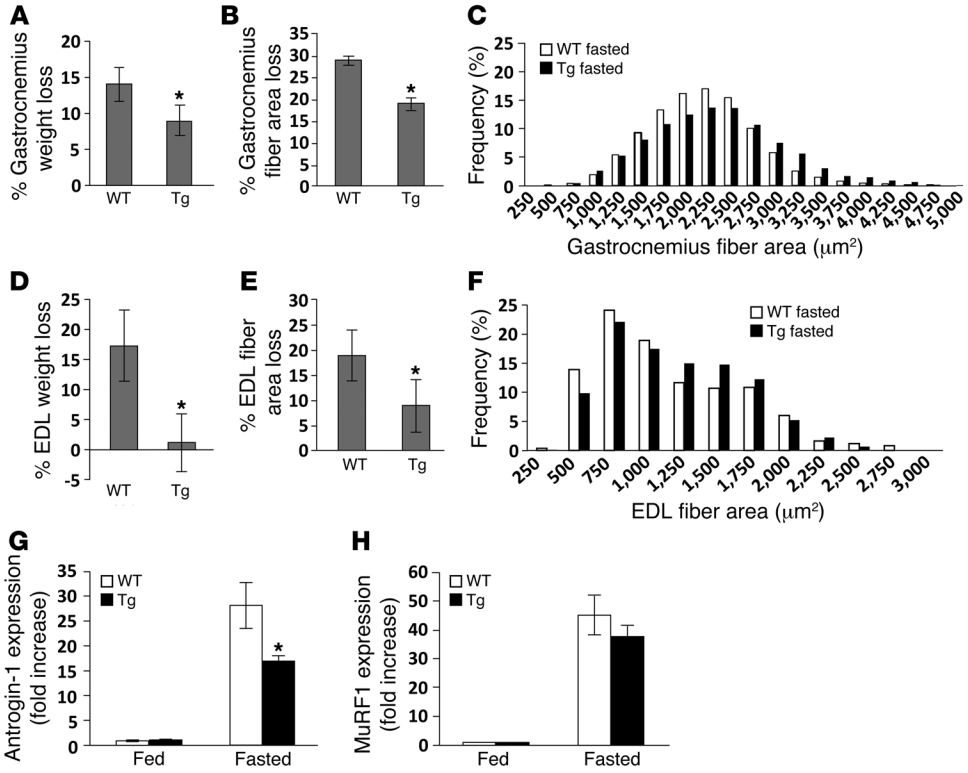

Figure 3

Myh6/Ghrl mice are protected from skeletal muscle atrophy induced by 48 hours of fasting. (**A**–**C**) Effect of fasting on gastrocnemii. Mean percentage of gastrocnemius weight loss (**A**) and CSA reduction (**B**) of fasted *Myh6/Ghrl* (Tg) mice and WT littermates compared with fed animals. (**C**) Frequency distribution of gastrocnemii CSA of fasted *Myh6/Ghrl* and WT mice. (**D**–**F**) Effect of fasting on EDL muscles. Mean percentage of EDL muscle weight loss (**D**), CSA reduction (**E**), and CSA frequency distribution (**F**) of fasted *Myh6/Ghrl* and WT littermates. (**G** and **H**) Atrogin-1 and MuRF1 expression in gastrocnemii of fed and fasted *Myh6/Ghrl* mice and their WT littermates, determined by real-time RT-PCR. *$P < 0.01$ vs. WT. $n = 7$ (fed WT and *Myh6/Ghrl*); 5 (fasted WT); 6 (fasted *Myh6/Ghrl*); 3 (CSA loss and distribution, WT and *Myh6/Ghrl*).

administration of exogenous UnAG at 100 μg/kg, a dose previously used for in vivo studies (6), induced phosphorylation of Akt^{S473}, $FoxO3a^{T32}$, and $p38^{T180/Y182}$ in WT gastrocnemii (Figure 5, A–C), which indicates that, in vivo, UnAG activates the same antiatrophic signaling pathway as it does in C2C12 myotubes.

Repeated administration (every 12 hours) of UnAG protected mice from skeletal muscle atrophy induced by either fasting or denervation (Figure 5, D–I). UnAG treatment preserved gastrocnemii from weight and mean fiber CSA loss (Figure 5, D and E). Accordingly, frequency distribution of gastrocnemii CSA of fasted mice injected with UnAG showed a dramatic shift toward bigger fiber areas compared with saline-injected mice (Figure 5F).

Similarly, UnAG treatment of denervated mice resulted in a 25% protection from gastrocnemius weight loss and a significantly lower decrease of mean fiber CSA, although the CSA distribution of UnAG-injected mice showed only a very mild shift compared with saline-injected animals (Figure 5, G–I). Although the plasma concentration of UnAG after injection dropped to basal levels in about 2–4 hours (Supplemental Figure 3A), these data indicate that repeated acute stimulation is sufficient to protect from experimentally induced skeletal muscle atrophy without affecting muscular IGF-1 expression (Supplemental Figure 3B).

AG and UnAG induce antiatrophic signaling and impair muscle atrophy in Ghsr$^{-/-}$ *mice*. The findings reported above, along with previous data on common binding sites for AG/UnAG in C2C12 lacking *Ghsr* (16), strongly suggest that AG and UnAG stimulate antiatrophic signaling in skeletal muscle through activation of a receptor distinct from GHSR-1a. To verify this hypothesis, we assayed AG/UnAG antiatrophic signaling and activity in *Ghsr*$^{-/-}$ mice, in which AG fails to activate the GH/IGF-1a axis or stimulate appetite (50). Injection of either AG or UnAG induced Akt^{S473} phosphorylation in gastrocnemii of *Ghsr*$^{-/-}$ mice (Figure 6A). Consistently, treatment of *Ghsr*$^{-/-}$ mice with 100 μg/kg AG or UnAG twice daily reduced gastrocnemii weight loss induced by 48-hour fasting by 30% compared with saline-treated animals (Figure 6B). Moreover, the mean CSA loss of AG- and UnAG-injected mice strongly decreased compared with saline-injected animals, and CSA distribution shifted toward bigger areas (Figure 6, C and D).

In summary, these findings demonstrated that both AG and UnAG activate a direct antiatrophic signaling pathway in skeletal muscle and protect from experimentally induced muscle atrophy, independently of the AG receptor GHSR-1a.

Discussion

Several studies have shown that AG protects from cachexia and prevents muscle proteolysis in vivo, supposedly through stimulation of appetite and activation of the GH/IGF-1 axis mediated by AG binding to GHSR-1a (6, 7, 18–21). However, here we provided in vitro and in vivo evidence that AG and UnAG exert antiatrophic activity by acting directly on the skeletal muscle, even in *Ghsr*$^{-/-}$ mice.

Upregulation of circulating UnAG, which does not bind GHSR-1a and does not activate the GH/IGF-1 axis, counteracted muscle atrophy induced by either fasting or denervation. Consistently, UnAG has been reported to reduce burn-induced skeletal muscle proteolysis and local TNF-α upregulation (51).

We achieved upregulation of circulating UnAG either by myocardial *Ghrl* overexpression in *Myh6/Ghrl* mice or by repeated administration. The antiatrophic activity of UnAG cannot be mediated by its conversion to AG in the plasma, since acylation occurs only intracellularly on the ghrelin precursor by the ghrelin-specific acyltransferase GOAT (11, 12). The negligible myocardial expression of GOAT might explain the increase of only the unacylated form

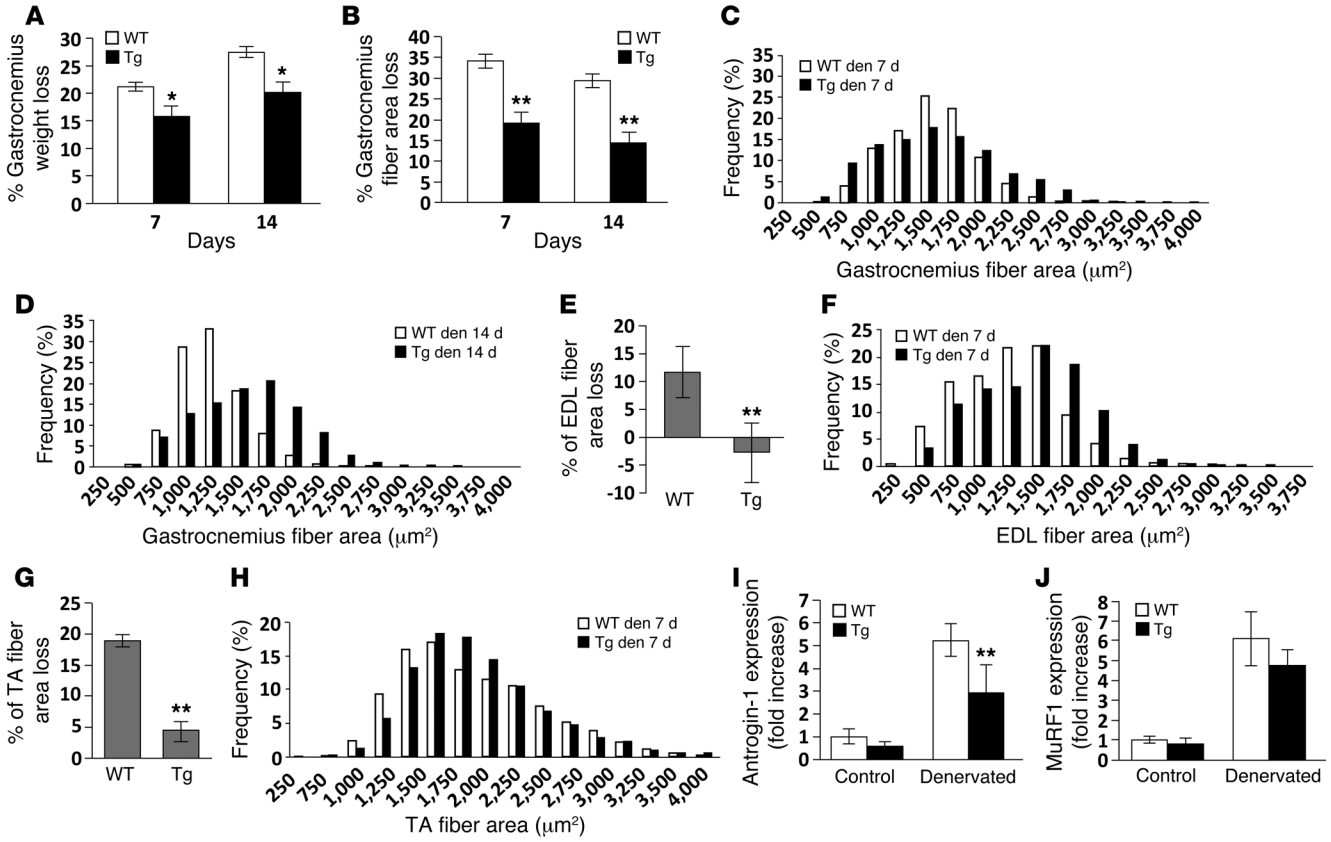

Figure 4

Myh6/Ghrl mice are protected from denervation-induced skeletal muscle atrophy induced by sciatic nerve resection. (**A** and **B**) Mean percentage of weight loss (**A**) and CSA reduction (**B**) of denervated gastrocnemius at 7 and 14 days after denervation, compared with the unperturbed side. (**C** and **D**) Frequency distribution of gastrocnemii CSA at 7 and 14 days after denervation in *Myh6/Ghrl* and WT mice. (**E**–**H**) CSA reduction and fiber area distribution of (**E** and **F**) EDL and (**G** and **H**) TA muscles at 7 days after denervation. (**I** and **J**) Atrogin-1 and MuRF1 expression, determined by real-time RT-PCR, in denervated gastrocnemii at 7 days after denervation, compared with the unperturbed side. $^{**}P < 0.01$, $^{*}P < 0.05$ vs. WT. $n = 6$ (WT); 5 (*Myh6/Ghrl*); 3 (CSA loss and distribution, WT and *Myh6/Ghrl*).

of circulating ghrelin in *Myh6/Ghrl* mice. This is in agreement with other tissue-specific *Ghrl* Tg mice featuring high UnAG circulating levels in the absence of significant changes of AG (43–45).

The observations that *Myh6/Ghrl* mice did not feature any change in circulating and muscular IGF-1 or in tibial or whole body length, along with the lack of skeletal muscle hypertrophy, further indicate that the GH/IGF-1 axis is not activated in these mice. Finally, the finding that both AG and UnAG impaired skeletal muscle atrophy in *Ghsr*$^{-/-}$ mice indicated that their antiatrophic activity is mediated by a receptor distinct from GHSR-1a. In these mice, AG exerted antiatrophic activity in the skeletal muscle independent of its role in modulating GH release and energy balance. Nevertheless, these data do not exclude the possibility that in WT animals, GHSR-1a may contribute to the antiatrophic activity of AG by also regulating the GH/IGF-1 axis and positive energy balance. For instance, AG has been suggested to prevent downregulation of muscular IGF-1 expression in an experimental model of cachexia through an indirect mechanism involving GHSR-1a activity on positive energy balance (20).

The hypothesis that AG/UnAG impairs muscle atrophy in vivo by acting directly on the skeletal muscle is further supported by our finding that UnAG administration rapidly stimulated antiatrophic signaling in the gastrocnemius. Moreover, AG/UnAG activated antiatrophic signaling in cultures of C2C12 myotubes, which do not express GHSR-1a, protecting them from dexamethasone-induced atrophy and atrogene upregulation. Although AG has previously been reported to fail in reducing dexamethasone-induced Atrogin-1 expression in C2C12 myotubes (20), the 10-fold lower dexamethasone concentration used in that study and the considerably weaker Atrogin-1 induction may explain the different results. Conversely, Sheriff et al. showed that UnAG reduces TNF-α/IFN-γ–induced cachexia in C2C12 myotubes in a PI3K/mTOR-dependent manner (51). The results of our present study not only confirmed the involvement of PI3K/mTOR pathways in AG/UnAG activity on skeletal muscle, but also showed the specific contribution of the mTORC2- over the mTORC1-mediated signaling pathway, which may explain, at least in part, the ability of AG/UnAG to protect from skeletal muscle atrophy without a concomitant induction of hypertrophy.

Indeed, the molecular mechanisms underlying AG/UnAG antiatrophic activity in the skeletal muscle involved the activation of mTORC2-mediated signaling pathways, leading to phosphorylation of Akt^{S473} and of its substrate FoxO3a^{T32}, which eventually impaired Atrogin-1 expression and muscle protein degradation. At

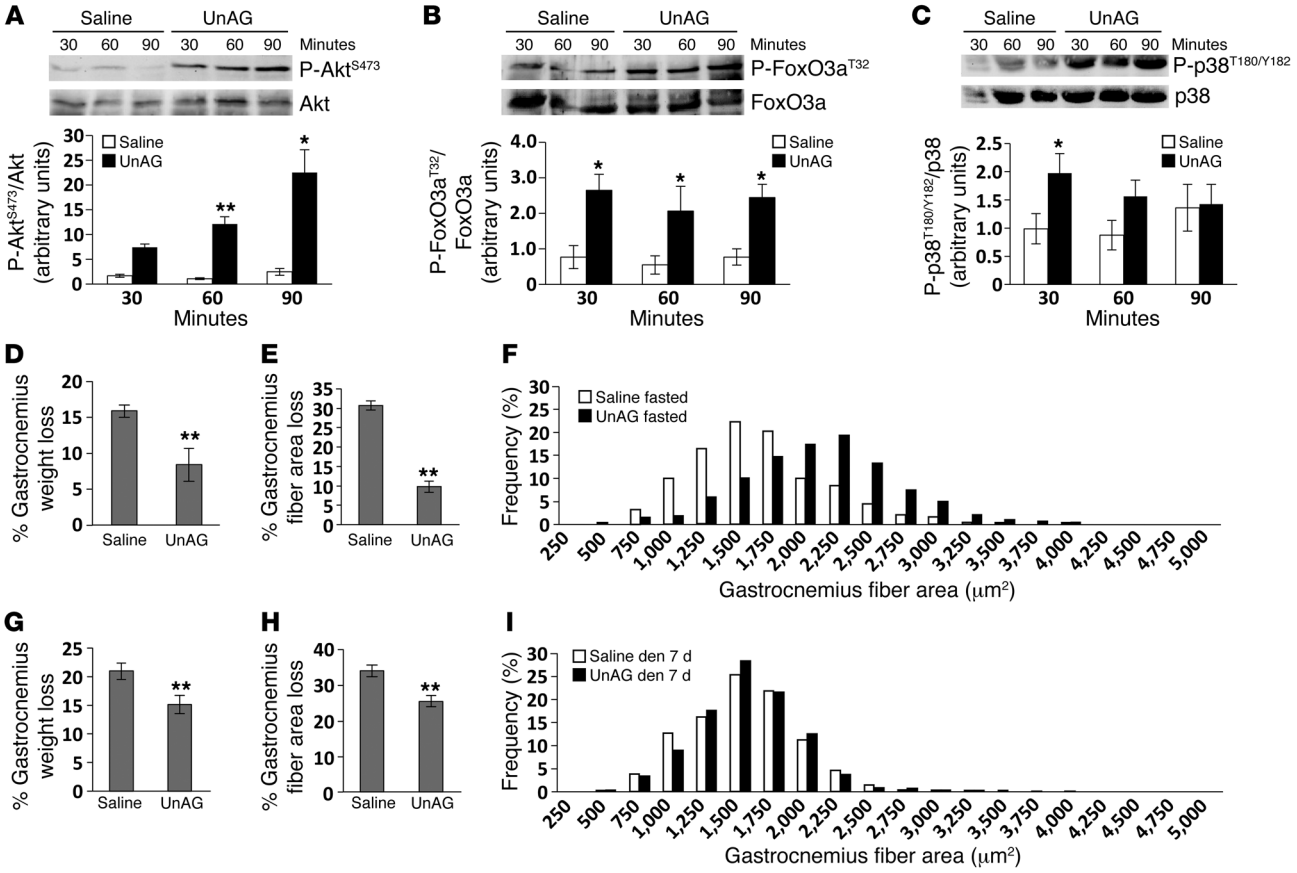

Figure 5

UnAG pharmacological treatment protects skeletal muscle from fasting- and denervation-induced atrophy in WT mice. (**A**–**C**) Phosphorylation of Akt^{S473}, FoxO3a^{T32}, and p38$^{T180/Y182}$ in gastrocnemii of WT mice treated with 100 μg/kg UnAG or saline. At the indicated time points, gastrocnemii were removed and processed for Western blot analysis. Shown are representative blots and densitometric analysis of 3 independent experiments, normalized to untreated animals (not shown). (**D**–**F**) Mean percent weight loss (**D**), CSA reduction (**E**), and CSA frequency distribution (**F**) of gastrocnemii from fed or 48-hour fasted mice treated twice daily with 100 μg/kg UnAG or saline (n = 5 per group). Frequency distribution was measured in 3 mice per group. In **D** and **E**, percent reduction shown is between fasted and fed mice. (**G**–**I**) Mean percent weight loss (**G**), CSA reduction (**H**), and CSA frequency distribution (**I**) of gastrocnemii from mice treated with 100 μg/kg UnAG or saline twice daily for 7 days after sciatic nerve resection (n = 5 per group). Frequency distribution was measured in 3 mice per group. In **G** and **H**, percent reduction shown is between denervated gastrocnemii and gastrocnemii from the unperturbed side. *P < 0.05, **P < 0.01 vs. saline treatment.

the same time, in C2C12 myotubes, AG/UnAG failed to stimulate mTORC1-mediated phosphorylation of S6K^{T389} and S6$^{S235/236}$, protein synthesis, and hypertrophy. Consistently, chronic upregulation of circulating UnAG in *Myh6/Ghrl* mice did not induce muscle hypertrophy. This finding highlights a remarkable difference between the antiatrophic activities of AG/UnAG and IGF-1 in the skeletal muscle, as IGF-1 stimulates both mTORC2-mediated impairment of protein degradation and mTORC1-dependent stimulation of protein synthesis and hypertrophy (23–26). Consistently, in TNF-α/IFN-γ–treated C2C12 myotubes, UnAG inhibited protein catabolism and impaired the induction of Atrogin-1 and MuRF1. Moreover, UnAG restored the basal phosphorylation state of proteins of mTORC1 and mTORC2 pathways, although the lack of UnAG-induced increase in Akt^{S473} phosphorylation observed herein may depend on receptor desensitization, given the higher concentration of UnAG used and the protracted treatment (51).

The finding that downregulation of the mTORC1-specific component raptor did not affect the antiatrophic activity of AG/UnAG, while impairing IGF-1 antiatrophic activity, further supports the conclusion that AG/UnAG antiatrophic activity does not involve mTORC1-mediated stimulation of protein synthesis. On the other hand, the finding that AG/UnAG antiatrophic activity was sensitive to downregulation of rictor, the specific component of mTORC2, demonstrated the key role of mTORC2 in mediating AG/UnAG antiatrophic activity. The finding that ghrelin-induced phosphorylation of Akt^{S473} was uncoupled from the activation of mTORC1-mediated pathways and hypertrophy may appear controversial, as IGF-1–induced phosphorylation of Akt^{S473} is associated with the activity of both mTOR complexes (29), and overexpression of constitutive active Akt in the skeletal muscle prevents denervation-induced atrophy and induces hypertrophy (22, 52). The lack of muscle hypertrophy observed in *Myh6/Ghrl* mice may depend on weaker stimulation of the PI3K/Akt pathway by UnAG. Indeed, although tissue-specific expression of constitutive active Akt in Tg mice induces strong phosphorylation of Akt and of its substrates (53), phosphorylation of Akt was not detectable in

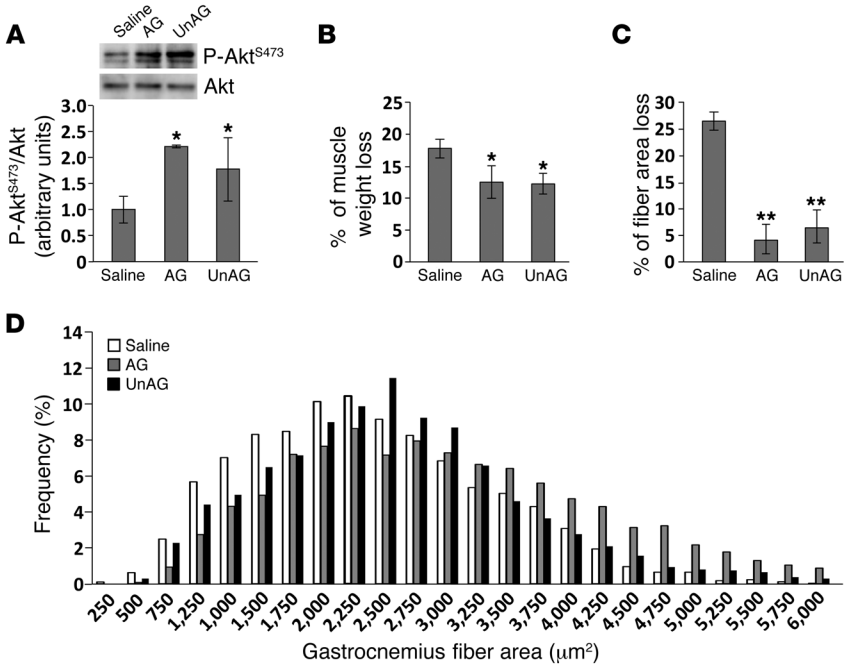

Figure 6
AG and UnAG pharmacological treatment of *Ghsr*$^{-/-}$ mice induces antiatrophic signaling and protects from fasting-induced skeletal muscle atrophy. (**A**) Phosphorylation of Akt^{S473} in gastrocnemii of *Ghsr*$^{-/-}$ mice injected with 100 μg/kg AG or UnAG or with saline. 60 minutes after treatment, gastrocnemii were removed and processed for Western blot analysis. Shown are representative blots and densitometric analysis of 3 independent experiments. (**B**–**D**) Mean percentage weight loss (**B**), CSA reduction (**C**), and CSA frequency distribution (**D**) of gastrocnemii from fed or 48-hour fasted *Ghsr*$^{-/-}$ mice injected s.c. twice daily with 100 μg/kg AG or UnAG or with saline (n = 5 per group). Frequency distribution was measured in 3 mice per group. In **B** and **C**, percent reduction is between fasted and fed mice. *P < 0.05, **P < 0.01 vs. saline treatment.

muscles of *Myh6/Ghrl* mice (data not shown). Indeed, we found that 2 distinct PI3K isoforms, namely PI3Kβ and PI3Kα, mediated the antiatrophic activity of AG/UnAG and IGF-1, respectively. This observation, along with the ability of a $G\alpha_s$-uncoupling drug to abolish the antiatrophic activity of AG/UnAG, but not IGF-1, is consistent with the hypothesis that the unknown receptor mediating the common activities of AG/UnAG is a GPCR (9). Moreover, these data further serve to rule out the hypothesis that AG/UnAG acts on myotubes by stimulating the autocrine release of IGF-1.

The inability of AG and UnAG to stimulate protein synthesis and hypertrophy in the skeletal muscle is consistent with their key role in the adaptive response to fasting and negative energy balance (13). The molecular mechanisms underlying the uncoupling of mTORC2 from mTORC1 remain to be investigated. AG and UnAG, which are released during fasting, might shift muscle metabolism toward amino acid oxidation, thereby decreasing the intracellular pool of free amino acids essential for mTORC1 activity (29). Alternatively, activation of PI3Kβ, whose enzymatic activity is lower than that of PI3Kα (54), may result in weaker activation of Akt. Finally, AMPK, which negatively regulates mTORC1 in skeletal muscle (55), may contribute to mTORC1 uncoupling, although AG was reported to be unable to stimulate AMPK in rat gastrocnemius (56).

The finding that p38 was required for AG/UnAG antiatrophic activity is consistent with previous findings that p38 cooperates with PI3K/Akt pathways to induce C2C12 differentiation (16, 57). However, the role of p38 in regulating muscle atrophy is complex, as its activation mediates muscle atrophy induced by oxidative stress and inflammatory cytokines (34, 36, 58). The role of p38 in signaling is determined by its association in distinct signaling complexes with different regulators and substrates and by its localization (35). Our findings are consistent with evidence indicating that, in myotubes, decreased p38 phosphorylation is associated with dexamethasone-induced atrophy, and that p38 mediates β-hydroxyl-β-methylbutyrate protection from dexamethasone-induced protein degradation (59, 60). Moreover, p38 activity can regulate cytoplasmic localization of FoxO3a independently of Akt, thereby impairing its transcriptional activity and Atrogin-1 induction (33, 61). Furthermore, activation of p38 stabilizes and activates the transcriptional coactivator PGC1α, which represses FoxO3a activity (62, 63). Although IGF-1 activated p38, this was dispensable for IGF-1 antiatrophic activity. In addition, IGF-1 and AG/UnAG antiatrophic activities differed in the inability of AG/UnAG to downregulate myostatin, a TGF-β–like inhibitor of muscle growth, which further supports the hypothesis that AG/UnAG and IGF-1 counteract muscle atrophy through distinct molecular mechanisms.

The data presented herein unveiled a novel component of the complex role of AG/UnAG, i.e., the direct activation of antiatrophic pathways in the skeletal muscle, eventually leading to reduced muscle wasting. This effect adds to the well-known capabilities of AG to stimulate appetite, regulate lipid metabolism, and release GH. Although the identity of the novel AG/UnAG receptor is yet unknown, these findings may have important biological and therapeutic implications, since they provide proof that UnAG has a strong and specific potential for the prevention or treatment of muscle atrophy, avoiding the diabetogenic side effects of AG (47) and the cancer risk associated with IGF-1 treatment (64).

Methods

Reagents. AG_{1-28} and $UnAG_{1-28}$ were purchased from PolyPeptide Laboratories. The PI3K p110α inhibitor PIK-75 hydrochloride was purchased from Axon Medchem, and the PI3K p110β inhibitor TGX-221 was a gift from U. Galli (Synthetic Medicinal Chemistry group, Università del Piemonte Orientale, Novara, Italy). Water-soluble dexamethasone and all other reagents, unless otherwise stated, were from Sigma-Aldrich. Anti–phospho-Akt^{S473}, anti-Akt, anti–phospho-FoxO3a^{T32}, anti-FoxO3a, anti–phospho-S6K^{T389}, anti-S6K, anti–phospho-S6$^{S235/236}$, anti-S6, anti-p38$^{T180/Y182}$, anti-p38, anti-raptor, and anti-rictor antibodies were from Cell Signaling Technology; anti-actin antibody was from Santa Cruz Biotechnology.

Cell cultures and myotube analysis. C2C12 myoblasts were differentiated in myotubes as previously described (16). For measurement of myotube diam-

eters, myotubes were fixed, and diameters were quantified by measuring a total of >100 myotube diameters from 5 random fields in 3 replicates at ×40 magnification using Image-Pro Plus software (MediaCybernetics) as described previously (24).

Raptor and rictor silencing. Raptor siRNA (*MISSION pre-designed siRNA* SASI_Mm01_00055293; Sigma-Aldrich), rictor siRNA (SASI_Mm01_00137731; Sigma-Aldrich), Block-iT, or siRNA negative control sequence (Invitrogen) were transfected with Lipofectamine2000 (Invitrogen) in C2C12 myotubes. Transfection efficiency was evaluated by the fluorescent siRNA negative control Block-iT, and silencing was verified by Western blot.

[^{3}H]-leucine incorporation assay. C2C12 myotubes were maintained for 24 hours with or without 10 nM AG or UnAG in differentiation medium supplemented with 2 μCi/ml [^{3}H]-leucine (Perkin Elmer) to evaluate the induction of protein synthesis. At the end of treatments, cells were washed with PBS, treated with 5% trichloroacetic acid, and lysed with 0.5 M NaOH and 0.5% SDS. The amount of incorporated [^{3}H]-leucine was evaluated by β counter (Tri-Carb 2800TR; Perkin Elmer) analysis. Data are the average of 4 replicates.

Western blot. C2C12 myotubes were serum starved overnight and then treated as indicated in the figure legends. Western blot was performed as previously described (16). Unless otherwise specified, after use of anti–phospho-specific antibodies, membranes were stripped with Re-Blot Plus (Chemicon, Millipore) and reblotted with the corresponding total protein antibodies.

Muscles of mice fasted for 6 hours were s.c. injected with 100 μg/kg UnAG or AG or with saline solution. At the indicated time points, gastrocnemii were removed, homogenized at 4°C in RIPA buffer (1% Triton X-100; 1% sodium deoxycholate; 0.1% SDS; 1 mM EDTA; 1 mM EGTA; 50 mM NaF; 160 mM NaCl; and 20 mM Tris-HCl, pH 7.4) containing 1 mM DTT, protease inhibitor cocktail, and 1 mM Na_3VO_4. Homogenates were then processed as above.

Tg animal generation and treatment. All experiments were conducted on young adult male FVB1 WT, FVB1 *Myh6/Ghrl*, and C57BL/6J *Ghsr*$^{-/-}$ mice (50), matched for age and weight.

Tg animals were obtained by cloning the murine ghrelin gene (*Ghrl*) under control of the cardiac promoter sequences of the β myosin heavy chain 3′ UTR and the first 3 exons of the α isoform *Myh6* (65). Transgene integration and expression were confirmed by PCR and real-time RT-PCR, respectively. Phenotypical characterization and experiments were carried out on hemizygote animals and littermate controls.

AG, UnAG, and IGF-1 plasmatic levels were measured by EIA kits (SPIbio Bertin Pharma for AG and UnAG; R&D Systems for IGF-1); insulin plasmatic levels were quantified with the Insulin (mouse) ELISA kit (ALPCO Diagnostics); and glycerol and free fatty acid plasmatic levels were evaluated by enzymatic assay kits (Cayman).

BMI was calculated as animal weight divided by the square of the nasoanal length.

Fasting-induced atrophy was achieved by 48 hours of food removal (63), while denervation-induced muscle atrophy was obtained by resection of the sciatic nerve under anesthesia with sevoflurane (Baxter) and evaluated 7 and 14 days later (66). Muscles were collected, weighed, and normalized for tibial length and processed either for RNA extraction or for histology.

Daily food intake was measured over a 12-day period, quantifying the food consumption of each mouse every day.

In all experiments with s.c. injection of AG and/or UnAG, controls were saline-injected animals.

Glucose and insulin tolerance tests. Glucose tolerance and insulin sensitivity tests were performed as previously described (43). For glucose tolerance evaluation, mice were injected i.p. with glucose at 1.5 mg/g body weight at 9:00 am, after 16 hours of fasting. Blood glucose was determined at the indicated time points on tail blood samples using the Accu-Chek Mobile blood glucose meter (Roche Diagnostics). For insulin sensitivity determination, Humulin R (0.75 U/kg body weight; Lilly) was administered i.p., and blood samples for glucose concentrations were collected as described above.

RNA extraction and analysis. Total RNA from cultured myotubes and from muscles was extracted by TRIreagent (Invitrogen). The RNA was retro-transcribed with High-Capacity cDNA Reverse Transcription Kit (Invitrogen), and real-time PCR was performed with the ABI7200 Sequence Detection System (Invitrogen) using the following assays: Mm00499518_m1 (*Fbxo32*, Atrogin-1), Mm01185221_m1 (*Trim63*, MuRF1), Mm00439560_m1 (*Igf1*), Mm00445450_m1 (*Ghrl*), Mm01254559_m1 (*Mstn*), Mm01247058_m1 (*Pck1*), Mm00446953_m1 (*Gusb*), and Mm00506384_m1 (*Ppif*).

Muscle sampling and staining for fiber size assessment. Muscles were embedded in Killik compound (Bio-optica) and frozen in liquid nitrogen–cooled isopentane. Serial transverse cryosections (7 μm thick) of the midbelly region of muscles were cut at –20°C and mounted on glass slides. The sections were air-dried, fixed for 10 minutes in 4% paraformaldehyde, and stained with H&E. The number of myofibers in TA, gastrocnemii, and EDL was measured from the histological preparations. Muscle fiber CSA was assessed as previously described (67). Data are expressed as fiber size distribution and as percent CSA reduction relative to controls.

Grip strength test. Skeletal muscle force was assessed using the BS-GRIP Grip Meter (2Biological Instruments) as previously described (68). Each animal was tested 3 times, and the average value of the maximum weight that the animal managed to hold was recorded and normalized to the mouse's weight.

Statistics. Data are presented as mean ± SEM. Variation among groups was evaluated using nonparametric Wilcoxon and Mann-Whitney *U* tests. Statistical significance was assumed for *P* values less than 0.05. All statistical analyses were performed with SPSS for Windows version 17.0.

Study approval. All animal experimental procedures were approved by the Institutional Animal Care and Use Committee at Università del Piemonte Orientale "Amedeo Avogadro."

Acknowledgments

We are grateful to Riccarda Granata and Cristina Grande for insulin measurements and to Thien-Thi Nguyen, Christian Zurlo, Laura Badà, and Giulia Bettas Ardisson for technical assistance. This work was supported by Telethon (grant no. GGP030386 to A. Graziani), Regione Piemonte CIPE (to A. Graziani, S. Geuna, and I. Perroteau), Regione Piemonte Ricerca Sanitaria (to A. Graziani), Italian Ministry for University and Research (PRIN grant to A. Graziani, S. Geuna, and I. Perroteau), and Opera Pia Eletto Lualdi.

Received for publication December 23, 2011, and accepted in revised form November 1, 2012.

Address correspondence to: Nicoletta Filigheddu, Department of Translational Medicine, Università del Piemonte Orientale "Amedeo Avogadro," Via Solaroli 17, 28100 Novara, Italy. Phone: 39.0321660529; Fax: 39.0321620421; E-mail: nicoletta.filigheddu@med.unipmn.it.

Paolo E. Porporato's present address is: Unit of Pharmacology and Therapeutics, Université Catholique de Louvain, Brussels, Belgium.

Viola F. Gnocchi's present address is: Research Center for Genetic Medicine, Children's National Medical Center, Washington, DC, USA.

Federica Chianale's present address is: Oncological Sciences Department, Systems Biology Unit, IRCC, Candiolo (TO), Italy.

1. Dodson S, et al. Muscle wasting in cancer cachexia: clinical implications, diagnosis, and emerging treatment strategies. *Annu Rev Med*. 2011;62:265–279.
2. Kojima M, Hosoda H, Date Y, Nakazato M. Ghrelin is a growth-hormone-releasing acylated peptide from stomach. *Nature*. 1999;402(6762):656–660.
3. Tschöp M, Smiley DL, Heiman ML. Ghrelin induces adiposity in rodents. *Nature*. 2000; 407(6806):908–913.
4. Nakazato M, Murakami N, Date Y, Kojima M. A role for ghrelin in the central regulation of feeding. *Nature*. 2001;409(6817):194–198.
5. Howard AD, Feighner SD, Cully DF, Arena JP. A receptor in pituitary and hypothalamus that functions in growth hormone release. *Science*. 1996; 273(5277):974–977.
6. Nagaya N, et al. Chronic administration of ghrelin improves left ventricular dysfunction and attenuates development of cardiac cachexia in rats with heart failure. *Circulation*. 2001;104(12):1430–1435.
7. Nagaya N, et al. Effects of ghrelin administration on left ventricular function, exercise capacity, and muscle wasting in patients with chronic heart failure. *Circulation*. 2004;110(24):3674–3679.
8. Baldanzi G, et al. Ghrelin and des-acyl ghrelin inhibit cell death in cardiomyocytes and endothelial cells through ERK1/2 and PI 3-kinase/AKT. *J Cell Biol*. 2002;159(6):1029–1037.
9. Granata R, et al. Acylated and unacylated ghrelin promote proliferation and inhibit apoptosis of pancreatic beta-cells and human islets: involvement of 3′,5′-cyclic adenosine monophosphate/protein kinase A, extracellular signal-regulated kinase 1/2, and phosphatidyl inositol 3-Kinase/Akt signaling. *Endocrinology*. 2007;148(2):512–529.
10. Chung H, Seo S, Moon M, Park S. Phosphatidylinositol-3-kinase/Akt/glycogen synthase kinase-3 beta and ERK1/2 pathways mediate protective effects of acylated and unacylated ghrelin against oxygen-glucose deprivation-induced apoptosis in primary rat cortical neuronal cells. *J Endocrinol*. 2008;198(3):511–521.
11. Yang J, Brown MS, Liang G, Grishin NV, Goldstein JL. Identification of the acyltransferase that octanoylates ghrelin, an appetite-stimulating peptide hormone. *Cell*. 2008;132(3):387–396.
12. Gutierrez JA, et al. Ghrelin octanoylation mediated by an orphan lipid transferase. *Proc Natl Acad Sci U S A*. 2008;105(17):6320–6325.
13. Chen C-Y, Asakawa A, Fujimiya M, Lee S-D, Inui A. Ghrelin gene products and the regulation of food intake and gut motility. *Pharmacol Rev*. 2009; 61(4):430–481.
14. Delhanty PJD, et al. Ghrelin and unacylated ghrelin stimulate human osteoblast growth via mitogen-activated protein kinase (MAPK)/phosphoinositide 3-kinase (PI3K) pathways in the absence of GHS-R1a. *J Endocrinol*. 2006;188(1):37–47.
15. Sato M, et al. Effects of ghrelin and des-acyl ghrelin on neurogenesis of the rat fetal spinal cord. *Biochem Biophys Res Commun*. 2006;350(3):598–603.
16. Filigheddu N, et al. Ghrelin and des-acyl ghrelin promote differentiation and fusion of C2C12 skeletal muscle cells. *Mol Biol Cell*. 2007;18(3):986–994.
17. Delhanty PJD, et al. Unacylated ghrelin rapidly modulates lipogenic and insulin signaling pathway gene expression in metabolically active tissues of GHSR deleted mice. *PLoS One*. 2010;5(7):e11749.
18. Nagaya N, et al. Treatment of cachexia with ghrelin in patients with COPD. *Chest*. 2005;128(3):1187–1193.
19. Balasubramaniam A, et al. Ghrelin inhibits skeletal muscle protein breakdown in rats with thermal injury through normalizing elevated expression of E3 ubiquitin ligases MuRF1 and MAFbx. *Am J Physiol Regul Integr Comp Physiol*. 2009;296(4):R893–R901.
20. Sugiyama M, et al. Ghrelin improves body weight loss and skeletal muscle catabolism associated with angiotensin II-induced cachexia in mice. *Regul Pept*. 2012;178(1–3):21–28.
21. DeBoer MD. Emergence of ghrelin as a treatment for cachexia syndromes. *Nutrition*. 2008;24(9):806–814.
22. Bodine SC, et al. Akt/mTOR pathway is a crucial regulator of skeletal muscle hypertrophy and can prevent muscle atrophy in vivo. *Nat Cell Biol*. 2001; t3(11):1014–1019.
23. Rommel C, et al. Mediation of IGF-1-induced skeletal myotube hypertrophy by PI(3)K/Akt/mTOR and PI(3)K/Akt/GSK3 pathways. *Nat Cell Biol*. 2001;3(11):1009–1013.
24. Sandri M, et al. Foxo transcription factors induce the atrophy-related ubiquitin ligase atrogin-1 and cause skeletal muscle atrophy. *Cell*. 2004;117(3):399–412.
25. Stitt TN, et al. The IGF-1/PI3K/Akt pathway prevents expression of muscle atrophy-induced ubiquitin ligases by inhibiting FOXO transcription factors. *Mol Cell*. 2004;14(3):395–403.
26. Latres E, et al. Insulin-like growth factor-1 (IGF-1) inversely regulates atrophy-induced genes via the phosphatidylinositol 3-kinase/Akt/mammalian target of rapamycin (PI3K/Akt/mTOR) pathway. *J Biol Chem*. 2005;280(4):2737–2744.
27. Bodine SC, et al. Identification of ubiquitin ligases required for skeletal muscle atrophy. *Science*. 2001;294(5547):1704–1708.
28. Foster KG, Fingar DC. Mammalian target of rapamycin (mTOR): conducting the cellular signaling symphony. *J Biol Chem*. 2010;285(19):14071–14077.
29. Laplante M, Sabatini DM. mTOR signaling in growth control and disease. *Cell*. 2012;149(2):274–293.
30. Copp J, Manning G, Hunter T. TORC-specific phosphorylation of mammalian target of rapamycin (mTOR): phospho-Ser2481 is a marker for intact mTOR signaling complex 2. *Cancer Res*. 2009; 69(5):1821–1827.
31. Sarbassov DD, et al. Prolonged rapamycin treatment inhibits mTORC2 assembly and Akt/PKB. *Mol Cell*. 2006;22(2):159–168.
32. Lamming DW, et al. Rapamycin-induced insulin resistance is mediated by mTORC2 loss and uncoupled from longevity. *Science*. 2012;335(6076):1638–1643.
33. Clavel S, Siffroi-Fernandez S, Coldefy AS, Boulukos K, Pisani DF, Dérijard B. Regulation of the intracellular localization of Foxo3a by stress-activated protein kinase signaling pathways in skeletal muscle cells. *Mol Cell Biol*. 2010;30(2):470–480.
34. Li YP, et al. TNF-alpha acts via p38 MAPK to stimulate expression of the ubiquitin ligase atrogin1/MAFbx in skeletal muscle. *FASEB J*. 2005; 19(3):362–370.
35. Cuadrado A, Nebreda AR. Mechanisms and functions of p38 MAPK signalling. *Biochem J*. 2010; 429(3):403–417.
36. McClung JM, Judge AR, Powers SK, Yan Z. p38 MAPK links oxidative stress to autophagy-related gene expression in cachectic muscle wasting. *Am J Physiol Cell Physiol*. 2010;298(3):C542–C549.
37. Kim J, et al. p38 MAPK participates in muscle-specific RING Finger 1-mediated atrophy in cast-immobilized rat gastrocnemius muscle. *Korean J Physiol Pharmacol*. 2009;13(6):491–496.
38. Hohenegger M, et al. 1998. Gsalpha-selective G protein antagonists. *Proc Natl Acad Sci U S A*. 1998; 95(1):346–351.
39. Jia S, et al. Essential roles of PI(3)K-p110beta in cell growth, metabolism and tumorigenesis. *Nature*. 2008;454(7205):776–779.
40. Ciraolo E, et al. Phosphoinositide 3-kinase p110beta activity: key role in metabolism and mammary gland cancer but not development. *Sci Signal*. 2008;1(36):ra3.
41. Morissette MR, Cook SA, Buranasombati C, Rosenberg MA, Rosenzweig A. Myostatin inhibits IGF-I-induced myotube hypertrophy through Akt. *Am J Physiol Cell Physiol*. 2009;297(5):1124–1132.
42. Trendelenburg AU, Meyer A, Rohner D, Boyle J, Hatakeyama S, Glass DJ. Myostatin reduces Akt/TORC1/p70S6K signaling, inhibiting myoblast differentiation and myotube size. *Am J Physiol Cell Physiol*. 2009;296(6):C1258–C1270.
43. Zhang W, Chai B, Li J-Y, Wang H, Mulholland MW. Effect of des-acyl ghrelin on adiposity and glucose metabolism. *Endocrinology*. 2008;149(9):4710–4716.
44. Iwakura H, et al. Analysis of rat insulin II promoter-ghrelin transgenic mice and rat glucagon promoter-ghrelin transgenic mice. *J Biol Chem*. 2005; 280(15):15247–15256.
45. Ariyasu H, et al. Transgenic mice overexpressing des-acyl ghrelin show small phenotype. *Endocrinology*. 2005;146(1):355–364.
46. Musarò A, et al. Localized Igf-1 transgene expression sustains hypertrophy and regeneration in senescent skeletal muscle. *Nat Genet*. 2001;27(2):195–200.
47. Delhanty PJ, van der Lely AJ. Ghrelin and glucose homeostasis. *Peptides*. 2011;32(11):2309–2318.
48. Mandard S, et al. The fasting-induced adipose factor/angiopoietin-like protein 4 is physically associated with lipoproteins and governs plasma lipid levels and adiposity. *J Biol Chem*. 2006;281(2):934–944.
49. Sharara-Chami RI, Zhou Y, Ebert S, Pacak K, Ozcan U, Majzoub JA. Epinephrine deficiency results in intact glucose counter-regulation, severe hepatic steatosis and possible defective autophagy in fasting mice. *Int J Biochem Cell Biol*. 2012;44(6):905–913.
50. Sun Y, Wang P, Zheng H, Smith RG. Ghrelin stimulation of growth hormone release and appetite is mediated through the growth hormone secretagogue receptor. *Proc Natl Acad Sci U S A*. 2004; 101(13):4679–4684.
51. Sheriff S, Kadeer N, Joshi R, Friend LA, James JH, Balasubramaniam A. Des-acyl ghrelin exhibits pro-anabolic and anti-catabolic effects on C2C12 myotubes exposed to cytokines and reduces burn-induced muscle proteolysis in rats. *Mol Cell Endocrinol*. 2012;351(2):286–295.
52. Pallafacchina G, Calabria E, Serrano AL, Kalhovde JM, Schiaffino S. A protein kinase B-dependent and rapamycin-sensitive pathway controls skeletal muscle growth but not fiber type specification. *Proc Natl Acad Sci U S A*. 2002;99(14):9213–9218.
53. Skurk C, et al. The FOXO3a transcription factor regulates cardiac myocyte size downstream of AKT signaling. *J Biol Chem*. 2005;280(21):20814–20823.
54. Zhao JJ, et al. The p110alpha isoform of PI3K is essential for proper growth factor signaling and oncogenic transformation. *Proc Natl Acad Sci U S A*. 2006;103(44):16296–16300.
55. Gwinn DM, et al. AMPK phosphorylation of raptor mediates a metabolic checkpoint. *Mol Cell*. 2008; 30(2):214–226.
56. Barazzoni R, et al. Ghrelin regulates mitochondrial-lipid metabolism gene expression and tissue fat distribution in liver and skeletal muscle. *Am J Physiol Endocrinol Metab*. 2005;288(1):E228–E235.
57. Serra C, et al. Functional interdependence at the chromatin level between the MKK6/p38 and IGF1/PI3K/AKT pathways during muscle differentiation. *Mol Cell*. 2007;28(2):200–213.
58. Puigserver P, et al. Cytokine stimulation of energy expenditure through p38 MAP kinase activation of PPARgamma coactivator-1. *Mol Cell*. 2001; 8(5):971–982.
59. Kewalramani G, et al. Acute dexamethasone-induced increase in cardiac lipoprotein lipase requires activation of both Akt and stress kinases. *Am J Physiol Endocrinol Metab*. 2008;295(1):E137–E147.
60. Aversa Z, Alamdari N, Castillero E, Muscaritoli M, Rossi Fanelli F, Hasselgren PO. beta-Hydroxy-beta-methylbutyrate (HMB) prevents dexamethasone-induced myotube atrophy. *Biochem Biophys Res Commun*. 2012;423(4):739–743.
61. Qin W, Pan J, Wu Y, Bauman WA, Cardozo C. Protection against dexamethasone-induced muscle atrophy is related to modulation by testosterone of FOXO1 and PGC-1α. *Biochem Biophys Res Commun*.

2010;403(3–4):473–478.
62. Hong T, et al. Fine-tuned regulation of the PGC-1α gene transcription by different intracellular signaling pathways. *Am J Physiol Endocrinol Metab*. 2011;300(3):E500–E507.
63. Sandri M, et al. PGC-1alpha protects skeletal muscle from atrophy by suppressing FoxO3 action and atrophy-specific gene transcription. *Proc Natl Acad Sci U S A*. 2006;103(44):16260–16265.
64. Fürstenberger G, Senn HJ. Insulin-like growth factors and cancer. *Lancet Oncol*. 2002;3(5):298–302.
65. De Acetis M, et al. Cardiac overexpression of melusin protects from dilated cardiomyopathy due to long-standing pressure overload. *Circ Res*. 2005; 96(10):1087–1094.
66. Hishiya A, Iemura S, Natsume T, Takayama S, Ikeda K, Watanabe K. A novel ubiquitin-binding protein ZNF216 functioning in muscle atrophy. *EMBO J*. 2006;25(3):554–564.
67. Geuna S, Tos P, Guglielmone R, Battiston B, Giacobini-Robecchi MG. Methodological issues in size estimation of myelinated nerve fibers in peripheral nerves. *Anat Embryol (Berl)*. 2001;204(1):1–10.
68. Tos P, et al. Employment of the mouse median nerve model for the experimental assessment of peripheral nerve regeneration. *J Neurosci Methods*. 2008;169(1):119–127.